UNIVERSITÀ
DI SIENA
1240

Department Biotechnology, Chemistry and Pharmacy

PhD Program in Biochemistry and Molecular Biology – Bibim 2.0

XXXVIII Cycle

Coordinator: Prof.ssa Lorenza Trabalzini

A PHGDH–Hedgehog Axis Drives 5-FU Chemoresistance in Colorectal Cancer

Scientific-Disciplinary Sector: Biochemistry and Molecular Biology

Candidate
Dott.ssa Caterina Mancini
Università degli Studi di Firenze

Supervisor
Prof.ssa Maria Letizia Taddei
Università degli Studi di Firenze

Academic year in which the PhD degree is conferred
2025/26

University of Siena
PhD program in Biochemistry and Molecular Biology – Bibim 2.0
XXXVIII Cycle

Date of the final exam

14 April 2026
Auditorium de Le Benedettine - Piazza S. Paolo a Ripa D'Arno 16, Pisa

Examining board

Prof.ssa Eleonora Da Pozzo, Università di Pisa
Prof.ssa Amalia Gastaldelli, IFC-CNR
Prof. Antonio Pezone, Università di Napoli

Substitutes

Prof.ssa Paola Antonia Corsetto, Università di Milano

30/03/2026 19:54:31
CATERINA MANCINI

Caterina Mancini

ABSTRACT

Phosphoglycerate dehydrogenase (PHGDH) is the rate-limiting enzyme in the de novo serine synthesis pathway (SSP), a highly regulated pathway overexpressed in several cancer types. It has been shown that high PHGDH levels correlate with accelerated proliferation of different tumor cells, while its depletion shows selective toxicity. Recently, it has emerged that PHGDH expression is dynamically regulated during different stages of tumor progression, promoting cancer aggressiveness.

Results show that the expression level of PHGDH is heterogeneous in colorectal cancer (CRC) cell lines and in tumor samples from CRC patients and correlates with aggressiveness and resistance of CRC cell lines to 5-Fluorouracil (5-FU) treatment. Furthermore, PHGDH expression correlates with upregulation of Hedgehog (HH) pathway, conferring resistance to 5-FU treatment. The combination of 5-FU and JC19, a GLI1 inhibitor, is able to enhance the chemo-sensitivity both *in vitro* (cells and organoids) and *in vivo* (mouse models).

SUMMARY

ABBREVIATIONS

- 5-FU: 5-Fluorouracil
- ABC: ATP-Binding Cassette
- ASCT: Alanine-Serine-Cysteine Transporter
- CD: Cluster of Differentiation
- CRC: Colorectal Cancer
- CSC: Cancer Stem Cells
- EMT: Epithelial-Mesenchymal Transition
- GSEA: Gene Set Enrichment Analysis
- HH: Hedgehog
- IHC: Immunohistochemistry
- MMR: Mismatch Repair
- NES: Normalized Enrichment Score
- NR: Non-Responder
- OS: Overall Survival
- PCA: Principal Component Analysis
- PDCO: Patient-Derived Cancer Organoid
- PHGDH: Phosphoglycerate Dehydrogenase
- R: Responder
- RFS: Recurrence-Free Survival
- ROS: Reactive Oxygen Species
- SER/GLY: Serine-Glycine
- SER: Serine
- SSP: Serine Synthesis Pathway
- TCGA: The Cancer Genome Atlas

Chapter 1. INTRODUCTION

1.1. Colorectal Cancer

Colorectal cancer (CRC) is a malignant neoplasm that originates from the glandular epithelium of the large intestine and represents one of the most widespread malignancies worldwide (1). The development of CRC occurs through a process of malignant transformation characterized by the progressive accumulation of genetic and epigenetic mutations that confer a proliferative advantage to the cells (1). Adenocarcinoma represents the predominant histological type, accounting for approximately 96% of all CRC cases (2).

According to GLOBOCAN 2020 data, CRC represents the third most frequently diagnosed malignancy and the second leading cause of cancer-related death worldwide (2). In 2020, an estimated 1.93 million new cases and 0.94 million deaths related to CRC were reported, corresponding to 10% of the global cancer incidence and 9.4% of all cancer-related deaths, respectively (2). The incidence shows a strong correlation with the Human Development Index (HDI), with rates in very high-HDI countries being approximately four times higher than those in low-HDI countries (2).

Regarding gender differences, CRC shows a higher incidence in men than in women, with a global rate 44% higher in 2020 (2). Women show a greater predisposition to proximal colon cancer, which is associated with a more aggressive form of the disease (1).

The risk factors for CRC are classified into two categories: non-modifiable factors and modifiable factors (3). Age is the main non-modifiable risk factor, with a dramatic increase in incidence after the age of 50 (1). A worrisome aspect is the increase in early-onset CRC incidence among individuals aged 20–49 years, with a 47.31% rise from 1975 to 2015 (1).

Genetic predisposition contributes to about 10% of CRC cases. The most common hereditary syndromes are Lynch syndrome and familial adenomatous polyposis (FAP) (3). Lynch syndrome, caused by mutations in DNA mismatch repair (MMR) genes, confers a risk of developing CRC of 70% in men and 40% in women (4). FAP, caused by mutations in the APC tumor suppressor gene, confers a nearly 100% risk of CRC (4). Inflammatory bowel diseases (IBD), such as ulcerative colitis and Crohn's disease, increase the risk of CRC by two to three times compared to the general population (5).

Among modifiable factors, diet plays a crucial role. High consumption of red and processed meat is associated with increased risk, while a diet rich in fiber, whole grains, fruits, and vegetables exerts a protective effect (6). Obesity, type 2 diabetes mellitus, alcohol consumption, and tobacco smoking are additional modifiable factors that significantly increase the risk of CRC (3). By contrast, regular physical activity is associated with a reduced risk through mechanisms that include decreased systemic inflammation and improved immune function (6).

The pathogenesis of CRC is based on the adenoma–carcinoma sequence model, proposed by Fearon and Vogelstein (7). This model describes the progression from precancerous polyp to invasive carcinoma (*Figure 1*) through the sequential accumulation of specific genetic mutations (8). The average progression time from adenoma to cancer ranges from 10.6 to 25.8 years, with higher progression rates in advanced adenomas, characterized by size greater than 10 mm, villous features, or high-grade dysplasia (8).

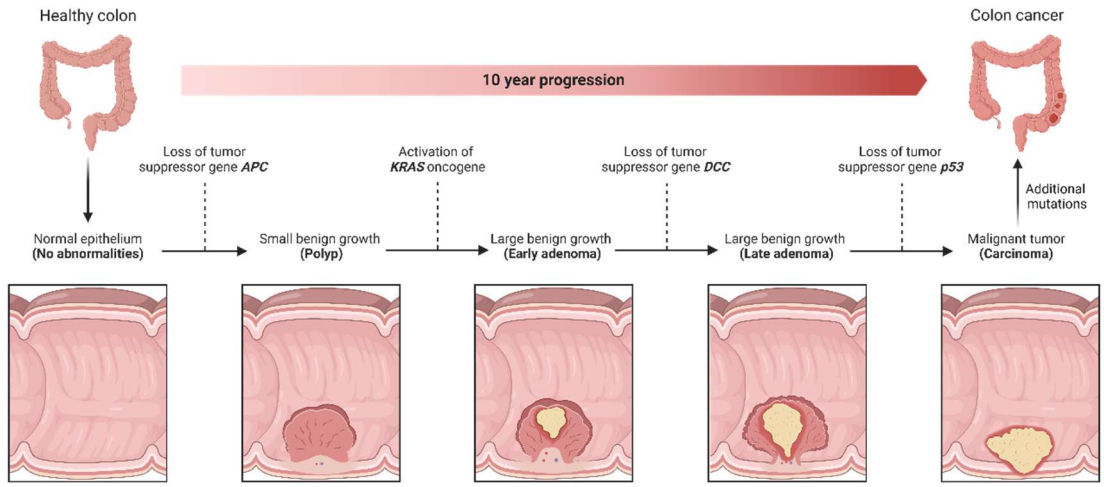

***Figure 1**: Schematic representation of colorectal cancer progression. (Illustration generated using BioRender).*

Based on genomic integrity, CRC tumors can be classified as microsatellite stable (MSS) or microsatellite unstable (MSI) (8). Chromosomal instability is responsible for about 70% of cases and is characterized by alterations such as aneuploidy and loss of heterozygosity. Mutations in APC represent the initial event in adenoma formation, activating the Wnt signaling pathway (8). Subsequently, mutations in KRAS (present in about 40% of tumors) lead to constitutive activation of the EGFR pathway, while late mutations in TP53 facilitate the transition to malignancy (8).

The MSI pathway is observed in about 15% of CRCs and is caused by a defect in the DNA MMR system (8). The most common cause of the sporadic MSI phenotype is epigenetic silencing of MLH1 due to promoter methylation. These tumors frequently exhibit BRAF mutations and present a CIMP phenotype (CpG island methylator phenotype) (8).

1.1.1. Staging, Treatment and Prognosis of Colorectal Cancer

The TNM system is the international standard for CRC staging (*Table 1*) and is crucial for treatment planning and prognosis (9). The T category assesses the depth of tumor invasion into the intestinal wall, the N category defines the status of regional lymph nodes based on the number of metastatic lymph nodes, while the M category evaluates the presence of distant metastases (10). Five-year survival varies significantly according to stage, from 97.1% for T1-2 N0 lesions to 21.7% for T4 N2 lesions (10).

Staging	**TNM**
0	Tis N0 M0
I	T1-2 N0 M0
IIA	T3 N0 M0
IIB	T4a N0 M0
IIC	T4b N0 M0
IIIA	T1-2 N1/N1c M0 T1 N2a M0
IIIB	T3-4a N1/N1c M0 T2-3 N2a M0 T1-2 N2b M0
IIIC	T4a N2a M0 T3-4a N2b M0 T4b N1-2 M0
IVA	any T, any N, M1a
IVB	any T, any N, M1b
IVC	any T, any N, M1c

Table 1*: TNM staging system for colorectal cancer (T=Tumor; N=Node; M=Metastases).*

The treatment of CRC is mainly based on the stage of the disease. For stage 0 and I tumors, endoscopic or surgical resection is generally sufficient (11). In stage II, the decision to add adjuvant chemotherapy depends on the presence of high-risk factors, such

as T4 tumors, lymphovascular invasion, intestinal obstruction, or perforation (12). Stage III requires surgical resection followed by adjuvant chemotherapy with regimens such as FOLFOX or XELOX (13).

For metastatic stage IV disease, systemic treatment is the cornerstone of therapy. First-line regimens include FOLFOX, XELOX, or FOLFIRI, often combined with targeted therapies such as monoclonal antibodies against VEGF (bevacizumab) or EGFR (cetuximab, panitumumab) for RAS wild-type tumors (14). Immunotherapy with immune checkpoint inhibitors, such as pembrolizumab and nivolumab, has shown significant efficacy in patients with MSI-H/dMMR tumors, which account for approximately 5% of metastatic CRCs (15).

The prognosis of CRC is influenced by multiple clinicopathological and molecular factors. The TNM stage remains the most important prognostic predictor (16). Histological grade, tumor location, and microsatellite status are additional significant prognostic determinants. Left-sided tumors are associated with a significantly lower risk of mortality compared to right-sided tumors (16). MSI-H status is generally associated with a better prognosis in localized tumors, whereas RAS and BRAF mutations are correlated with a less favorable prognosis (16).

Recurrence after curative treatment represents a significant clinical challenge, with approximately 20–25% of patients presenting with metastases at initial diagnosis (17). The most common sites of distant metastases include the liver (40–50% of cases) and the lung (10–20% of cases) (17).

1.2. Treatment and Limitations of 5-Fluorouracil (5-FU) Therapy

5-Fluorouracil (5-FU) has constituted the first-line treatment for CRC for several decades and is classified as an antimetabolite and pyrimidine antagonist. The molecule was synthesized in 1957 by Heidelberger's group, who demonstrated that it is avidly internalized by tumor cells compared to healthy tissues, thereby exhibiting selective cytotoxicity (18). 5-FU is an aromatic heterocyclic organic compound analogous to uracil, in which a fluorine atom replaces the hydrogen at the C5 position (19). This modification, while not altering the molecular weight or the stability of the compound, enables it to interfere with nucleotide synthesis, to be incorporated into RNA, and to inhibit DNA synthesis with a cytotoxic effect (18,19).

In CRC, adjuvant chemotherapy is recommended after surgical resection in patients with stage III disease or in patients with stage II disease who are at high risk of recurrence. 5-FU can be administered intravenously or orally in the form of Capecitabine, an antimetabolite developed to mimic the continuous infusion of the drug, reducing plasma doses and consequently the side effects (20). Capecitabine is absorbed in the gastrointestinal tract and converted into the liver through hepatic carboxylesterases and cytidine deaminases into active pro-metabolites, which are expressed both in the liver and in the tumor. However, the response rate to 5-FU alone is 10–15%, while in combination with other antitumor agents it increases to 50% (18,19). To date, the first-line treatment involves the administration of 5-FU in combination regimens such as FOLFOX, which includes oxaliplatin, leucovorin (LV), and 5-FU; FOLFIRI, which consists of irinotecan, LV, and 5-FU; and FOLFOXIRI, which combines all three cytotoxic agents (18,21). In the third-line setting, 5-FU is co-administered with biological agents such as Bevacizumab, Ramucirumab, Aflibercept, or Regorafenib, which inhibit the tyrosine kinase activity of membrane receptors involved in tumor angiogenesis, and with monoclonal antibodies such as Panitumumab and Cetuximab, which directly inhibit EGFR (18,21,22). These therapeutic combinations enhance treatment efficacy and patient survival but also increase toxicity (18,21).

1.2.1. Mechanism of action of 5-FU

5-FU itself does not exert direct cytotoxic effects; instead, its pro-metabolites are the true mediators of the antitumor activity. The drug is internalized by tumor cells through specific transporters and passive diffusion (23). Once inside the cell, 5-FU is converted into two major active metabolites: fluorodeoxyuridine triphosphate (FdUTP) and fluorouridine triphosphate (FUTP), which are incorporated into DNA and RNA, respectively (18,24). 5-FU can be phosphorylated through several enzymatic pathways to generate fluorouridine monophosphate (FUMP), which is subsequently converted into fluorouridine diphosphate (FUDP) and fluorouridine triphosphate (FUTP). FUTP is erroneously incorporated into cellular RNA, causing damage due to impaired maturation, as the modification of uridine to pseudouridine is prevented (19,25). In parallel, FUDP can be reduced to fluorodeoxyuridine diphosphate (FdUDP) by ribonucleotide reductase and subsequently phosphorylated to FdUTP, which is incorporated in place of thymidine triphosphate by DNA polymerases, leading to double-strand breaks in DNA (18,24).

The principal mechanism of 5-FU cytotoxicity arises from the formation of fluorodeoxyuridine monophosphate (FdUMP), which covalently binds to the nucleotide-binding site of thymidylate synthase (TS), preventing the entry of deoxyuridine monophosphate (dUMP), the physiological substrate of the enzyme, and thereby blocking the conversion of dUMP to deoxythymidine monophosphate (dTMP) (18,26). In summary, as a pyrimidine analog antimetabolite, 5-FU becomes a substrate for the enzymes involved in the normal synthesis of deoxythymidine triphosphate (dTTP) within tumor cells. However, its conversion leads to multiple cytotoxic effects that converge toward programmed cell death through inhibition of DNA synthesis, misincorporation into DNA and RNA, and disruption of RNA maturation processes (*Figure 2*).

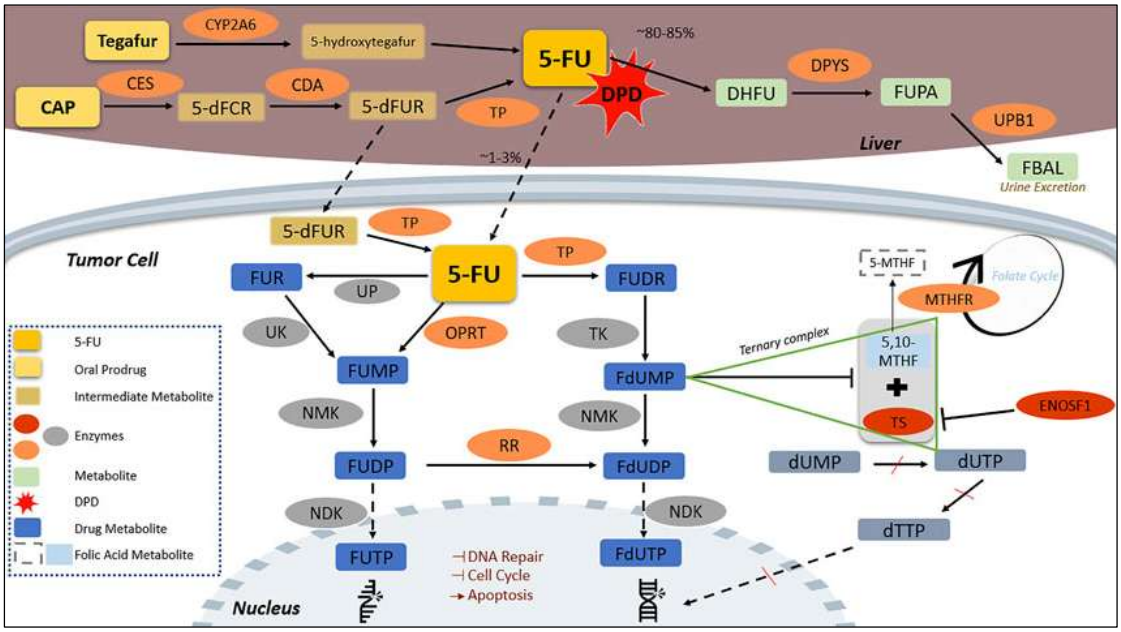

***Figure 2**: Metabolism and mechanism of action of 5-fluorouracil: 5-FU is converted into three active metabolites - fluorodeoxyuridine monophosphate (FdUMP), fluorodeoxyuridine triphosphate (FdUTP), and fluorouridine triphosphate (FUTP) - FdUTP and FUTP are misincorporated into DNA and RNA, interfering with normal nucleic acid metabolism. FdUMP inhibits thymidylate synthase (TS), thereby preventing DNA synthesis (27).*

1.2.2. Limitations and Critical Issues of 5-FU Therapy

Despite the efficacy of 5-FU in the treatment of CRC, most patients experience side effects such as fever, fatigue, mucositis and stomatitis, nausea, vomiting and diarrhea, leukopenia, neutropenia, thrombocytopenia, skin rash, and hand-foot syndrome (18,19,21). Neurological alterations, such as cerebellar ataxia and cognitive dysfunction, have been reported in approximately 1% of patients (18,21). The bioavailability of 5-FU in patients is highly variable, due both to the circadian regulation of dihydropyrimidine

dehydrogenase (DPD) - the enzyme responsible for drug catabolism - and to the presence of polymorphisms and deficiencies in this enzyme (18). In patients with DPD deficiency, there is a severe risk of toxicity following administration of a standard dose of 5-FU, while in patients with DPD overexpression, rapid hepatic elimination of the drug leads to reduced therapeutic efficacy (19). Chemoresistance represents one of the main obstacles to the effectiveness of therapy and to the development of recurrences in patients. It is a hallmark of highly plastic and aggressive tumors, often manifesting as resistance to multiple anticancer drugs (18,28). Resistance can be acquired during treatment, when chemotherapy exerts selective pressure on the tumor bulk and certain clones, equipped with compensatory mechanisms, adapt and survive (18,29). In other cases, resistance is intrinsic; tumor cells are physiologically resistant to chemotherapeutic agents due to the overexpression of membrane transporters that actively expel the drug (29). In CRC, overexpression of certain ATP-binding cassette (ABC) transporters such as ABCB5 and MRP2 has been observed, facilitating the efflux of 5-FU. Their expression appears to be induced by Notch signaling via the transcription factor HES1, which regulates both transporter gene transcription and the epithelial-mesenchymal transition. Cancer stem-like cells can also enter a dormant or quiescent state to survive treatment, and, under permissive conditions, may contribute to tumor recurrence (18,30). Clonal heterogeneity in CRC also arises from features of the tumor microenvironment, such as hypoxia, acidity, and the availability of growth factors, which enable certain clones within the tumor bulk to develop resistance to 5-FU (31). Despite 5-FU-based chemotherapy as first-line treatment, chemoresistance frequently emerges, and the 5-year survival rate remains approximately 12–14%, reflecting the limited efficacy of current 5-FU regimens (21,32).

The primary target of fluorodeoxyuridine monophosphate is thymidylate synthase, encoded by the TYMS gene (18). Several studies have shown that exposure to 5-FU induces the expression of thymidylate synthase: binding of FdUMP inhibits TS catalysis, but at the same time triggers a compensatory response that increases translation of TS mRNA (18,24). Formation of the ternary complex renders thymidylate synthase unable to inhibit its own translation, thereby signaling a need for increased TS levels. Consequently, higher availability of thymidylate synthase correlates with resistance to 5-FU and serves as a prognostic marker of reduced therapeutic efficacy and increased tumor aggressiveness (33). Mutations, gene amplifications, and tandem repeat polymorphisms in the promoter region of the TYMS gene can also increase enzyme expression with the

same outcome (18). Overexpression of TS is also linked to oncogenic activation of FOXM1, a transcription factor that binds to the promoters of genes encoding enzymes involved in nucleotide synthesis, and regulates the expression of cyclins D1 and B1, DNA repair genes (RAD and BRCA2), metalloproteases (MMP2 and MMP9), and the transporter ABCC10. Collectively, FOXM1 mediates a phenotype that is resistant to 5-FU, aggressive, and pro-invasive (34). Thymidine phosphorylase (TP), a cytosolic enzyme that converts thymidine into thymine, is essential for pyrimidine recycling during RNA degradation. TP plays a fundamental role in tumor growth, metastasis, and angiogenesis, and is also involved in the inhibition of apoptosis (18,35).

DNA repair systems are capable of correcting damage caused by endogenous or exogenous agents, including chemotherapeutic drugs. Aberrant activation of the repair system is associated with increased CRC aggressiveness and poorer patient response to chemotherapy. Physiologically, the system recognizes uracil as an abnormal base in DNA through uracil glycosylase, which removes it - a mechanism that is also involved in eliminating 5-FU derived bases (36). The MMR system also plays an important role in determining response to chemotherapy regimens. CRC can be classified according to MMR proficiency or deficiency, which correlate with microsatellite stability or instability, respectively (18). In tumors with mismatch repair deficiency, altered base - including fluorodeoxyuridine - are not recognized, and apoptosis is not induced in response to DNA damage (18,37). Impaired function of these systems is also influenced by p53 inactivation, which prevents recognition of DNA mutations and induction of apoptosis (38).

1.2.3. Role of Tumor Metabolism in Chemoresistance

The tumor bulk is characterized by high clonal heterogeneity at the epigenetic, signaling, metabolic, and phenotypic levels; this very heterogeneity enables certain clones to withstand chemotherapy treatment (31,39). Within the tumor microenvironment, a metabolic symbiosis is established not only among the bulk tumor cells themselves, which exhibit different metabolic profiles (oxidative phosphorylation and Warburg-type glycolytic metabolism), but also with other surrounding cells, such as cancer-associated fibroblasts (CAFs), which are induced by the tumor to acquire a reverse Warburg phenotype (40). Under chronic 5-FU treatment, some CRC cells revert their metabolism from glycolytic to respiratory in order to meet the increased energy demand under stress conditions (41). This metabolic shift is enabled by the re-expression of enzymes such as

pyruvate kinase M1 and by mitochondrial biogenesis induced by the sirtuin1-PGC1α axis. These processes allow the cells to maximize energy production from glucose through the reactivation of the Krebs cycle and oxidative phosphorylation (42). This metabolic reprogramming is driven by the treatment, which acts as selective pressure, inducing stem-like cells to adapt for survival. The dependence of these clones on mitochondrial activity is crucial for the development of chemoresistance, but at the same time makes them susceptible to therapies targeting respiratory metabolism, such as Metformin (41).

Several studies have highlighted that the availability of both endogenous and exogenous serine is a key factor in the development of resistance to 5-FU (43,44). The metabolism of serine is closely interconnected, through the folate cycle, to the cellular availability of NADPH and nucleotides, both required to sustain tumor expansion. Overexpression of the enzyme PHGDH diverts the glycolytic intermediate 3-phosphoglycerate toward sustained biosynthesis of this amino acid, and the acquisition and maintenance of 5-FU resistance is permitted by the availability of serine (45–47). In 5-FU resistant cells, an increase in the serine hydroxymethyltransferase SHMT2/SHMT1 isoform ratio is observed, along with a compartmentalization of the one-carbon group derived from serine at the mitochondrial level. This allows tumor cells to maximize the biosynthesis of nitrogenous bases and cytoplasmic NADPH in order to overcome the DNA damage induced by the chemotherapeutic agent (43). Studies conducted in xenograft mouse models with CRC cells silenced for the enzyme phosphoserine aminotransferase have shown that a serine-deficient diet reduces tumor volume and increases markers of DNA damage (43,47).

Despite the numerous resistance mechanisms, chemotherapy regimens based on 5-FU remain the most effective treatments for CRC. A deeper understanding of the molecular and metabolic mechanisms underlying resistance could pave the way for the identification of new therapeutic targets, as well as for the selection of the most appropriate therapy according to patients' specific mutational and signaling profiles (18). Numerous ongoing studies are evaluating the use of PHGDH inhibitors as potential co-treatments alongside conventional chemotherapy in order to revert the drug-resistant tumor phenotype (45). Through compound library screenings, the essential characteristics required for PHGDH inhibitors have been identified: these molecules must be sufficiently small to enter the PHGDH substrate-binding pocket and possess one or more negatively charged residues to create stabilizing ionic interactions (45). Some of the inhibitors currently under

investigation display these characteristics and exhibit a certain degree of efficacy in PHGDH-overexpressing tumors. Indole derivatives, such as BI-4916, classified as orthosteric inhibitors, inhibit PHGDH by competing with NAD+ for binding (48,49). Compound 9 is an allosteric inhibitor that binds to a cysteine residue within the ASB domain and alters the equilibrium between the enzymatically active tetrameric and dimeric forms; however, it has demonstrated toxicity in *in vivo* models (48,50). Natural compounds have also been identified as allosteric inhibitors of PHGDH (50). Starting from piperazine-1-carbothioamide, the molecule NCT-503 was derived. NCT-503 reversibly inhibits PHGDH without competing with its substrates, and reduces the incorporation of the one-carbon unit into nucleotides (51). These small inhibitory molecules downregulate PHGDH through different mechanisms and reduce serine biosynthesis, thereby impacting tumor cell proliferation and inducing apoptosis in a dose-dependent manner, although various studies have reported differing degrees of toxicity (48–51).

1.3. Role of the Serine Pathway in Tumor Progression

Serine is a non-essential amino acid that plays a central role in cellular metabolism. It is particularly important in highly proliferative cells such as tumor cells. Cells can obtain serine through two main ways: uptake from the extracellular environment via specific membrane transporters, such as ASCT (Alanine-Serine-Cysteine Transporter) systems, or through endogenous synthesis, known as the Serine Synthesis Pathway (SSP) (52,53) Serine is essential in tissues with high biosynthetic demand, such as the brain, and in tumor cells to support their proliferative activity (54).

De novo serine biosynthesis derives from the glycolytic pathway (*Figure 3*).

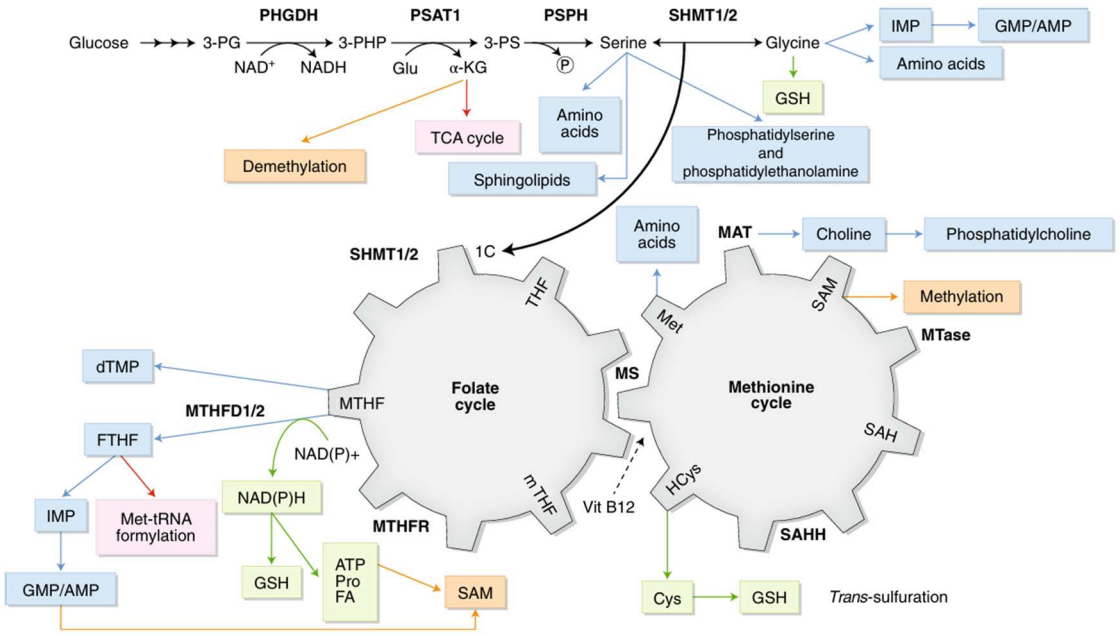

***Figure 3**: De novo serine synthesis pathway. The figure also illustrates glycine metabolism and the one-carbon cycle, highlighting the interconnections between these metabolic pathways and the key enzymes involved (55).*

This allows cells to divert intermediates from glucose catabolism toward essential anabolic pathways. The process starts from 3-phosphoglycerate (3PG), an intermediate of glycolysis or gluconeogenesis. It develops through three sequential enzymatic reactions (53). This metabolic pathway enables cells to maintain intracellular serine levels independent of its extracellular availability. This is a valuable characteristic for tumor cells situated in microenvironments poor in oxygen and nutrients.

Neoplastic cells show a marked dependence on serine. They utilize both exogenous sources and endogenous synthesis to meet their elevated metabolic requirements (56). Numerous studies highlight that serine is the second most consumed amino acid by tumor cells after glutamine. This underlines the importance of this nutrient in cancer metabolism. The ability of tumor cells to modulate SSP activity in response to available serine represents a significant example of metabolic plasticity. This plasticity allows adaptation to variable conditions and promotes tumor progression (57,58).

1.3.1. Metabolic and Non-Metabolic Functions of PHGDH in Tumor Progression

PHGDH catalyzes the first and main rate-limiting step of the serine synthesis pathway. It oxidizes 3PG to 3-phosphohydroxypyruvate (3PHP) through an NAD-dependent mechanism (53). Subsequently, 3PHP is converted to 3-phosphoserine (3PS) by

phosphoserine aminotransferase 1 (PSAT1) through a transamination reaction that uses glutamate. This generates α-ketoglutarate, an important anaplerotic intermediate of the Krebs cycle. Finally, phosphoserine phosphatase (PSPH) dephosphorylates 3PS, releasing serine (53).

The activity of the SSP is subject to refined regulation. A key mechanism is negative feedback in which serine itself allosterically regulates pyruvate kinase isoform M2 (PKM2). This enzyme catalyzes the last reaction of glycolysis (59,60). Serine acts as an allosteric activator of PKM2, promoting the continuation of glycolysis. Under conditions of serine deficiency, PKM2 activity decreases. This causes an accumulation of upstream intermediates, particularly 3PG, which is then directed toward the SSP, restoring the necessary serine levels.

Another regulator is 2-phosphoglycerate (2PG), which directly activates PHGDH. Since PKM2 inhibition leads to 2PG accumulation, this mechanism facilitates the flux of 3PG toward the SSP (61). At the transcriptional level, the GCN2-ATF4 pathway responds to low amino acid levels by increasing the expression of SSP genes (60,62). Moreover, the NRF2 factor, often deregulated in cancer and a regulator of the antioxidant system, stimulates PHGDH, PSAT1 and SHMT2 to ensure glutathione and nucleotide synthesis in tumor cells (62).

Serine is essential not only as a metabolic component but also as a donor of one-carbon units to the folate cycle. This process is crucial for de novo nucleotide synthesis, methylation reactions and maintenance of cellular redox balance (53,63). Through SHMT, serine is converted to glycine. It transfers a methylene group to tetrahydrofolate (THF) to form 5,10-methylene-THF, an essential precursor for thymidylate synthesis (catalyzed by thymidylate synthase, TYMS) and purines. Serine deficiency in tumor cells drastically reduces proliferation and purine nucleotide levels (57,58).

Maintenance of redox homeostasis is critical for tumor cells, which experience elevated levels of reactive oxygen species (ROS) from intensified mitochondrial metabolism. Serine contributes to oxidative stress control in two main ways: as a precursor of glycine and cysteine, two components of glutathione (GSH), the main cellular antioxidant (53), and through the folate cycle that fuels NADPH production, an essential cofactor for antioxidant defenses. ROS have a dual role in tumorigenesis: moderate levels promote

proliferation and metabolic adaptation, while excessive levels cause cellular damage and death (64,65).

Finally, serine fuels the methionine cycle by providing one-carbon units necessary for the remethylation of homocysteine to methionine. This is catalyzed by methionine synthase in the presence of 5-methyl-THF (53). Subsequently, methionine is converted to S-adenosylmethionine (SAM), the main methyl group donor for epigenetic methylation reactions on DNA, histones, proteins and lipids. These reactions are essential for gene expression regulation. Interestingly, serine also supports ATP production necessary for the conversion of methionine to SAM through de novo purine synthesis (66)

Since the 1980s (67), it has been known that the activity of SSP enzymes is increased in cancer tissues compared to normal tissues. Recent genomic studies have rediscovered the importance of PHGDH in cancer, with frequent amplifications of its chromosomal locus. In colorectal carcinoma, PHGDH overexpression has been associated with worse clinicopathological parameters: advanced stage, lymph node metastasis, larger tumor size, vascular invasion and unfavorable prognosis (46). Studies indicate that tumors can be stratified into two categories according to their serine dependence: those that depend on exogenous serine, with low SSP levels, and those that adopt endogenous synthesis through PHGDH overexpression (68,69).

For exogenous-dependent tumors, dietary restriction of serine and glycine has proven effective preclinically in reducing plasma levels of these amino acids by up to 50% without significant side effects (58). This delays tumor growth by increasing oxidative stress due to reduced glutathione synthesis and deficits in nucleotide production (59).

In tumors with high PHGDH expression, the use of selective pharmacological inhibitors is proposed, such as the molecule NCT-503, successfully tested both *in vitro* and *in vivo* (51). This treatment not only reduces serine synthesis but also causes an imbalance in cytosolic one-carbon units. It decreases the 5,10-methylene-THF pool for thymidylate synthesis, regardless of exogenous serine presence. A recent work demonstrated that the combination of PHGDH inhibitors and a serine/glycine-poor diet produces a synergistic effect against tumors with intermediate PHGDH levels. These tumors are able to partially compensate for dietary restriction with internal synthesis (51,70). The authors emphasize the importance of precise molecular characterization to identify tumors truly dependent on this metabolic pathway. From a clinical perspective, it is essential to identify reliable

biomarkers for tumor classification based on serine dependence. PHGDH expression detected by immunohistochemistry is a promising candidate. However, related enzymes (PSAT1, PSPH, SHMT1/2, MTHFD1/2) and transporters (ASCT2) must also be considered.

1.3.2. PHGDH in Therapeutic Resistance

Beyond its catalytic role, PHGDH contributes to tumor progression and chemoresistance through metabolic and non-metabolic mechanisms. Its expression is associated with resistance to several chemotherapeutic agents, including 5-fluorouracil (5-FU), a key drug in colorectal carcinoma (43,71). In 5-FU resistance, the compartmentalization of serine catabolism in the mitochondrion is crucial (43). The mitochondrial isoform SHMT2 enables the production of glycine and mitochondrial one-carbon units. This supports purine synthesis and NADPH production, which are essential for mitochondrial redox balance. This shift reduces the cytosolic concentration of 5,10-methylene-THF. It limits the formation of the ternary complex 5-fluorodeoxyuridine monophosphate (FdUMP), thymidylate synthase and 5,10-methylene-THF, which is indispensable for the cytotoxic action of 5-FU. Resistant cells also show upregulation of PHGDH, PSAT1 and PSPH, indicating a general activation of the SSP (71). PHGDH also supports antioxidant defenses, allowing cells to resist the increase in ROS induced by oncological therapies. PHGDH inhibition restores sensitivity to therapies in resistant cells (71,72).

An emerging aspect concerns the nuclear functions of PHGDH, which interacts with transcription factors and regulatory proteins of gene expression (73,74). In particular, PHGDH binds FOXM1, a transcription factor that promotes proliferation. It prevents its degradation and increases transcriptional activity (75). Moreover, PHGDH interacts with the oncogene c-Myc, a master regulator of metabolism and proliferation. This contributes to remodeling of the tumor microenvironment (76).

1.3.3. Therapeutic Targeting of SSP and PHGDH

The multiple roles of PHGDH in tumor progression and therapeutic resistance make its targeting a promising strategy, acting on both metabolic and non-metabolic functions. Pharmacological inhibitors such as NCT-503 have demonstrated reduced tumor growth in preclinical models (77,78). Particularly interesting is the combined use with conventional chemotherapeutics to overcome resistance.

Historically, targeting the folate cycle with drugs such as methotrexate (a dihydrofolate reductase inhibitor, DHFR) represents an established approach. Methotrexate, introduced in 1958 (79), remains effective in various neoplasms, as does 5-FU with its action on thymidylate synthase. However, the importance of folate-dependent metabolism in healthy cells often leads to significant side effects, especially in the bone marrow and intestinal epithelium (24,80).

Recent studies indicate that combined inhibition of cytosolic (SHMT1) and mitochondrial (MTHFD2) enzymes of the folate cycle enhances antitumor efficacy. This prevents metabolic compensation since one-carbon intermediates do not cross the mitochondrial membrane (81).

The non-metabolic roles of PHGDH open new therapeutic opportunities. Interactions with transcription factors such as FOXM1 and c-Myc suggest a modulatory role in gene expression independent of enzymatic activity. In some models, genetic inhibition of PHGDH produces stronger antiproliferative effects compared to pharmacological inhibition. This indicates the importance of non-catalytic functions (74). In pancreatic carcinoma, PHGDH interacts with translation initiation factors (eIF4A1, eIF4E), stabilizing the complex and facilitating protein synthesis (82). In hepatocellular carcinoma, it can promote mitochondrial function and tumor growth (83).

Although preclinical data are promising, clinical translation presents challenges. Reliable predictive biomarkers are needed to select patients who are candidates for serine-targeted therapies. PHGDH expression by immunohistochemistry is a first step, but it must be integrated with other parameters. Tumors with high PHGDH levels may still depend on exogenous serine and vice versa (77). Tumor metabolic plasticity represents a major difficulty: cells can activate alternative pathways to compensate for the inhibition of single enzymes. For example, blockade of the mitochondrial folate cycle can be compensated by the cytosolic pathway due to the reversibility of cycle reactions (81). This suggests that therapies based on multiple targeting will likely be more effective and durable.

A study by Chen et al. (84) found that PHGDH deletion after the initiation of tumor formation does not inhibit tumor growth in mouse models. This indicates that dependence on serine synthesis is stage-specific or that compensatory mechanisms are activated

during neoplastic progression. Understanding these dynamics is essential to define the most vulnerable moments for therapeutic intervention.

Finally, the high toxicity associated with antifolate drugs, such as methotrexate, derives from the fact that folate metabolism and nucleotide synthesis are essential processes even in rapidly proliferating healthy cells (bone marrow, intestinal epithelium, hair follicles) (81). Dietary restriction of serine and glycine in animal models has not shown significant adverse effects. This suggests a possible favorable therapeutic window (58). Combined use of diet and pharmacological inhibitors at moderate doses could maximize therapeutic efficacy while reducing toxicity.

Future prospects include the development of more selective and potent inhibitors, the identification of predictive biomarkers, and the design of clinical studies that integrate dietary interventions and pharmacological therapies. Moreover, it is essential to investigate the non-catalytic role of PHGDH to identify new therapeutic targets (74,75).

In conclusion, serine metabolism and PHGDH represent promising therapeutic targets in cancer treatment, especially in tumors with high dependence on this metabolic pathway. The integration of metabolic, molecular and nutritional approaches could open new avenues to improve the efficacy of oncological therapies and counteract resistance mechanisms.

1.4. Hedgehog Pathway

The Hedgehog (HH) signaling pathway was first identified in Drosophila (85). The Hedgehog pathway is activated in many biological processes, particularly in the embryo where Hedgehog acts as a morphogen in some organogenesis processes, such as the generation of the neural tube (86). In adults, it is substantially active in the stem cell population, where it is fundamental in repair processes (87) and maintenance of this population (88).

There are three types of proteins belonging to the Hedgehog family: Sonic hedgehog (Shh), Indian hedgehog (Ihh), and Desert-hedgehog (Dhh) (85). The most studied protein is Shh, and its functions are particularly important in the development of the nervous system (86).

The Shh signaling pathway can be activated through two different mechanisms, both dependent on the presence of the primary cilium (89) (*Figure 4*).

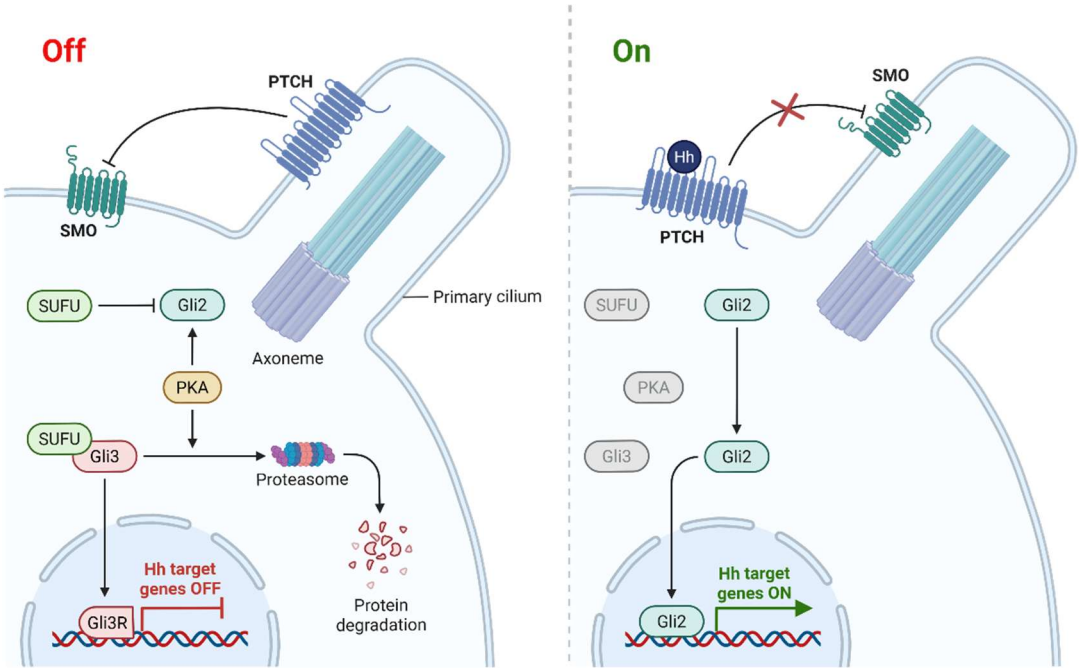

***Figure 4**: Schematic representation of the Hedgehog signaling pathway in its inactive (OFF) and active (ON) states, illustrating the key components, molecular interactions, and downstream effects on gene transcription.*

1.4.1. Signaling and Activation Mechanisms

Activation of the HH signaling pathway requires a specialized cellular structure called the primary cilium, an organelle that is essential for signal transduction (89). Structurally, the primary cilium has a highly conserved organization. Internally, it consists of an axoneme formed by nine pairs of microtubules arranged in a circular configuration, lacking the central pair typical of motile cilia, a structure defined as 9+0. The primary cilium is anchored to the cell via the basal body, a highly specialized structure. This anchorage not only ensures the structural stability of the cilium but also coordinates intracellular trafficking mechanisms required for the proper positioning of the signaling pathway components. The presence of the primary cilium is absolutely necessary for both activation mechanisms of the HH pathway: the canonical mechanism, which is the most well-characterized mode of signal transduction, and the non-canonical mechanism, which involves alternative signaling mechanisms independent of Gli transcription factor activation. The functional importance of the primary cilium is evidenced by the observation that defects in its formation or function are associated with severe developmental diseases characterized by multiple organ and system alterations, reflecting the pleiotropic role of the HH pathway during embryogenesis (89).

1.4.1.1. Canonical mechanism

The canonical signal transduction mechanism of HH is based on a cascade of molecular events that occur at the level of the primary cilium. Under basal conditions, that is, in the absence of the Shh ligand, the Patched1 (Patch1) receptor, a transmembrane protein, is located on the membrane of the primary cilium where it exerts a constitutive inhibitory action on the Smoothened (Smo) receptor, preventing its accumulation and activation on the ciliary membrane. This basal repression mechanism ensures that the pathway remains inactive in the absence of appropriate stimuli. The binding of the Shh ligand to its receptor Patch1 triggers a series of molecular events that culminate in the activation of the signaling pathway. This binding induces the internalization of Patch1 via a receptor-mediated endocytosis process (90), followed by the degradation of the receptor through the ubiquitin-proteasome system. The degradation of Patch1 is finely regulated by post-translational modifications, particularly ubiquitination mediated by specific ubiquitin ligases, which mark the protein for proteasomal degradation (91). The removal of Patch1 from the ciliary membrane eliminates the constitutive inhibition exerted on Smo, allowing the accumulation and activation of Smo on the primary cilium membrane (90). Once activated, Smo transduces the signal through interaction with multiple intracellular effectors, coordinating a complex cascade of phosphorylation and dephosphorylation events that regulate the activity of Gli transcription factors. The activation of Smo promotes the formation of the GLIA (Gli Activator) complex, mainly composed of the active forms of Gli2 and Gli3 proteins (92). This complex represents the primary initiator of the transcriptional response to HH signaling. The response is subsequently amplified and maintained by Gli1, which itself is a target gene of the pathway and acts as a signal amplifier through a positive feedback mechanism (92). In contrast, in the absence of HH signaling, the Gli2 and Gli3 proteins are maintained in an inactive state known as GLIR (Gli Repressor) through the combined action of protein kinase A (PKA) and the regulatory protein SUFU (Suppressor of Fused), which sequester the Gli factors in the cytoplasm and promote their partial proteolytic processing (91,93). This generates truncated forms of Gli2 and Gli3, which function as transcriptional repressors. These truncated forms migrate to the nucleus where they actively inhibit the expression of HH target genes. The dynamic balance between the activating and repressive forms of Gli factors is therefore a central element in the fine regulation of the transcriptional output of the pathway (92). The molecular mechanisms by which Smo coordinates the formation of the GLIA complex involve multiple effectors and are the subject of intense investigation. Among

the identified effectors is the protein KIF7, a kinesin localized at the tip of the primary cilium (94). Another important mechanism involves the interaction of Smo with heterotrimeric G proteins, particularly the Gαi subunit. The activation of this G protein leads to a decrease in intracellular levels of cyclic adenosine monophosphate (cAMP), which in turn causes the inactivation of protein kinase A (PKA), removing the phosphorylative inhibition on Gli factors and promoting the formation of the activator complex (95). Additionally, Smo can interact with the Evc-Evc2 protein complex, located at the base of the primary cilium, which contributes to signal transduction (96). The integration of these multiple levels of regulation ensures an appropriate and proportional cellular response to the intensity of the HH signal. Among the major transcriptional targets of the HH pathway are Patch1 and Gli1. Other important target genes include the oncogene c-Myc, which promotes cell proliferation, members of the Wnt family that coordinate additional developmental signaling pathways, and the transforming growth factor beta (TGFβ) factor, involved in regulating multiple cellular processes (97). Additionally, the HH pathway directly regulates the expression of cell cycle regulators, particularly cyclins D and E, which promote progression through the G1 phase and entry into the S phase of the cell cycle, providing a direct link between HH signaling and the control of cell proliferation (98).

1.4.1.2. Non canonical mechanism

The HH pathway can be activated through non-canonical mechanisms, independent of Gli transcription factor activation. The first of these mechanisms involves direct modulation of the cell cycle through the physical interaction between Patch1 and cyclin B1, a key regulator of the G2 to M phase transition of the cell cycle (99). In the absence of Shh, Patch1 sequesters cyclin B1, preventing its proliferative action and contributing to the maintenance of cell cycle arrest. The second non-canonical mechanism involves regulation of the actin cytoskeleton through the activation of small GTPases from the Rho family. In this context, the presence of Shh leads to the activation of Smo, which in turn activates the Gαi protein, triggering the activation of two important effectors: phosphoinositide 3-kinase (PI3K) and phospholipase C (PLC) (100). PLC induces the release of calcium ions from intracellular stores, particularly from the endoplasmic reticulum, generating a calcium signal that modulates various cellular processes. PI3K, on the other hand, phosphorylates and activates the small GTPases RhoA and Rac1 (101,102). Activation of these GTPases promotes cell migration, cytoskeletal

rearrangement, and, in developing neurons, axon formation - processes that are essential for the development and function of the nervous system.

Aberrant activation of the Hedgehog signaling pathway represents a critical event. This occurs through the molecular mechanisms described. It is important not only during embryonic development but also in pathological contexts. These mechanisms are normally finely regulated. When they become altered, the HH pathway can contribute significantly to neoplastic transformation and tumor progression. The pathway transitions from physiological function to promotion of malignant phenotype. This transition occurs through several molecular mechanisms. These mechanisms exploit and subvert the normal regulatory circuits of the pathway

1.4.2. The Hedgehog Pathway in Tumor Development

The HH signaling pathway can contribute to tumorigenesis through several molecular mechanisms that lead to aberrant pathway activation. These mechanisms can be classified based on their dependence or independence from the extracellular ligand. They include genetic alterations, autocrine and paracrine signaling, and dysfunctions in regulatory circuits. The first and most direct mechanism of aberrant activation involves the acquisition of genetic mutations. These mutations confer tumor cells with independence from ligand presence. Loss-of-function mutations in the PTCH1 gene eliminate the constitutive inhibitory function of Patch1 on Smo. This results in constitutive activation of the signaling pathway even in the absence of the Shh ligand (103). This mechanism is particularly frequent in sporadic basal cell carcinoma and in nevoid basal cell carcinoma syndrome. The second type of genetic alteration involves gain-of-function mutations in the SMO gene. These mutations render Smo constitutively active, independently of the Patch1 state (104,105). These mutations have been identified in sporadic basal cell carcinomas and medulloblastomas. The HH pathway can also be aberrantly activated through autocrine signaling mechanisms. This occurs when tumor cells acquire the ability to autonomously produce and secrete Shh. This self-stimulation circuit has been demonstrated in colorectal carcinoma, where it is essential for tumor growth, metastasis formation, and maintenance of cancer stem cells (106), in breast carcinoma (107), in advanced prostate and lung carcinoma (108,109), and in ovarian carcinoma (110).

An additional mechanism involves paracrine signaling through bidirectional interaction between tumor cells and stroma. Tumor cells secrete Shh which activates stromal cells.

These cells respond by producing growth factors, cytokines, and extracellular matrix components that promote tumor growth and angiogenesis (111). In particular, HH activation in stromal perivascular cells induces VEGF-A, increasing tumor vascularization (112). This modality has been documented in prostate carcinoma (113) and in pancreatic adenocarcinoma (114). In the reverse modality, stromal cells produce Shh which acts on tumor cells. This has been demonstrated in chronic myeloid leukemia, where bone marrow stroma provides essential HH signals for leukemic stem cells (115).

A relevant aspect concerns the alteration of negative feedback mechanisms. Under physiological conditions, transcriptional induction of Patch1 limits HH signaling through negative feedback. In tumor cells, this circuit is frequently dysfunctional due to activating mutations. This results in amplified and persistent signaling (103).

1.4.3. Hedgehog Pathway-Mediated Chemoresistance: Molecular Mechanisms and Therapeutic Implications

The Hedgehog signaling pathway plays a central role in the induction and maintenance of tumor chemoresistance through multiple interconnected molecular mechanisms. These include the maintenance of cancer stem cells, regulation of drug efflux transporters, modulation of apoptosis, and induction of epithelial-mesenchymal transition. Understanding these mechanisms is fundamental for the development of more effective therapeutic strategies capable of overcoming resistance to conventional treatments.

One of the most relevant mechanisms through which the HH pathway promotes chemoresistance is the maintenance and expansion of cancer stem cells (CSCs). This is a cellular subpopulation characterized by unlimited self-renewal capacity and intrinsic resistance to chemotherapeutic and radiotherapeutic treatments (116). The HH pathway is essential for maintaining the stem cell phenotype through direct regulation of key genes that determine stemness. NANOG is a master transcription factor that controls self-renewal of stem cells. It represents a direct transcriptional target of the HH pathway and is essential for the survival and expansion of CSCs (106). In parallel, HH signaling induces the expression of other stemness regulators, including OCT4, SOX2, and BMI1, in multiple tumor types. This consolidates the stem cell phenotype and therapeutic resistance (106). The functional importance of this mechanism has been demonstrated in glioblastoma. There, inhibition of the HH pathway through cyclopamine determines a significant reduction in the expression of NANOG, OCT4, and SOX2. This completely

abolishes the tumor engraftment capacity of glioblastoma stem cells, highlighting the critical role of this pathway in maintaining the stem cell properties necessary for tumor growth and recurrence (117).

Another fundamental mechanism through which the Hedgehog pathway confers chemoresistance involves the regulation of ABC (ATP-Binding Cassette) transporters. These are ATP-dependent efflux pumps that actively remove cytotoxic drugs from the intracellular environment. This reduces their therapeutic concentration and therefore decreases the efficacy of chemotherapeutic treatment. The HH signaling pathway directly upregulates the expression of ABCB1 (P-glycoprotein/MDR1) and ABCG2 (BCRP, Breast Cancer Resistance Protein). These are two of the main transporters responsible for multidrug resistance in different tumor types (118). In epithelial ovarian carcinoma, treatment with cyclopamine, an inhibitor of the HH pathway, significantly reduces the expression of both transporters. This resensitizes cells to drugs. Similarly, in osteosarcoma, inhibition of the HH pathway determines a reduction in ABCG2 expression. This consequently increases the sensitivity of tumor cells to chemotherapy (119).

Particularly relevant is the observation that non-canonical activation of the Hedgehog pathway, mediated by factors such as osteopontin (OPN), induces multidrug resistance through Gli-dependent upregulation of ABCB1 and ABCG2. This mechanism presents significant therapeutic implications. Cells with non-canonical activation are refractory to Smo inhibition but remain sensitive to GANT61 (a Gli inhibitor). This suggests that targeting Gli transcription factors downstream in the signaling cascade may represent a more effective strategy to overcome this type of resistance (120).

The HH pathway confers resistance to chemotherapy-induced apoptosis through modulation of the balance between pro-apoptotic and anti-apoptotic proteins of the BCL-2 family. In particular, activation of Gli transcription factors promotes the expression of anti-apoptotic proteins such as BCL-2, BCL-XL, and MCL-1. Simultaneously, it downregulates the expression of pro-apoptotic proteins such as BAX and BAD. This shifts the cellular balance toward survival and protects tumor cells from programmed cell death. In colon carcinoma, pharmacological inhibition of the HH pathway determines a reduction in BCL-2 expression accompanied by an increase in BAX. This activates the mitochondrial apoptotic pathway and sensitizes tumor cells to the cytotoxic effects of

chemotherapy. In multiple myeloma, HH signaling produced by the stromal microenvironment exerts a protective role on malignant cells. It inhibits chemotherapy-induced apoptosis through upregulation of BCL-2 and therefore sustains the survival of neoplastic cells in the presence of therapeutic stress (121,122).

The HH pathway also promotes chemoresistance through induction of Epithelial-Mesenchymal Transition (EMT). Hedgehog signaling upregulates the expression of key EMT transcriptional factors, including SNAIL, SLUG, and ZEB1. These orchestrate the transcriptional reprogramming necessary for phenotypic transition (120). In breast carcinoma, treatment with OPN induces characteristic EMT changes in a Gli-dependent manner. This determines a reduction in the expression of epithelial markers such as E-cadherin and keratin 18, accompanied by a simultaneous increase in mesenchymal markers such as N-cadherin, vimentin, and Twist (120).

The clinical relevance of the HH pathway in promoting chemoresistance has stimulated the development of therapeutic strategies aimed at pathway inhibition. Smo inhibitors, particularly Vismodegib and Sonidegib, represent second-generation cyclopamines characterized by optimized pharmacokinetic properties. Vismodegib was approved by the Food and Drug Administration (FDA) for the treatment of locally advanced or metastatic basal cell carcinoma. It demonstrated a clinical response rate of 50% in patients with metastatic disease. This result represented a milestone in the development of targeted therapies against the HH pathway (123). Sonidegib was subsequently approved for the same indication. It has demonstrated efficacy in reducing EMT and invasiveness in several tumor types, including glioblastoma, renal cell carcinoma, and prostate carcinoma (124).

However, the clinical use of these drugs presents significant limitations related to the development of therapeutic resistance. This manifests as either innate resistance or acquired resistance. Acquired mutations in the SMO gene represent the most common mechanism of acquired resistance. Different variants alter the drug binding site without compromising the activating function of the receptor (125). An alternative mechanism of resistance, particularly insidious, involves non-canonical activation of Gli transcription factors through alternative pathways such as STAT3, PI3K/AKT, or RAS/MAPK. These completely bypass the dependence on Smo, rendering tumor cells refractory to Smo inhibitors but maintaining sensitivity to GANT61 (120). Other identified resistance

mechanisms include loss of primary cilia, which are essential for signal transduction (126), genomic amplification of GLI2 or CCND1, and compensatory crosstalk with other oncogenic signaling pathways (125).

To overcome these limitations, direct inhibitors of Gli transcription factors have been developed. These act downstream of Smo and should therefore maintain efficacy even in the presence of resistance to Smo inhibitors. GANT61 represents the main Gli inhibitor. It functions through direct interference with the binding of Gli1 and Gli2 to target DNA sequences. This blocks the transcription of pathway target genes (127). However, despite promising preclinical results, the clinical application of GANT61 is limited by its chemical instability under physiological conditions. It is characterized by rapid spontaneous hydrolysis that generates two metabolites, GANT61-A (inactive) and GANT61-D (active). This makes *in vivo* administration and standardization of therapeutic doses problematic (128). Promising strategies to overcome resistance to HH inhibitors include the development of dual inhibitors that combine targeting of the HH pathway with that of other molecular targets (129), the use of combination therapies that associate HH inhibitors with conventional chemotherapy or radiotherapy, demonstrating synergistic effects in controlling tumor growth (117), and the employment of alternative compounds that directly antagonize Gli factors, or that have inhibitory activity on the HH pathway, or that suppress aberrant HH signaling (130).

Chapter 2. RATIONALE

CRC remains a major global health challenge. Despite better surgical and medical treatments, many patients still cannot overcome chemotherapy resistance. This is still the main barrier to improved patient outcomes. 5-FU has been the standard chemotherapy for CRC for many decades. When 5-FU is combined with other drugs - such as oxaliplatin in FOLFOX or irinotecan in FOLFIRI - response rates improve significantly. However, many patients either fail initial therapy or develop resistance during treatment. Understanding why cancer cells resist 5-FU is critical to developing better strategies. Recent research shows that cancer metabolism plays a central role in both tumor growth and treatment resistance. Among the metabolic pathways, serine metabolism has emerged as particularly important. PHGDH is frequently overexpressed in cancers, including CRC. High PHGDH levels support tumor cell survival under stress. The enzyme fuels the production of nucleotides for DNA synthesis, NADPH for antioxidant defense, and one-carbon units needed for rapid cell division. A major gap exists in the current literature. While PHGDH is known to promote cancer growth, its specific role in driving 5-FU resistance has not been systematically studied. Furthermore, the molecular pathways connecting PHGDH to chemotherapy resistance remain unclear. This knowledge gap limits the development of targeted therapies. Recent evidence suggests that PHGDH may function beyond its classical metabolic role. Some PHGDH protein localizes to the cell nucleus, where it may interact with transcription factors and influence gene expression directly. This dual functionality - both metabolic and non-metabolic - suggests that PHGDH likely coordinates with key oncogenic signaling pathways to drive chemoresistance and promote tumor aggressiveness. The HH signaling pathway is a strong candidate for such crosstalk. The HH pathway is a well-established driver of cancer stem cell maintenance, drug resistance, and aggressive tumor behavior. It operates through the transcriptional effectors GLI1 and GLI2, which activate genes that promote stemness, stop apoptosis, and enhance drug efflux. Multiple studies show that HH pathway activation correlates with poor response to chemotherapy in many cancer types. However, no prior work has investigated whether PHGDH and HH signaling are functionally connected or whether they cooperate to drive 5-FU resistance in CRC. This possible PHGDH–Hedgehog axis represents a novel therapeutic opportunity, as simultaneous targeting of both metabolic and signaling components might overcome resistance more effectively than targeting either pathway alone.

This study aims to investigate the link between PHGDH, HH pathway and 5-FU resistance. To this end, CRC cell lines, patient-derived organoids, clinical tissue samples, and animal models were used to determine whether PHGDH predicts chemotherapy response, to elucidate the underlying molecular mechanisms, to explore its interaction with HH signaling, and to test whether combined targeting of PHGDH and HH can restore drug sensitivity. Identifying PHGDH as a predictive biomarker and validating combination therapy with HH inhibitors and 5-FU could improve outcomes for chemoresistant CRC patients and provide a framework for precision medicine approaches.

Chapter 3. MATERIAL AND METHODS

3.1. Cell lines and treatments

Human colorectal carcinoma cell lines HCT8, RKO, LS174T, and HCT116 were procured from ATCC. Tumor cells were cultured in high glucose Dulbecco's modified Eagle's medium (DMEM) (Euroclone) supplemented with 10% fetal bovine serum (Euroclone), 1% penicillin and streptomycin (Euroclone), and 1% L-glutamine (Euroclone) in cell culture flasks until reaching 70-80% cell confluence. Cells were maintained in a humidified atmosphere containing 5% CO2 at 37°C. All cell lines underwent Mycoplasma testing using the Mycoalert detection kit (Lonza). HCT116 cells resistant to 5-FU (HCT116R) were generated by exposing HCT116 parental cells to progressively increasing concentrations of 5-FU over six months until achieving the final concentration of 20 μM, as previously described (43). HCT116R cells were continuously cultured in the presence of 20 μM 5-FU to maintain 5-FU resistance. 5-FU (#F6627) and GANT61 (#G9048) were obtained from Merck Sigma. JC19 was synthesized as previously described (131).

3.2. Cell transfection and transduction

HCT8 and LS174T cells were transfected with PHGDH human shRNA plasmid (Origene) or scrambled shRNA (Origene) using Lipofectamine 3000 (Thermo Fisher Scientific) following the manufacturer's protocol. After 24 h incubation, transfected cells were exposed to 2 μM puromycin for one month to select stable shPHGDH-expressing clones. RKO cells underwent transfection with plasmid pLHCX expressing the PHGDH cDNA - provided by Sarah-Maria Fendt, VIB KU Leuven, Belgium - or negative control. Subsequently, after 24 h, transfected cells were treated with 400 μg/mL hygromycin for 1 month until selection of stable PHGDH overexpressing cells.

Lentiviral particles for GLI1 silencing were generated in HEK-293T cells as previously described (131). The shRNA vectors utilized were pLKO.1-puro (Lv-C) and pLKO.1 puro-shGLI1 (Lv-shGLI1). HCT8 cells were seeded in 6-well plates and transduced with Lv-C or Lv-shGLI1 lentiviruses diluted 1:4 in culture medium in the presence of 8 μg/mL polybrene (Merck Sigma). Following 24 h, the culture medium containing viral particles was replaced with complete medium, and 72 h post-transduction, 3.5 μM puromycin was

added to select transduced cells. After 5 days of selection, GLI1 protein levels were evaluated.

3.3. Western blot analysis

Cells were lysed in RIPA buffer (Thermo Fisher Scientific) supplemented with Protease Inhibitor and Phosphatase inhibitor (Merck Sigma). Protein lysates were centrifuged at 14,000 rpm at 4°C for 10 min, and protein concentrations were quantified using Bicinchoninic Acid (BCA) assay (Euroclone). Subsequently, 20 μg of total proteins were loaded onto SDS-PAGE gels (BioRad) and transferred to PVDF membranes (BioRad). Membranes were blocked for 1 h at room temperature in 5% non-fat dry milk (Santa Cruz Biotechnology) in PBS-Tween 0.1% and then incubated overnight with primary antibodies against PHGDH (Thermo Fisher Scientific, #PA5-54,360), GLI1 (Cell Signaling Technology, #2643), c-Myc (Cell Signaling Technology, #5605), phospho-ERK1/2 (Cell Signaling Technology, #9101), ERK1/2 (Cell Signaling Technology, #4348), phospho-AKT (Cell Signaling Technology, #9271), AKT (Cell Signaling Technology, #9272), phospho-P38 (Cell Signaling Technology #4511), P38 (Abcam, ab59461), phospho-H2AX (Cell Signaling Technology, #2577), H3 (Cell Signaling Technology, #9715), H2AX (Cell Signaling Technology, #2595), HSP90 (Santa Cruz Biotechnology, sc-69703), Vinculin (Merck, #V9131), and β-Actin (Santa Cruz Biotechnology, sc-47778). Following 1 h incubation at room temperature with anti-rabbit horseradish peroxidase-conjugated (Santa Cruz Biotechnology, #2357) or anti-mouse horseradish peroxidase-conjugated (Santa Cruz Biotechnology, #516102) secondary antibodies, membranes were visualized using Clarity Western ECL Substrate (BioRad) and images were acquired using Amersham Imager 600 (Amersham). Vinculin, HSP90 or β-Actin served as loading controls. All western blot images represent at least three independent experiments.

3.4. Cytosolic and nuclear fraction isolation

Cells were seeded in P100 plates and allowed to adhere. Upon reaching sub-confluence, cells were detached with trypsin and centrifuged at 1000 g for 5 min. Cell pellets were resuspended in hypotonic solution (10 mM Hepes pH 8, 10 mM KCl, 1.5 mM MgCl, 1 mM DTT, 0.1 mM EDTA) containing 0.2% NP-40, phosphatase and protease inhibitors. The resuspended cell pellet was homogenized using a glass pestle for 15 min on ice. The solution was centrifuged to pellet nuclei at 16,000 g for 10 min at 4°C. The supernatant

(cytosolic fraction) was collected, while the pellet was lysed with RIPA buffer. Protein content of both fractions was determined using the BCA method. Cytosolic and nuclear purity was confirmed by western blot analysis with antibodies against β-Actin or histone H3, respectively.

3.5. Immunoprecipitation

Colon cancer cells ($2x10^6$) were lysed with RIPA buffer, and 500 μg of nuclear fraction proteins were incubated with specific antibodies at 4°C overnight with gentle agitation. Subsequently, A/G protein (Thermo Fisher Scientific) was added to the antibody-lysate complex and incubated for 1 h at 4°C with gentle shaking. The complexes were washed with PBS 1X to remove impurities and centrifuged at 14,000 rpm for 10 min at 4°C. Immunoprecipitated proteins were then resuspended in Laemmli buffer without reduction agent and separated by SDS-PAGE.

3.6. RNA isolation and Quantitative Real-Time Polymerase Chain Reaction (qPCR)

Total RNA was extracted from cells or tissue using the RNeasy Plus Mini Kit (Qiagen #74134) according to the manufacturer's instructions. RNA quantity and purity were determined using a NanoDrop Microvolume Spectrophotometer and Fluorometer (Thermo Fisher Scientific). cDNA was synthesized by incubating 1 μg of total RNA with High-Capacity cDNA Reverse Transcription Kit (Applied Biosystems) according to the manufacturer's instructions. qPCR was performed using Luna Universal qPCR Master Mix (New England Biolabs). The qPCR analysis was conducted in triplicate using CFX96 Real-Time PCR System (BioRad). Data were reported as relative quantity with respect to the reference sample using the $2^{-\Delta\Delta Ct}$ method. β2-microglobulin served as the reference gene.

Specific primers were provided by Thermo Fisher Scientific, see *Table 2*.

Gene	Sequence
PHGDH-FW PHGDH-REV	AGGCTCGCATCAGTGTCC ATCTCTCACGGGGGTTGTG
EpCAM-FW EpCAM-REV	TGTGGTGATAGCAGTTGTTGC CTATGCATCTCACCCATCTCC
LGR5-FW LGR5-REV	CTTCCAACCTCAGCGTCTTC TTTCCCGCAAGACGTAACTC
CD133-FW CD133-REV	GCTTCAGGAGTTTCATGTTGG GGGGAATGCCTACATCTGG
VEGFA-FW VEGFA-REV	CACTGAGGAGTCCAACATCAC AGGAAGCTCATCTCTCCTATGT
ALDH1-FW ALDH1-REV	GCACGCCAGACTTACCTGTC CCACTCACTGAATCATGCCA
ABCB1-FW ABCB1-REV	AGTGAAAAGGTTGTCCAAG AGTCTGCATTCTGGATGG
CMYC-FW CMYC-REV	CGGAACTCTTGTGCGTAAGG ACTCAGCCAAGGTTGTGAGG
ECAD-FW ECAD-REV	AGGCCAAGCAGCAGTACATT ATTCACATCCAGCACATCCA
KLF4-FW KLF4-REV	AGACAGTCTGTTATGCACTGTGG TGTTCTGCTTAAGGCATACTTGG
NCAD-FW NCAD-REV	CCTCCAGAGTTTACTGCCATGAC GTAGGATCTCCGCCACTGATTC
BCL2-FW BCL2-REV	ATCGCCCTGTGGATGACTGAGT GCCAGGAGAAATCAAACAGAGGC
GLI1-FW GLI1-REV	CCCAGTACATGCTGGTGGTT GCTTTACTGCAGCCCTCGT
GLI2-FW GLI2-REV	CTCAGCCCCGCTGATGTGGC TCAGCAGGTCCCCGTAGGGC
PATCH1-FW PATCH1-REV	GGCAGCGGTAGTAGTGGTGTTC TGTAGCGGGTATTGTCGTGTGTG
B2M-FW B2M-REV	AGTATGCCTGCCGTGTGAAC GCGGCATCTTCAAACCTCCA

***Table 2**: Forward and reverse primers used for the analyzed genes.*

3.7. Viability assay

$3x10^4$ cells/well were seeded in 24-well plates and allowed to adhere for 24 h. Triplicate wells were prepared for each experimental condition. Culture medium was replaced with experimental media. At each endpoint, cells were detached with trypsin (Euroclone), resuspended in DMEM and counted.

3.8. Colony formation assay

Following 48 h of 5 μM 5-FU treatment, $1x10^3$ cells were seeded into six-well plates and cultured for 10 days in complete medium. Subsequently, cells were fixed and stained with Crystal Violet solution. Colonies were photographed. The total colony area was calculated using the Colony Area plugin of ImageJ imaging system as follows

$$\text{Colony area } \% = \frac{\text{\# of pixels in the region with an intensity above zero}}{\text{Total \# of pixels in the same region}} x100.$$

3.9. Invasion assay

Invasion was assessed using a Boyden chamber equipped with 8 μm pore filters (Greiner Bio-One) coated with 50 $\mu g/cm^2$ Matrigel (Corning). $8x10^4$ cells were detached and resuspended in starvation medium in the upper chamber. Complete medium containing 10% FBS was added to the lower chamber as chemoattractant. After 16 h, invaded cells were fixed and stained with Crystal Violet. Invasion values were expressed as the average number of invading cells per microscopic field across five fields.

3.10. Colonsphere formation

Cells were cultured under anchorage-independent conditions in poly 2-hydroxyethyl methacrylate (poly-HEMA) coated dishes (Merck Sigma) with selective serum-free DMEM/F12 medium supplemented with 50x B27 (Gibco), 20 ng/mL bFGF (Bio-Techne), and 20 ng/mL EGF (Relia Tech). Briefly, CRC cells were treated with 5-FU for 48 h, then 700 cells/well were seeded in 96-well plates pre-coated with poly-HEMA under anchorage-independent conditions. After 7-10 days, photographs were taken to determine sphere number. Data represents the average number of formed spheres/fields across at least 5 randomly chosen fields. Total colonsphere volume was calculated after measuring length (L) and height (H) using ImageJ with the following formula: $V = (L^2*H)/2$, as previously reported (132). Data represent the average sphere volume/field across at least 5 fields. For self-renewal evaluation (P2 generation), individual colonspheres were dissociated with Trypsin EDTA and diluted to one cell per well in 96-well poly-HEMA pre-coated plates. After 7-10 days, photographs were taken to determine sphere formation. The percentage of spheroids was calculated as the number of spheres formed/number of seeded wells.

3.11. Flow cytometric analysis

Colonspheres, enzymatically dissociated into single cell suspension, were resuspended in 100 µL PBS 1X and stained with fluorochrome-conjugated antibodies: anti-CD133 1:100 (BD Pharmigen, #566596), anti-CD24 1:10 (BD Pharmigen, #560991), anti-CD44 1:50 (BD Pharmigen, #560977), and anti-EpCAM 1:100 (Invitrogen, #17579182) for 30 min at 4°C in darkness. Cells were subsequently washed with PBS and analyzed using a BD-FACS Canto II flow cytometer. Gating strategies included initial selection of viable cells based on forward scatter (FSC) and side scatter (SSC) parameters, followed by singlet discrimination (FSC-H versus FSC-A). Unstained controls were used to establish background auto-fluorescence and determine gating thresholds for each marker. Mean fluorescence intensity (MFI) was recorded, quantified, and normalized to the experimental control (shCTRL or CTRL). Acquired data were processed using BD FACSDiva Software (BD Biosciences).

3.12. Human tissues and organoid generation

Human tissues were obtained from patients undergoing surgery at the Azienda Ospedaliero Universitaria Careggi, Florence, Italy. Written informed consent was obtained from all patients. The study was conducted in accordance with the Helsinki Declaration and approved by the ethics committee (RC_AUT_DG_24030_BIO). Tissues were transported to the laboratory on ice and further processed for molecular analysis and organoid generation as previously described (133–135) Briefly, for patient-derived cancer organoid (PDCO) generation, biopsies were washed in PBS 1x with Penicillin/Streptomycin 1% (Euroclone) and 100 µg/ml Primocin (InvivoGen). Tissue was minced into small pieces of 1-2 mm^3 and digested in 5 mL Advanced DMEM F/12 (Gibco) containing 5 mg/mL Collagenase type IV (Merck Sigma), 10 µL Deoxyribonuclease I from bovine pancreas (2000 Kunitz units/mg, Sigma Aldrich), and 2 µM Y27632 dihydrochloride (Tocris) for 1 h at 37°C with pipetting every 10 min. The digested tissue was filtered through a 100 µm cell strainer and DMEM supplemented with 10% fetal bovine serum was added to stop digestion. The digestion mixture was centrifuged for 5 min at 300 RCF. The tube was placed on ice, the pellet was resuspended in Matrigel (Corning) and seeded as droplets in pre-warmed 12-well plates. After 20 min, growth factor-supplemented medium was added. Medium was changed every 2 days. Advanced DMEM F/12 was supplemented with 10 mM HEPES (Euroclone), 2 mM GlutaMax (Gibco), Primocin (InvivoGen), 1x B-27 supplement (Gibco), 10 mM

Nicotinamide (Sigma Aldrich), 1.25 mM N-acetyl-l-cysteine (Cayman), 500 nM A83-01 (Cayman), 50 ng/mL EGF (ReliaTech), 100 ng/mL Recombinant human Noggin (PrepoTech), 500 ng/mL hRSPO1-FC (ImmunoPrecise Antibodies), 10 µM Y27632 dihydrochloride (Tocris), 10 nM Prostaglandin E2 (Selleckchem), 25 ng/mL SB202190 (AdipoGen), and 10 mM Gastrin I human (Sigma Aldrich) (136,137).

3.13. Organoid viability assay

PDCOs were dissociated with Trypsin-EDTA 0.25% (Gibco) and seeded in 96-well plates at a density of $5x10^3$ cells in 7 µL Matrigel droplets. Prior to treatment, cells were allowed to recover and form organoids for 2-3 days. PDCOs were treated with 5-FU, JC19, or in combination, and cell viability was assessed after 7 days using CellTiter-Glo 3D reagent (Promega, #G9682). Luminescence was measured. All experiments were performed twice in triplicate.

3.14. Formalin-fixed paraffin embedded (FFPE) organoids

Following PDCOs generation and growth, medium was removed from wells and 150 µL of 2 mg/mL Dispase II (Merck Sigma) was added to each well. After 1 h incubation at 37°C, 1 mL of PBS 1x was added. Droplets were collected into 15 mL Falcon tubes, filled with PBS 1x, and centrifuged at 300 RCF at room temperature for 5 min. The supernatant was discarded and pellets were stored at 4°C in 1 mL of 4% formalin. Fixed PDCOs were resuspended in 80 µL of pre-warmed HistoGel (Epredia) and placed as single droplets on parafilm. After solidification (1 h), HistoGel droplets were transferred to tissue cassettes for paraffin embedding.

3.15. Immunohistochemistry (IHC) analysis

Human- or mouse-derived tumors were fixed in 4% formalin and subsequently embedded in paraffin wax. 7 µm tissue sections of paraffin-embedded PDCOs, human- or mouse-derived tumors were prepared for histology and IHC analysis. Hematoxylin & Eosin (H&E, #3801698, Leica Biosystems) staining was performed on individual specimens. Human-derived tumor (#CRC) and PDCOs sections were immunostained using antibody specific to PHGDH (1:1000, #PA5-54360 Invitrogen, Waltham, Massachusetts), while mouse-derived tumor sections were stained with Ki67 (#GA626, Dako Omnis) antibody. IHC was performed using the Leica BOND-MAX automated staining system. Staining was developed with 3,3'-diaminobenzidine (DAB) and counterstained with Hematoxylin

(#DS9800, Leica Biosystems). Digital images were acquired with an Aperio LV1 slide scanner and analyzed using ImageScope software.

Archive formalin-fixed paraffin-embedded (FFPE) 3 μm tissue sections from the Section of Pathological Anatomy, University of Florence, were prepared for immunohistochemical analysis. Sample processing was performed using an automated immunostainer (Ventana Discovery ULTRA, Ventana Medical Systems, Tucson, AZ). Sections were deparaffinized in EZ prep (#950-102; Ventana Medical Systems, Tucson, AZ), and antigen retrieval was achieved by incubation with cell-conditioning solution 1 (CC1) (#950-124; Ventana Medical Systems, Tucson, AZ). Sections were then incubated with antibody against PHGDH (#PA5-54360, 1:500 Rabbit polyclonal; Invitrogen, Waltham, Massachusetts). Signal was developed with Ultra Map diaminobenzidine anti-mouse or anti-rabbit HRP detection kit (Ventana Medical Systems, Tucson, AZ). PHGDH expression score was classified into 4 categories: 0 (no staining), 1+ (weak staining), 2+ (moderate staining), 3+ (strong staining). The product of staining intensity score and percentage of positive tumor cells (0% to 100%) was considered the final PHGDH expression score, ranging from 0 (no staining) to 300 (100% of cells with 3+ staining intensity) (46). Quantification was conducted by analyzing three representative fields for each CRC sample, with expression levels reported as Cytoplasm H-score mean values. H-scores were stratified into low and high-expression groups based on the overall mean value across all analyzed CRC samples.

3.16. *In vivo* experiment

Animal experiments were performed in accordance with national guidelines and approved by the ethical committee of the Animal Welfare Office of Italian Health Ministry. All procedures conformed to legal mandates and Italian guidelines for laboratory animals. All animals received humane care and study protocols complied with institutional guidelines. Studies involving animal experiments conform to the Animal Research: Reporting of In Vivo Experiments (ARRIVE) guidelines (http://www.nc3rs.org.uk/arriveguidelines), developed by the National Centre for the Replacement, Refinement and Reduction of Animals in Research (NC3Rs) to improve standards and reporting of animal research. Female Fox1 nu/nu mice (Charles River Laboratories International) were injected subcutaneously into both flanks with $8x10^6$ HCT8 cells in 100 μL PBS. Once tumors became palpable, mice were randomized and treated for two weeks with vehicle (PBS, 5% ethanol/PBS, 10% DMSO), 5-FU (25 mg/kg in PBS, 5% ethanol) using a cyclic

regimen consisting of three daily injections followed by two recovery days, JC19 (15 mg/kg in PBS, 10% DMSO) twice daily, or combination treatment. All treatments were administered by intraperitoneal injection (IP). Treatment doses were adjusted according to mouse weight with a maximum injection volume of 100 µL. Animals (6 per group) were monitored daily. Tumors were measured using calipers, and average tumor volume was calculated using the formula: volume = length × width^2/2. Humane endpoints were determined according to parameters indicated in the project authorized by the Italian ethical committee of Animal Welfare Office of Italian Health Ministry (authorization number: n° 981/2024-PR), specifically the maximal tumor volume permitted by our ethics committee was 1200 mm^3. Tumor volume did not exceed this limit at any point during the study.

3.17. Ultrasound and photoacoustic imaging

At the endpoint of the *in vivo* experiment, tumor volumes were determined using high-frequency ultrasound (HF-US) imaging with Vevo F2 LAZR-X system (Fujifilm Visualsonics) performing 3D acquisition in B-Mode on live mice. During acquisitions, mice were anesthetized with continuous isoflurane flow (initial induction at 4% and maintenance at 2%) and positioned on a mouse handling table heated to 37°C in prone position. Respiration rate, body temperature, and electrocardiogram (ECG) were monitored during analysis. A 55-MHz transducer was used for echography. Obtained data were analyzed using Vevo LAB software (Fujifilm Visualsonics) to measure tumor volumes.

3.18. Library preparation and RNA-sequencing

Total RNA was isolated from cells using the RNeasy Plus Mini Kit (QIAGEN) according to the manufacturer's protocol. Universal Plus mRNA-Seq kit (Tecan Genomics, Redwood City, CA) was used for library preparation following manufacturer's instructions (library type: fr-secondstrand). RNA samples were quantified and quality-tested using Agilent 2100 Bioanalyzer RNA assay (Agilent technologies, Santa Clara, CA). Final libraries were verified using both Qubit 2.0 Fluorometer (Invitrogen, Carlsbad, CA) and Agilent Bioanalyzer DNA assay. Libraries were then prepared for sequencing and sequenced in paired-end 150 bp mode on NovaSeq 6000 (Illumina, San Diego, CA).

3.19. Computational analyses

FastQC was employed to perform comprehensive quality assessment on all fastq files, ensuring that sequencing data met predefined quality standards prior to downstream analyses. Transcript abundance was estimated using Salmon (138), a widely-used tool for accurate and bias-aware RNA-seq quantification. The latest version of the human reference transcriptome (hg38) was used for this purpose. Following transcript quantification, raw counts were imported into the R environment using the tximport package (139). Differential expression analysis was then performed using the DESeq2 package (140) in R. Results from Wald test were utilized to rank differentially expressed genes (DEGs). To further explore biological themes associated with identified DEGs, gene set enrichment analysis (GSEA) was conducted using the most recent version of the fGSEA R packages and the most updated HALLMARK msig gene sets (141). Following recommendations of GSEA software authors, all results with False Discovery Rate (FDR) < 0.25 were considered statistically significant.

RNA-seq and clinical data from colorectal adenocarcinoma patients were obtained from The Cancer Genome Atlas (TCGA) database, specifically from TCGA-COAD (colon adenocarcinoma) and TCGA-READ (rectal adenocarcinoma) projects. Only patients with documented 5-FU-based chemotherapy treatment were included in the analysis. Patients were stratified into responders (R) and non-responders (NR) based on clinical outcomes following treatment. Expression data in the TCGA database had been previously calculated using STAR alignment and quantified with featureCounts. Expression profiles were imported into R, and raw counts were processed following standard DESeq2 procedures for normalization and differential expression analysis. Gene Set Enrichment Analysis was subsequently performed using the fGSEA package with HALLMARK gene sets from MSigDB to identify significantly enriched pathways between R and NR groups.

Analysis of correlation between PHGDH mRNA expression and overall survival (OS) and Relapse Free Survival (RFS) in CRC patients was performed using the open-access database Kaplan-Meier plotter (http://www.kmplot.com). Expression of PHGDH in normal, primary tumors, and metastases was obtained from The Cancer Genome Atlas dataset on TNM plot database (http://www.tnmplot.com). Classification into low and high PHGDH was performed using the "Auto select best cutoff" option, where lower and upper quartiles define the range for all possible cutoff values. The threshold yielding optimal performance within this range was selected as the cutoff.

3.20. Statistical analysis

Statistical analysis of data was performed using unpaired Student t-test or One-way ANOVA for pairwise comparison of groups with GraphPad Prism version 8.0 (GraphPad Software). All data were expressed as mean ± SEM. A p value ≤ 0.05 was considered statistically significant. All statistical analyses were carried out on three biological replicates. Levene's test for equality of variance was performed to assess heterogeneity in PHGDH expression between tumors and healthy patient cohorts. The significance level was set at 5%. Bliss independence analysis was used to evaluate drug combination effects. Bliss score: = 0, no functional interaction; > 0, synergism; < 0, antagonism.

Chapter 4. RESULTS

4.1. Expression Analysis of PHGDH in Colorectal Cancer Tissue and Patient-Derived Organoids

To investigate the clinical relevance of PHGDH in colorectal cancer, expression patterns were initially examined in patient-derived cancer organoids (PDCOs) established from freshly isolated surgical CRC samples. Immunohistochemical (*Figure 5A*) and Western blot analyses (*Figure 5B*) revealed marked inter-patient variability in PHGDH protein levels, allowed us to stratify PDCOs into distinct "high PHGDH" and "low PHGDH" categories (*Figure 5C*).

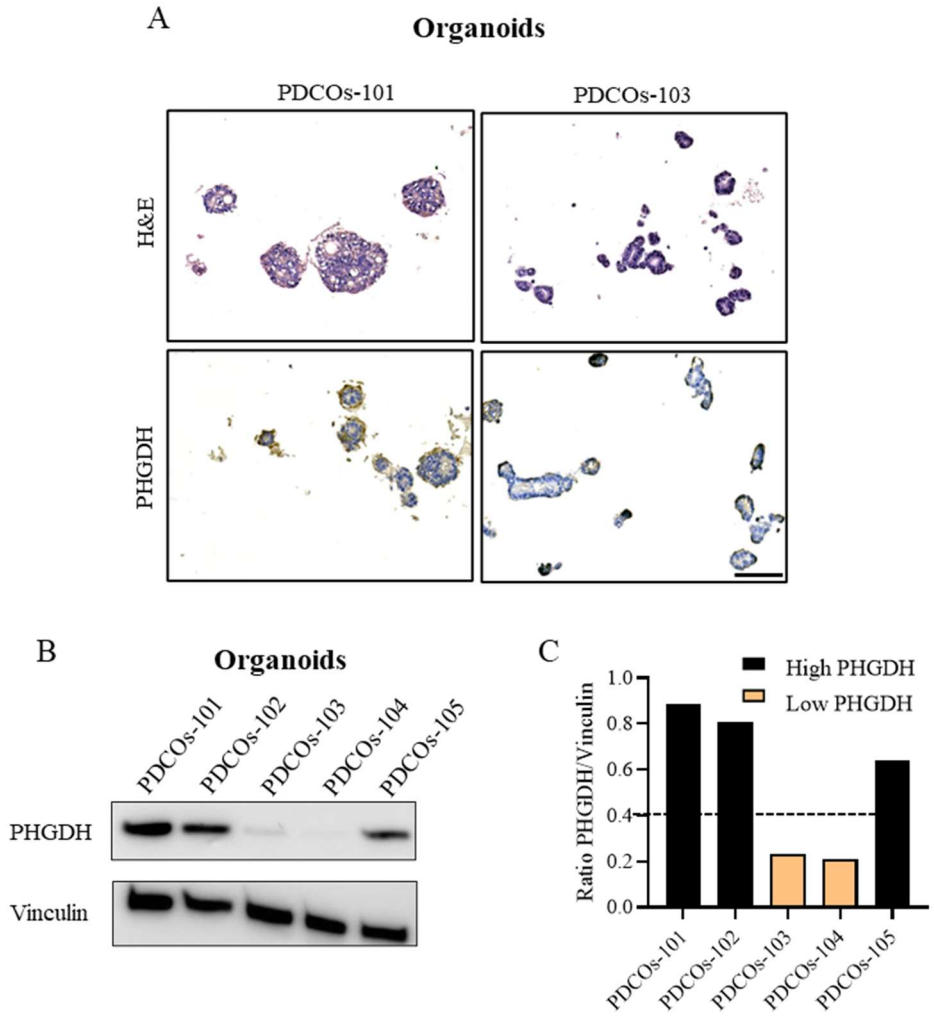

***Figure 5**: PHGDH expression is heterogeneous in CRC. **A)** Representative H&E and PHGDH staining of PDCOs by IHC detection (left, high PHGDH; right, low PHGDH) (magnification 20x, scale bar: 100 µm). **B-C)** PHGDH protein expression levels in PDCOs (western blot and relative bargraph, showing quantification of PHGDH protein levels). Vinculin was used as loading control. The organoids were divided into high and low PHGDH. Western blot image is representative of at least three independent experiments.*

This heterogeneity was further confirmed through comparative analysis of matched tumors and adjacent healthy tissues obtained from surgical explants (*Table 3*).

Patient n°	Histological diagnosis	Grade	pTMN stage	Relapse (YES=1; NO=0)
#1	Intestinal mucinous adenocarcinoma	G1	pT3N1a	0
#3	Invasive intestinal adenocarcinoma NOS, moderately differentiated	G1	N/A	0
#4	Adenocarcinoma NOS with colloid features	G1	pT3N1c	0
#5	Invasive intestinal adenocarcinoma NOS	G1	pT2N1b	1
#6	Invasive intestinal adenocarcinoma NOS	G1	pT3N1b	N/A
#7	Invasive intestinal adenocarcinoma NOS	G1	pT3N0	N/A
#8	Invasive intestinal adenocarcinoma NOS with micropapillary (20%) and colloid (20%) features	G2	pT3N2b	0
#9	Adenocarcinoma NOS, well differentiated	G1	pT3N1b	1
#10	Adenocarcinoma NOS	G2	pT3N0	0
#11	Intestinal adenocarcinoma NOS	G2	pT3N1b	N/A
#12	Adenocarcinoma NOS with mucinous features (25%)	G2	pT3N0	0
#13	Adenocarcinoma	N/A	N/A	0
#14	Adenocarcinoma NOS	G1	pT2N0	N/A
#15	Adenocarcinoma NOS	G1	pT3N0	N/A
#16	Intestinal adenocarcinoma with colloid features, poorly differentiated	G3	pT4N1aM1	1
#17	Adenocarcinoma NOS	G1	pT3N0	0
#18	Adenocarcinoma	N/A	N/A	0
#19	Adenocarcinoma	N/A	N/A	N/A
#20	Intestinal adenocarcinoma NOS	G2-G3	pT3N0	N/A
#21	Adenocarcinoma intestinale invasivo, NOS	G1	pT2N0	N/A
#22	Adenocarcinoma NOS	G3	pT3N1b	1
#23	Adenocarcinoma NOS with colloid features (40%)	G1	pT2N1a	0
#24	Adenocarcinoma NOS	G1	pT1N0	N/A
#25	Intestinal adenocarcinoma NOS	G2	pT2N0	N/A
#26	Adenocarcinoma NOS	G3	pT4aN1b	0
#27	Adenocarcinoma	N/A	N/A	N/A
#33	Adenocarcinoma NOS	G1	pT3N0	1

Table 3*: Clinicopathological characteristics of CRC patients.*

While PHGDH expression demonstrated considerable heterogeneity across tumor specimens, the corresponding healthy tissues exhibited more homogeneous expression levels (*Figure 6A* and *Figure 6B*). Hematoxylin and eosin staining combined with immunohistochemical detection of PHGDH (*Figure 6C*) confirmed this differential expression pattern. The quantification of PHGDH, as measured by H-score, revealed significant variability between different tumors, allowing to categorize patients into "low" and "high PHGDH" expression groups (*Figure 6D*).

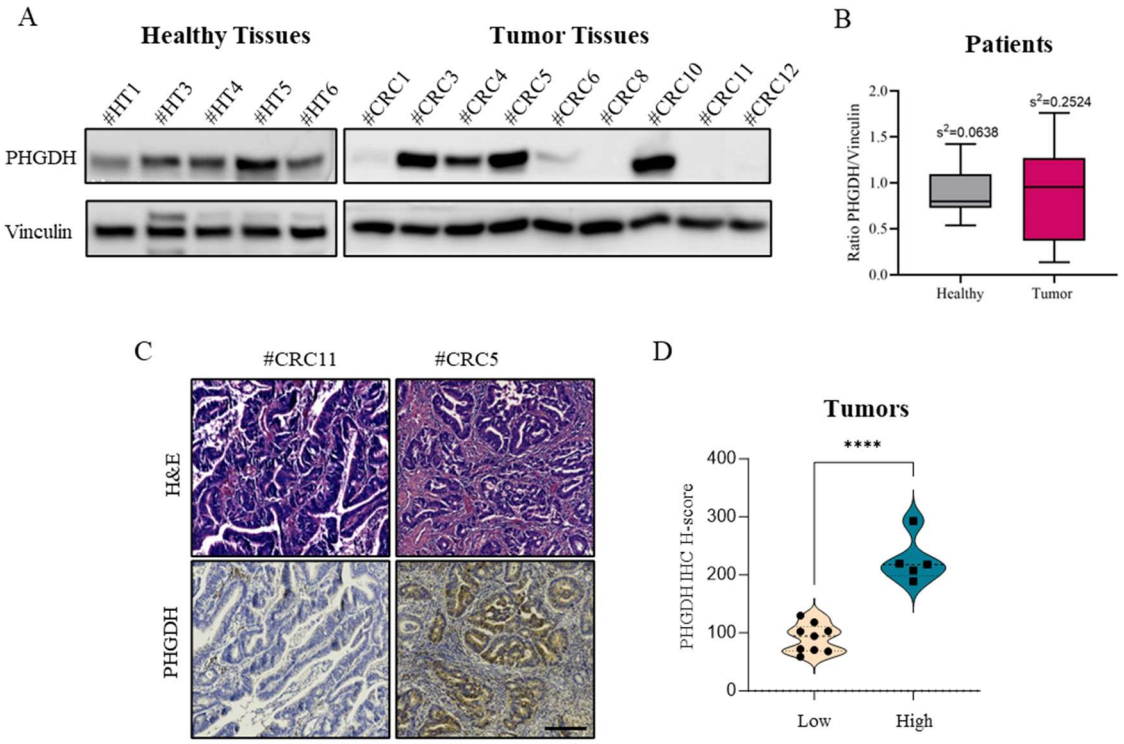

***Figure 6**: **A)** PHGDH protein expression levels in healthy and tumor tissues from CRC patients' specimens. Western blot of representative samples within the cohort. Vinculin was used as loading control. **B)** Box and Whisker plot comparing the expression distribution of PHGDH in healthy (n = 19) and tumor (n = 24) CRC tissues. Values of variance of the two groups are reported at the top of each box (healthy, s2 = 0.0638; tumor, s2 = 0.2524). Levene's test for equality of variance resulted in a f-ratio value of 14.86044 and a p-value of 0.0004, indicating that the variances of the two populations are significantly different from each other. **C)** Representative images of H&E and low (left) and high (right) PHGDH IHC staining on human-derived tumors (magnification 10x, scale bar: 200 µm), along with the corresponding quantification (PHGDH H-score) across 14 different tumor samples **(D)**. Tumors are categorized into low and high PHGDH expression groups based on H-score values. t-test **** $p < 0.0001$.*

These observations led to the hypothesis that inter-patient variability in baseline PHGDH protein expression and its potential modulation during 5-FU treatment, may contribute to differential therapeutic efficacy and impact disease progression and clinical outcomes. Notably, while long-term follow-up remain limited for this recently established patient cohort, preliminary analysis revealed that all four patients who developed disease

recurrence (*Table 3*) demonstrated elevated PHGDH levels compared to representative non-relapsing patients (*Figure 7*). This observation suggested a potential association between increased PHGDH expression and adverse prognosis, prompting further investigation using larger CRC patient-derived tissue repositories.

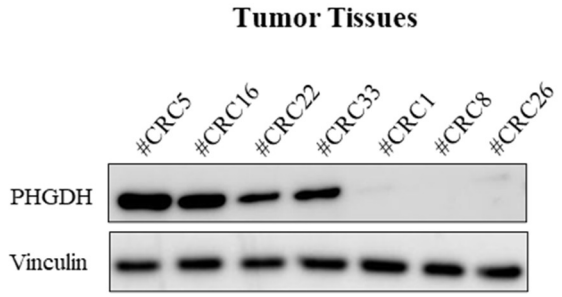

***Figure** 7: PHGDH expression level correlates with CRC patient relapses. PHGDH protein expression in representative CRC human tissues of relapsing patients (#CRC5, #CRC16, #CRC22, #CRC33) and non-relapsing patients (#CRC1, #CRC8, #CRC26).*

4.2. Functional Role of PHGDH in Mediating 5-FU Chemoresistance in CRC patients

To establish the clinical relevance of PHGDH expression in determining patient outcomes, a retrospective analysis was conducted on 50 tumors collected during the previous 10 years from patients with advanced CRC who received post-surgery 5-FU-based therapy (*Table 4*). This investigation aimed to determine whether PHGDH expression levels correlate with chemotherapeutic response. Patients were categorized as responders (R) or non-responders (NR) based on clinical outcomes over a minimum five-year follow-up period. PHGDH immunohistochemical quantification was performed using an H-score methodology, calculated as the product of staining intensity (scored as 0, 1+, 2+, or 3+) and the percentage of positive tumor cells (ranging from 0% to 100%). Interestingly, specimens with higher PHGDH expression were significantly more prevalent in the NR group compared to the R cohort, indicating a positive association between PHGDH levels and 5-FU resistance (*Figure 8*).

Patient	Age at surgery	Sex	Tumor location	Surgery	Histological diagnosis	Grade of differentiation	pTNM stage	PHGDH score	Adjuvant therapy	Response/Non-response
A1	78	F	Sigmoid colon	Anterior rectal resection	Adenocarcinoma NOS	G2	T3N0Mx	160	5-Fluorouracil	R
A2	73	F	Sigmoid colon	Anterior rectal resection	Adenocarcinoma NOS	G2	T3N0Mx	0	5-Fluorouracil	NR
A3	64	F	Transverse colon	Transversal resection	Adenocarcinoma NOS	G2	T3N2bM1a	80	5-Fluorouracil	R
A4	64	M	Rectum	Anterior rectal resection	Adenocarcinoma NOS	G2	T3N2M1a	0	5-Fluorouracil	NR
A5	61	M	Right flexure	Right hemicolectomy	Adenocarcinoma NOS	G2	T2N1aMx	5	5-Fluorouracil	R
A6	68	M	Sigmoid colon	Anterior rectal resection	Adenocarcinoma NOS	G2	T3N1b M1a	160	5-Fluorouracil	NR
A7	61	F	Sigmoid colon	Anterior rectal resection	Adenocarcinoma with colloid features	G2	T3N2aMx	10	5-Fluorouracil	NR
A8	62	F	Rectum	Anterior rectal resection	Adenocarcinoma NOS	G2	T3N2aM1a	0	5-Fluorouracil	NR
A9	61	F	Recto-sigmoid junction	Anterior rectal resection	Adenocarcinoma NOS	G1	T3N1aMx	160	5-Fluorouracil	NR
A10	72	F	Recto-sigmoid junction	Anterior rectal resection	Adenocarcinoma with colloid features	G2	T3N1cMx	10	5-Fluorouracil	R
A11	71	M	Recto-sigmoid junction	Anterior rectal resection	Adenocarcinoma NOS	G2	T2N1aMx	0	5-Fluorouracil	R
A12	74	M	Cecum	Right hemicolectomy	Adenocarcinoma NOS	G2	T3N1aMx	30	5-Fluorouracil	R
A13	75	M	Signoid Colon	Anterior rectal resection	Adenocarcinoma NOS	G2	T2N1aM1a	0	5-Fluorouracil	NR
A14	70	F	Rectum	Anterior rectal resection	Adenocarcinoma NOS	G2	T2N1bMx	N/A	5-Fluorouracil	R
A15	64	M	Rectum	Anterior rectal resection	Adenocarcinoma NOS	G2	T3N0M1a	70	5-Fluorouracil	R
A16	43	F	Rectum	Anterior rectal resection	Adenocarcinoma NOS	G2	T3N1bMx	60	5-Fluorouracil	R
A17	63	M	Recto-sigmoid junction	Anterior rectal resection	Adenocarcinoma NOS	G2	T3N1cMx	15	5-Fluorouracil	R
A18	46	F	Recto-sigmoid junction	Anterior rectal resection	Adenocarcinoma NOS	G2	T3N1cMx	120	5-Fluorouracil	R
A19	75	M	Ascending colon	Right hemicolectomy	Adenocarcinoma NOS	G2	T3N1aMx	0	5-Fluorouracil	R
A20	70	M	Descending colon	Left hemicolectomy	Adenocarcinoma NOS	G2	T2N1aM1a	10	5-Fluorouracil	NR
A21	68	M	Descending colon	Left hemicolectomy	Adenocarcinoma NOS	G2	T3N2aMx	150	5-Fluorouracil	NR

Patient	Age at surgery	Sex	Tumor location	Surgery	Histological diagnosis	Grade of differentiation	pTNM stage	PHGDH score	Adjuvant therapy	Response/Non-response
A22	52	F	Rectum	Anterior rectal resection	Adenocarcinoma NOS	G2	T0N1aMx	N/A	5-Fluorouracil	NR
A23	77	M	Descending colon	Left hemicolectomy	Adenocarcinoma NOS	G2	T3N1aMx	140	5-Fluorouracil	R
A24	79	F	Descending colon	Left hemicolectomy	Adenocarcinoma NOS	G2	T3N1aMx	80	5-Fluorouracil	R
A25	81	F	Cecum	Right hemicolectomy	Adenocarcinoma NOS	G2	T3N1bMx	0	5-Fluorouracil	NR
A26	45	F	Rectum	Anterior rectal resection	Adenocarcinoma NOS	G2	T3N2aM1a	0	5-Fluorouracil	R
A27	55	M	Descending colon	Left hemicolectomy	Adenocarcinoma NOS	G2	T3N2aM1a	0	5-Fluorouracil	NR
A28	66	F	Rectum	Anterior rectal resection	Adenocarcinoma NOS	G2	T3N0Mx	N/A	5-Fluorouracil	NR
A29	72	F	N/A	N/A	Adenocarcinoma NOS	G2	T2N1cM1a	40	5-Fluorouracil	NR
A30	72	M	Left flexure	Left hemicolectomy	Adenocarcinoma NOS	G2	T3N1aM1a	15	5-Fluorouracil	NR
A31	59	F	Ascending colon	Right hemicolctomy	Adenocarcinoma NOS	G2	T3N1aMx	180	5-Fluorouracil	NR
A32	64	F	Descending colon	Anterior rectal resection	Adenocarcinoma NOS	G2	T3N1bMx	20	5-Fluorouracil	R
A33	63	M	Descending colon	Left hemicolectomy	Adenocarcinoma NOS	G2	T3N1bMx	60	5-Fluorouracil	NR
A34	68	F	Cecum	Right hemicolectomy	Adenocarcinoma NOS	G2	T3N1bM1a	40	5-Fluorouracil	NR
A35	48	F	Ascending colon	Right hemicolectomy	Adenocarcinoma NOS	G2	T3N0Mx	30	5-Fluorouracil	R
A36	80	M	Rectum	Anterior rectal resection	Adenocarcinoma NOS	G2	T3N2aMx	270	5-Fluorouracil	NR
A37	69	F	Sigmoid colon	Anterior rectal resection	Adenocarcinoma NOS	G2	T3N2bMx	30	5-Fluorouracil	NR
A38	75	M	Sigmoid colon	Anterior rectal resection	Adenocarcinoma NOS	G2	T2N1aMx	120	5-Fluorouracil	R
A39	53	F	Ascending colon	Right hemicolectomy	Adenocarcinoma NOS	G2	T3N1bMx	240	5-Fluorouracil	NR
A40	66	F	Descending colon	Left hemicolectomy	Mucinous adenocarcinoma	G3	T3N2bMx	140	5-Fluorouracil	NR
A41	67	M	Sigmoid colon	Anterior rectal resection	Adenocarcinoma NOS	G2	T3N1cMx	120	5-Fluorouracil	NR
A42	68	M	Rectum	Anterior rectal resection	Adenocarcinoma NOS	G2	T3N2aMx	5	5-Fluorouracil	R

Patient	Age at surgery	Sex	Tumor location	Surgery	Histological diagnosis	Grade of differentiation	pTNM stage	PHGDH score	Adjuvant therapy	Response/Non-response
A43	68	M	Transverse colon	Transverse resection	Adenocarcinoma NOS	2	T3N2aMx	0	5-Fluorouracil	R
A44	57	M	Rectum	Anterior rectal resection	Adenocarcinoma NOS	3	T4bN1bMx	5	5-Fluorouracil	NR
A45	76	M	Rectum	Anterior rectal resection	Adenocarcinoma NOS	2	T3N2aMx	100	5-Fluorouracil	R
A46	62	F	Sigmoid colon	Anterior rectal resection	Adenocarcinoma NOS	2	T3N0M1a	240	5-Fluorouracil	R
A47	60	M	Rectum	Anterior rectal resection	Adenocarcinoma NOS	2	T2N1aMx	0	5-Fluorouracil	R
A48	48	F	Descending colon	Left hemicolectomy	Adenocarcinoma NOS	2	T3N1bMx	120	5-Fluorouracil	R
A49	62	M	Sigmoid colon	Anterior rectal resection	Adenocarcinoma NOS	2	T3N1aMx	25	5-Fluorouracil	R
A50	81	M	Sigmoid colon	Anterior rectal resection	Adenocarcinoma NOS	2	T3N1bMx	160	5-Fluorouracil	NR
A51	70	F	Sigmoid colon	Anterior rectal resection	Adenocarcinoma NOS	2	T3N1aMx	160	5-Fluorouracil	R
A52	66	M	Sigmoid colon	Anterior rectal resection	Adenocarcinoma NOS	2	T2N1aMx	10	5-Fluorouracil	R
A53	58	F	Rectum	Anterior rectal resection	Adenocarcinoma NOS	2	T3N1aMx	0	5-Fluorouracil	R

Table 4*: Clinicopathological characteristics of CRC patients and relationship between PHGDH expression and response to therapy. R: Response; NR: Non-response.*

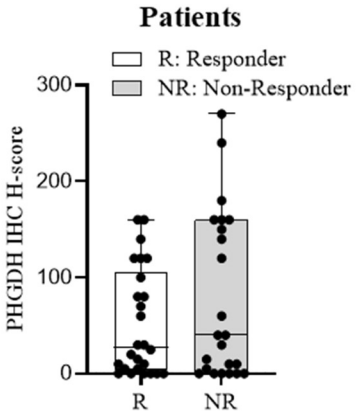

***Figure 8**: Retrospective analysis of 50 CRC patients showing the correlation between PHGDH expression level and therapy response (R: Responder, NR: Non-Responder).*

Complementary analysis of publicly available databases (https://www.cbioportal.org/) revealed that both primary CRC tumors and metastatic lesions exhibit elevated PHGDH expression with respect to their normal counterparts, suggesting that increased PHGDH levels are associated with unfavorable prognosis in CRC patients (*Figure 9*).

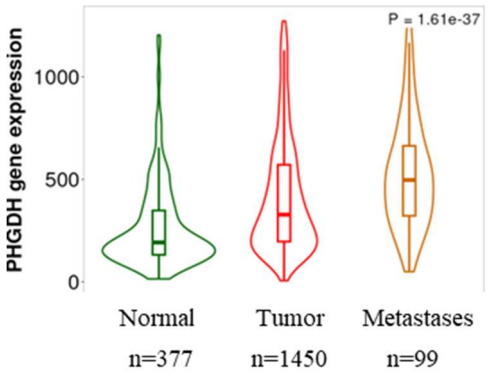

***Figure 9**: Violin plots show PHGDH gene expression profile in normal colon (Normal), primary (Tumor) and metastases (Metastases) of colon cancer obtained by online analysis platform on TNMplot.*

The prognostic significance of PHGDH expression was further evaluated by analyzing overall survival (OS) and relapse-free survival (RFS) using Kaplan-Meier analysis. In line with the previous result, elevated PHGDH expression was associated with reduced OS ($P < 0.05$, HR = 1.3) and diminished RFS ($P < 0.001$, HR = 1.47) in CRC patients (*Figure 10*).

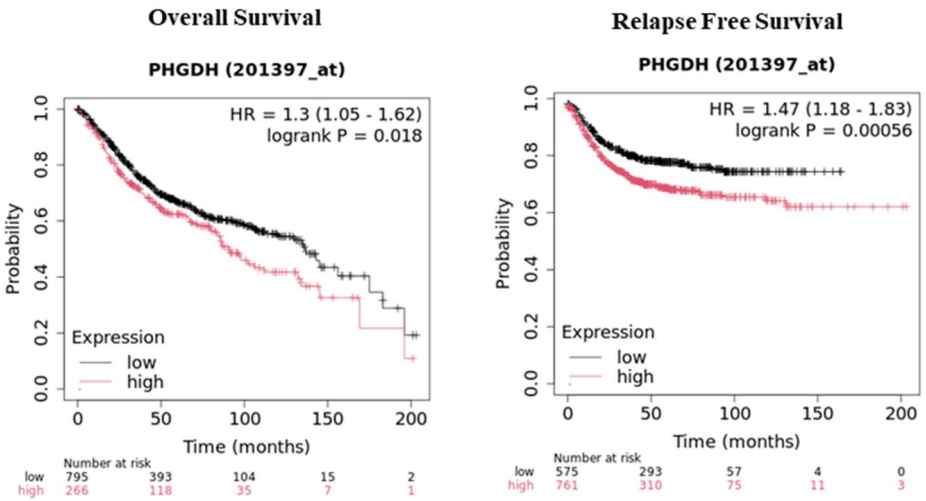

Figure 10: *Kaplan–Meier plotter of high and low PHGDH expression in CRC. OS and RFS in CRC patients expressing high PHGDH (red) and low PHGDH (black) levels.*

The relationship between PHGDH expression and 5-FU sensitivity was additionally validated using PDCOs. Significant inter-sample variability in 5-FU response was observed (*Figure 11*), with increased drug sensitivity consistently associated with reduced PHGDH expression levels (*Figure 5B* and *Figure 11*).

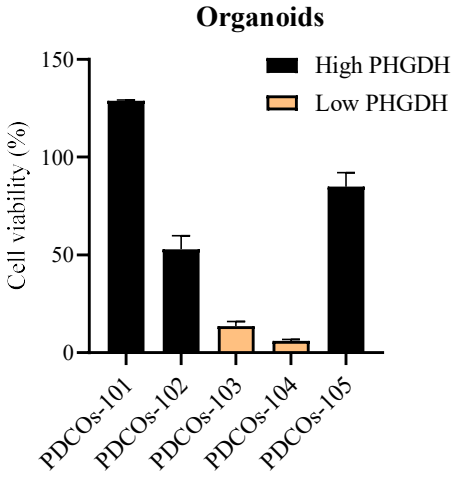

Figure 11: *PDCOs response to 5 μM 5-FU treatment. Cell viability was assayed after 7 days of treatment by CellTiter-Glo 3D reagent.*

The results reveal significant heterogeneity in PHGDH expression among patient-derived CRC samples, supporting PHGDH as a potential predictive biomarker for therapeutic outcomes in 5-FU-based chemotherapy regimens.

4.3. PHGDH Enhances Aggressiveness in CRC

To investigate the functional role of PHGDH in 5-FU resistance, both loss-of-function and gain-of-function approaches were used to manipulate PHGDH expression in CRC cell lines with differing baseline expression levels. PHGDH knockdown was carried out in high-expressing HCT8 cells, while overexpression was induced in low-expressing RKO cells (*Figure 12A*). The initial results demonstrated that PHGDH expression levels do not significantly influence basal proliferative capacity, as both PHGDH-silenced HCT8 cells (HCT8 shPHGDH) and PHGDH-overexpressing RKO cells (RKO OE PHGDH) exhibited proliferation rates similar to those of their respective parental lines under standard culture conditions (*Figure 12B* and *Figure 12C*).

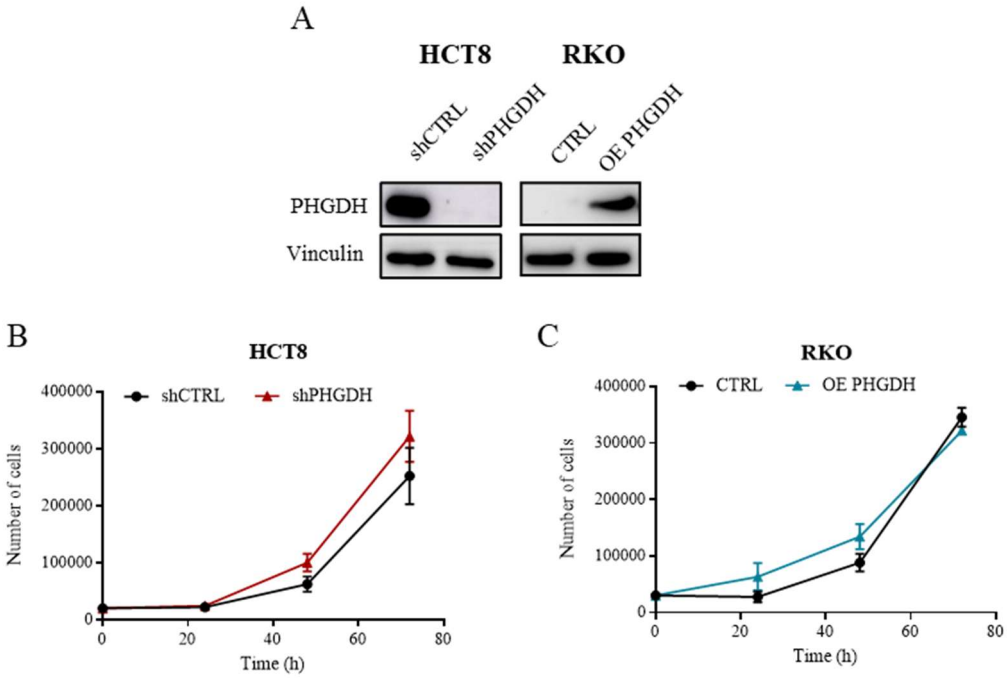

***Figure 12**: PHGDH supports resistance to 5-FU. **A)** PHGDH protein levels in HCT8 and RKO cells following shRNA silencing or overexpression, respectively. Vinculin immunoblot was performed to ensure equal loading. **B-C)** Proliferation rate of HCT8 and RKO cells after stable transfection. Data are reported as mean ± SEM from three independent experiments.*

In contrast, cell viability under 5-FU treatment was strongly dependent on PHGDH expression (*Figure 13A* and *Figure 13B*).

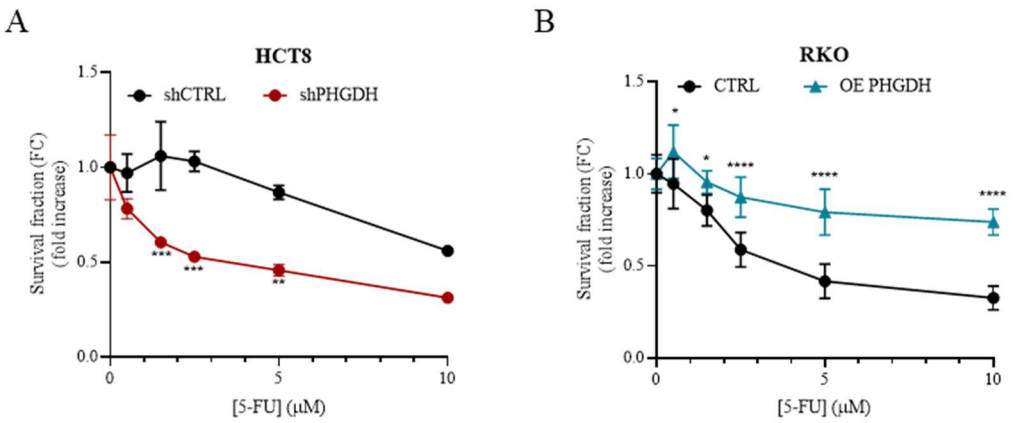

***Figure 13**: **A-B**) Survival fraction of HCT8, HCT8 shPHGDH, RKO and RKO OE PHGDH treated with increasing concentration of 5-FU for 48 h. Data are reported as mean ± SEM from three independent experiments; t-test; * $p < 0.05$, ** $p < 0.01$, *** $p < 0.001$, **** $p < 0.0001$.*

To better understand how PHGDH mediates resistance to chemotherapy, phosphorylation of histone H2AX (γH2AX), a marker of DNA double-strand breaks, was quantified. This analysis revealed that PHGDH expression enhances cellular capacity to mitigate DNA damage accumulation following 5-FU treatment. In particular, RKO OE PHGDH cells displayed reduced γH2AX levels compared to wild-type counterparts under both basal and 5-FU-treated conditions, whereas HCT8 shPHGDH cells exhibited elevated DNA damage accumulation, particularly following drug exposure (*Figure 14*).

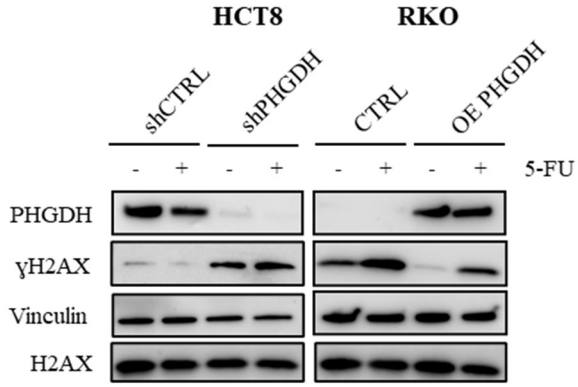

***Figure 14**: γH2AX levels in transfected and parental HCT8 and RKO cells. H2AX and vinculin were used as controls. Each image is representative of at least three independent experiments*

Similar results were obtained in PHGDH-silenced LS174T cells (LS174T shPHGDH) (*Figure 15*).

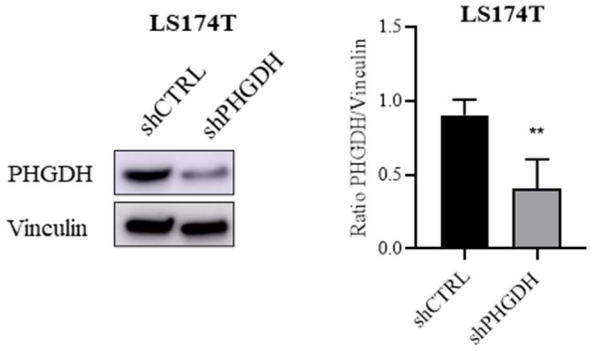

***Figure 15**: PHGDH protein levels in PHGDH silenced LS174T cells. Vinculin immunoblot was performed to ensure equal loading. Bargraph reports quantification of PHGDH level compared to vinculin and show the mean ± SEM of three independent experiments; t-test ** $p < 0.01$.*

Results demonstrated increased 5-FU sensitivity (*Figure 16A*) and elevated γH2AX levels relative to parental cells (*Figure 16B*). Collectively, data indicate that PHGDH expression is critical for promoting CRC aggressiveness through improved DNA repair mechanisms.

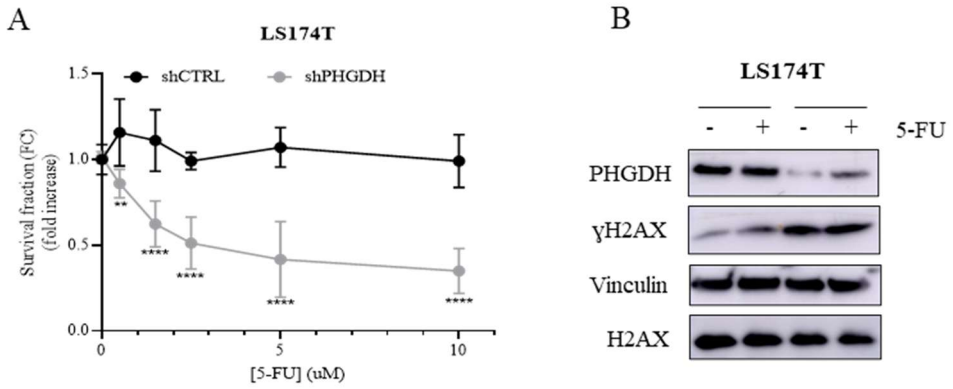

***Figure 16**: **A)** Survival fraction of LS174T cells transfected with shCTRL or shPHGDH after 48h of 5-FU treatment. Data are reported as mean ± SEM from three independent experiments; t-test ** $p < 0.01$, **** $p < 0.0001$. **B)** γH2AX levels in transfected and parental LS174T cells. Vinculin and H2AX were used as loading control.*

In addition, elevated PHGDH levels also promoted a more aggressive cell phenotype. RKO cells overexpressing PHGDH formed more colonies after 5-FU treatment than control cells, while PHGDH-silenced HCT8 cells were more sensitive to the drug and formed fewer colonies (*Figure 17*).

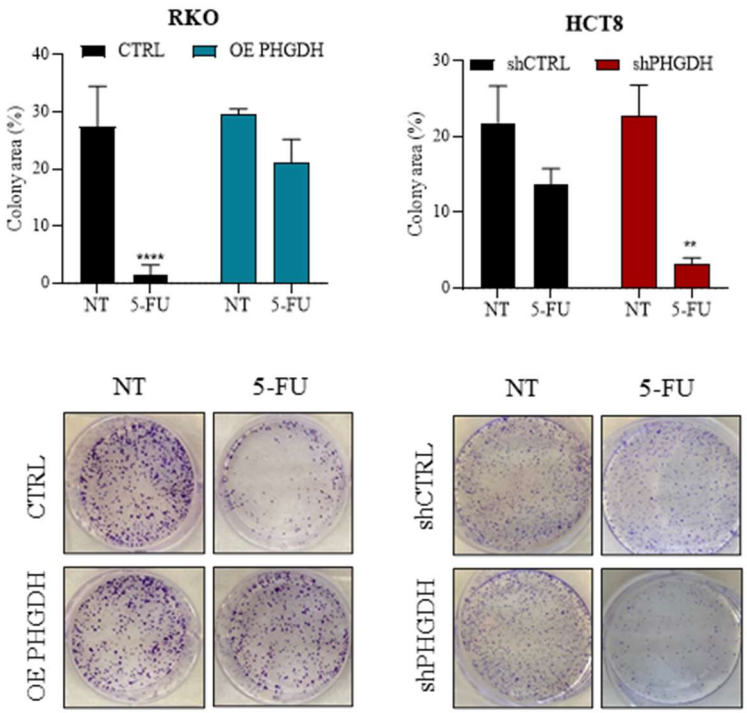

***Figure 17**: Colony formation assay of RKO, RKO OE PHGDH, HCT8 and HCT8 shPHGDH cells grown either in the absence or presence of 5 μM 5-FU. After 48 h, cells were detached, counted, and 1000 cells were plated in new dishes, and incubated for at least 10 days. Formed colonies were stained with Crystal Violet. Representative images are shown. Data are reported as mean ± SEM from three independent experiments; t-test; ** $p < 0.01$, **** $p < 0.0001$.*

Besides becoming resistant to drugs, cancer cells often become more invasive and gain stem cell-like properties as the tumor progresses. PHGDH expression levels directly influenced the invasive behavior of CRC cells: knockdown in HCT8 and in LS174T cells led to a marked reduction in invasive capacity, while overexpression in RKO cells enhanced invasion (*Figure 1*8).

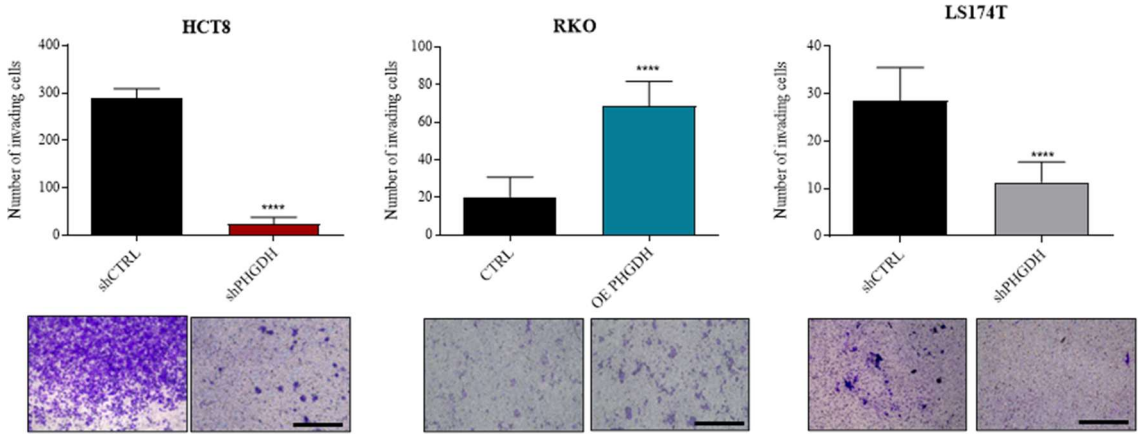

***Figure 18**: PHGDH confers aggressiveness to CRC cells. Invasive abilities of PHGDH-silenced or PHGDH-overexpressing cells. CRC cells were seeded in the upper compartment of 8 µm Transwell system coated with Matrigel. After 16 h invaded cells were stained with Crystal Violet and counted. Representative images of invaded CRC cells are shown below the bargraphs (magnification 20x, scale bar: 100 µm). Data are reported as mean ± SEM from three independent experiments; t-test; **** $p < 0.0001$.*

To investigate whether PHGDH expression influences cancer stem cell properties, the following assays were performed: (a) assessment of primary colon-spheres formation (P1 generation) and secondary colon-spheres formation (P2 generation) to evaluate self-renewal capacity; (b) evaluation of the expression of key stemness genes by qPCR; and (c) flow cytometric quantification of cancer stem cell surface markers. P1 colon-spheres formation after 5-FU exposure revealed a direct correlation between their number and size and PHGDH expression (*Figure 19A*). Secondary colon-sphere formation through serial passaging was assessed to evaluate self-renewal capacity. High PHGDH expression was found to enhance self-renewal ability, as indicated by an increased number of P2 colon-spheres in RKO OE PHGDH cells compared to control cells, even following 5-FU treatment. In contrast, PHGDH silencing markedly impaired the self-renewal capacity of HCT8 cells under both basal conditions and after 5-FU exposure (*Figure 19B*).

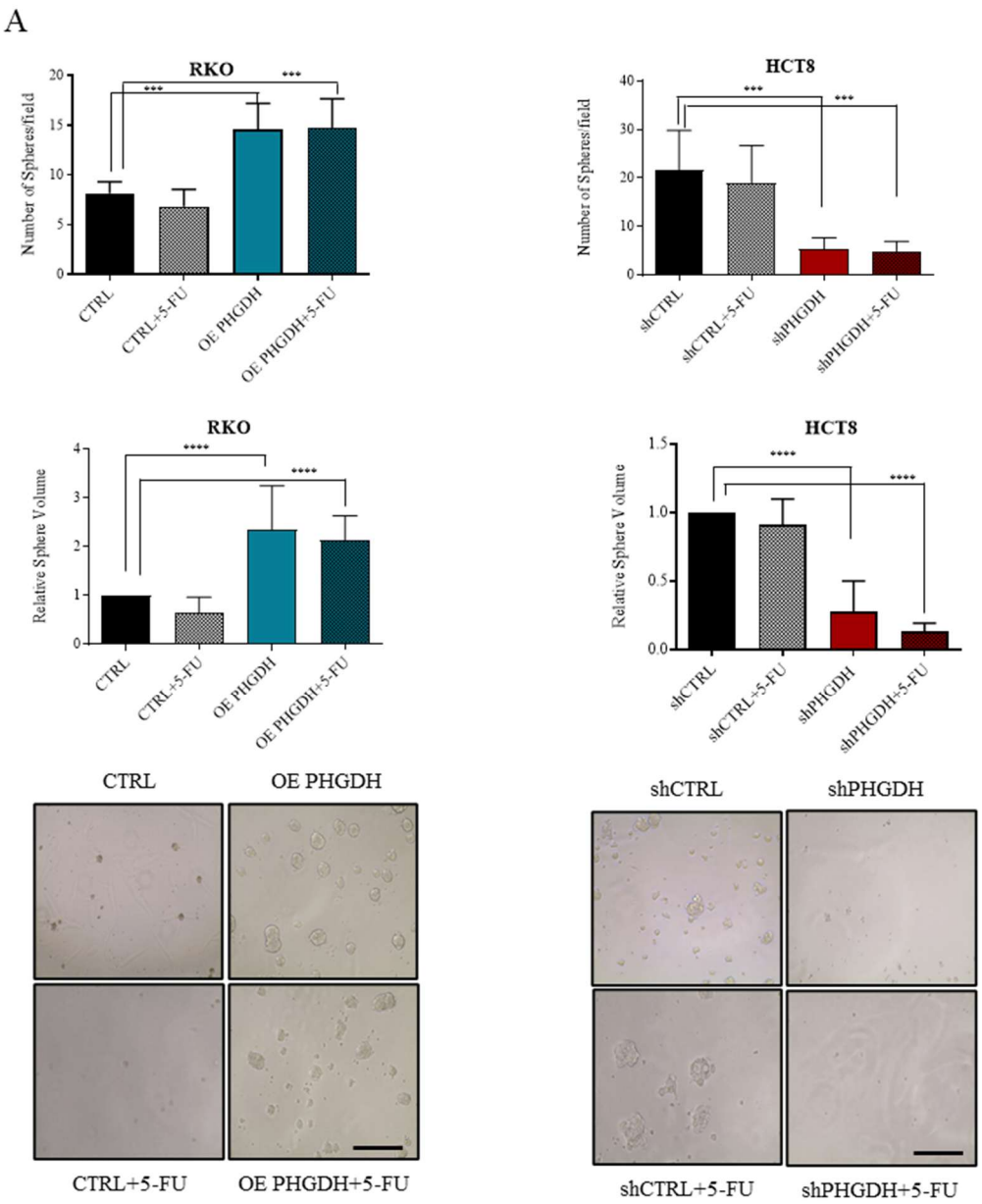
A
RKO
Number of Spheres/field
CTRL
CTRL+5-FU
OE PHGDH
OE PHGDH+5-FU
HCT8
shCTRL
shCTRL+5-FU
shPHGDH
shPHGDH+5-FU
Relative Sphere Volume
CTRL
OE PHGDH
CTRL+5-FU
OE PHGDH+5-FU
shCTRL
shPHGDH
shCTRL+5-FU
shPHGDH+5-FU

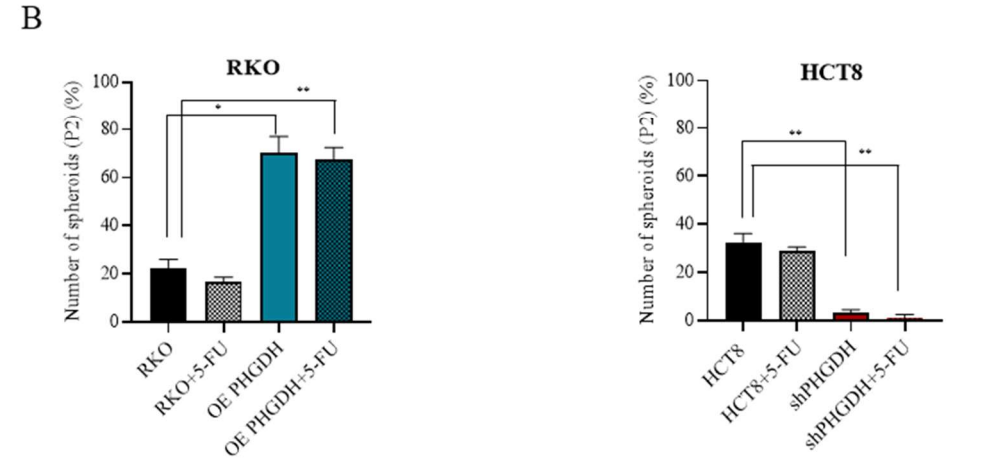
B
RKO
Number of spheroids (P2) (%)
RKO
RKO+5-FU
OE PHGDH
OE PHGDH+5-FU
HCT8
HCT8
HCT8+5-FU
shPHGDH
shPHGDH+5-FU

***Figure 19**: **A)** PHGDH overexpressing or silenced cells were treated with 5 μM 5-FU for 48 h then P1 spheres forming ability was performed seeding 700 cells/well in 96-well plate. After 7 days colonspheres were counted, and volumes were calculated as described in Methods. Representative images of CRC spheroids are shown below the bargraphs (magnification 20x, scale bar: 100 μm). Data are reported as mean ± SEM from three independent experiments; bargraph represents the fold increase relative to respective CTRL; t-test; *** p < 0.001, **** p < 0.0001. **B)** Cells disaggregated from P1 spheres were re-plated to test secondary spheroid (P2) formation ability in RKO, RKO OE PHGDH, HCT8 and HCT8 shPHGDH cells. Data are reported as mean ± SEM from three independent experiments; t-test; * p < 0.05, ** p < 0.01.*

Furthermore, qPCR analysis of P1 colon-spheres from RKO OE PHGDH or HCT8 cells revealed elevated expression of genes associated with stemness and epithelial-mesenchymal transition (EMT) compared to their low-PHGDH-expressing counterparts (*Figure 20*).

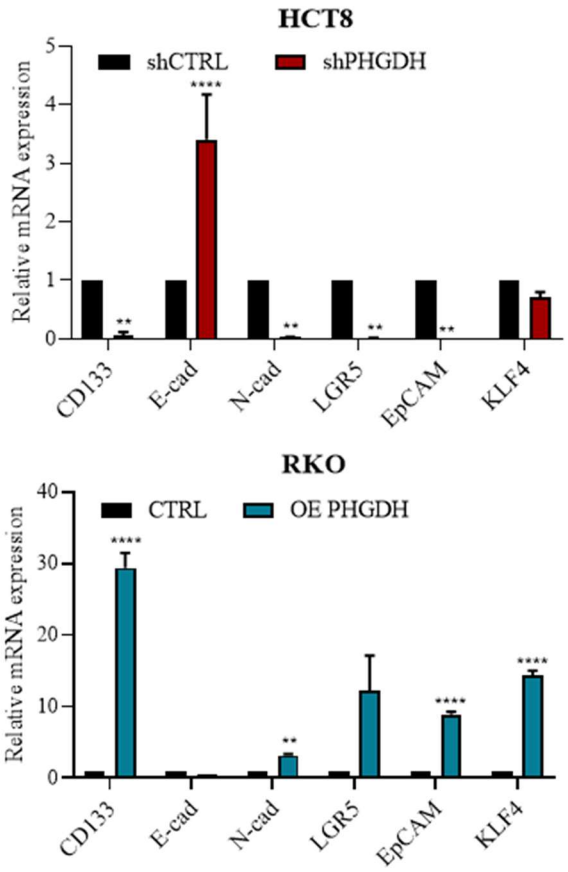

***Figure 20**: mRNA expression levels of genes involved in CSC phenotype acquisition and EMT program in P1 colonspheres. Data are reported as mean ± SEM from three independent experiments; t-test; ** p < 0.01, **** p < 0.0001.*

Flow cytometric evaluation of cancer stem cell surface markers - EpCAM, CD24, CD133, and CD44 - confirmed a direct correlation between stemness marker expression and PHGDH levels in both HCT8 and RKO P1 colon-spheres (*Figure 21*).

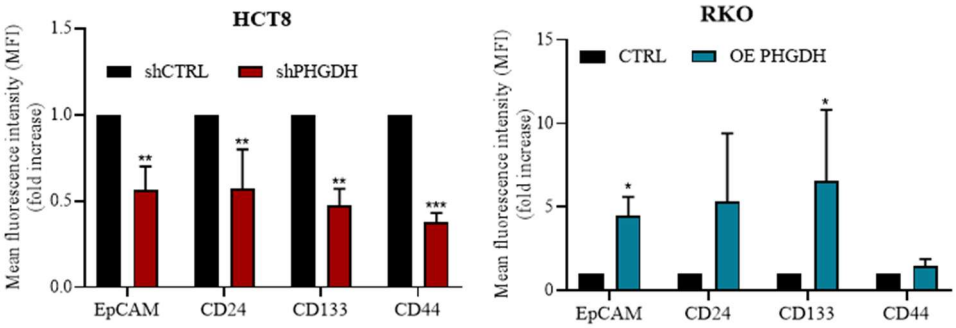

***Figure 21**: Membrane EpCAM, CD24, CD133 and CD44 expression levels in CRC cells evaluated in P1 colonspheres by flow cytometry. Data are reported as mean ± SEM from three independent experiments; t-test; * $p < 0.05$, ** $p < 0.01$, *** $p < 0.001$.*

Collectively, these results indicate that PHGDH expression enhances cancer aggressiveness and promotes enrichment of stem cell-like properties in CRC cell lines, thereby facilitating both therapeutic resistance and increased metastatic potential.

4.4. Transcriptomic Profiling Reveals Hedgehog Signaling Activation upon PHGDH Silencing

Accumulating evidence has highlighted non-metabolic roles of PHGDH in cancer, frequently mediated through its nuclear localization. Consistent with prior reports, Western blot analysis confirmed nuclear localization of PHGDH in HCT8 cells (*Figure 22A*). Emerging data suggest that nuclear PHGDH can modulate transcriptional programs through interactions with key transcription factors, such as c-Myc. c-Myc, a master regulator of cellular proliferation and metabolism, is often dysregulated in CRC. Coimmunoprecipitation experiments demonstrated that PHGDH and c-Myc physically associate within the nuclear compartment of HCT8 cells (*Figure 22B*), corroborating previous findings and supporting the hypothesis that PHGDH may exert catalytically independent functions through interactions with the transcriptional machinery.

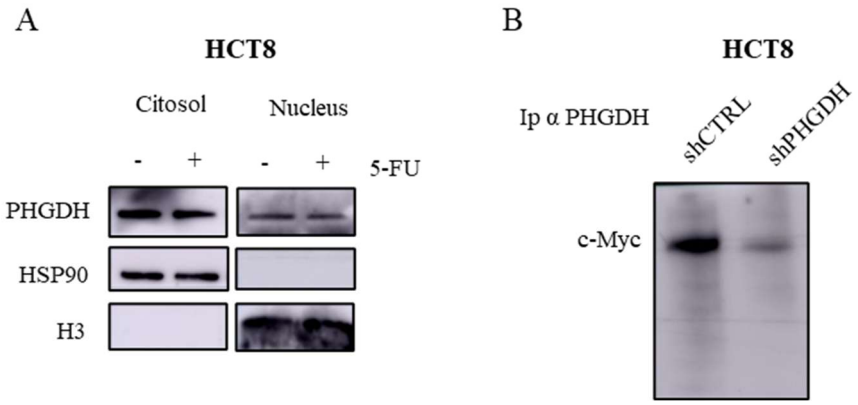

***Figure 22**: PHGDH modulation affects Hedgehog signaling pathway. **A)** PHGDH protein level in cytosolic or nuclear compartment in HCT8 cells treated with 5 μM 5FU for 48 h. HSP90 and H3 were used as loading control for cytosolic and nuclear compartment, respectively. **B)** Co-immunoprecipitation of PHGDH and c-Myc in shCTRL or shPHGDH cells. An anti-PHGDH antibody was used to pull down PHGDH, then western blotting for c-Myc was performed.*

To elucidate potential non-metabolic roles of PHGDH in therapeutic resistance, RNA-sequencing analysis was performed on HCT8 parental cells and two independent PHGDH-silenced clones (HCT8 shPHGDH). Principal Component Analysis (PCA) demonstrated robust reproducibility among biological replicates and distinct experimental groups (*Figure 23*).

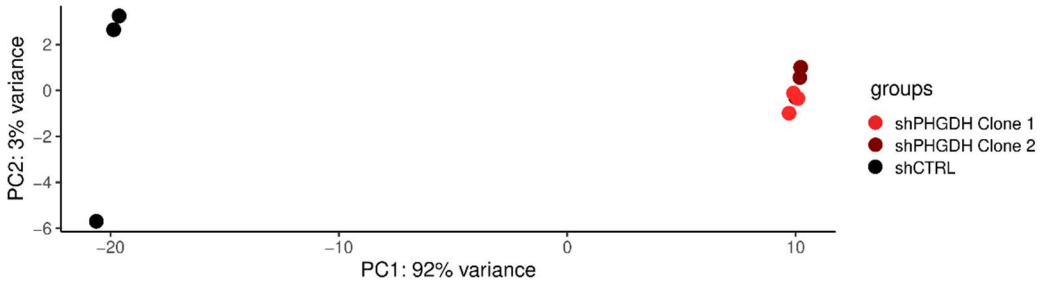

***Figure 23**: PCA displays the distribution of samples based on their gene expression profiles, projected onto the first two principal components (PC1 and PC2). PC1 (x-axis) captures 92% of the total variance, while PC2 (y-axis) captures 3%. Samples are color-coded according to their group: black points indicate shCTRL replicates, red and brown points indicate shPHGDH replicates.*

Pathway Enrichment Analysis revealed significant upregulation of pathways associated with unfolded protein response, mTORC1 signaling, hypoxia response, and p53 signaling in HCT8 shPHGDH cells relative to parental controls. The Hedgehog (HH) signaling cascade emerged as one of the most significantly suppressed pathways in PHGDH-silenced cells (*Figure 24*).

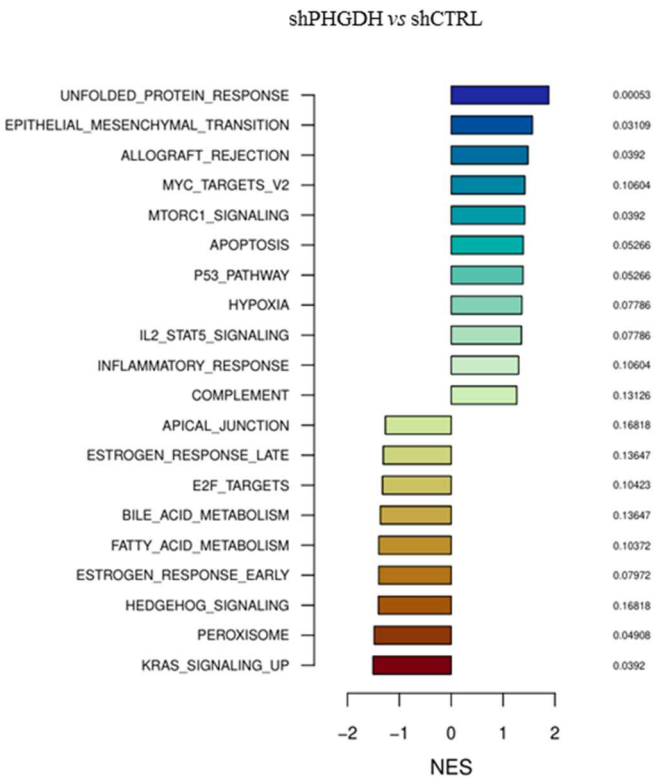

***Figure 24**: Pathway Enrichment Analysis of Differentially Expressed Genes illustrating the top enriched pathways in the comparison between shCTRL and shPHGDH samples. The analysis was performed using the MSigDB Hallmark gene set. The x-axis represents the Normalized Enrichment Score (NES), which indicates the up/down-regulation degree of the altered pathways: Pathways with positive NES values are up-regulated in shPHGDH samples compared to shCTRL, while pathways with negative NES values down-regulated. The associated adjusted p-values (Benjamini-Hochberg) are displayed to the right of each bar.*

Given the established role of HH signaling in maintaining stem cell properties and promoting chemoresistance, particularly in relation to 5-FU, further analyses were conducted to investigate the mechanistic relationship between PHGDH, HH signaling, and therapeutic resistance. Targeted pathway analysis was performed to characterize alterations in HH signaling following PHGDH modulation. Consistent with Gene Set Enrichment Analysis (GSEA) results (*Figure 25A*), expression of multiple HH pathway target genes decreased in PHGDH-silenced cells (*Figure 25B)*.

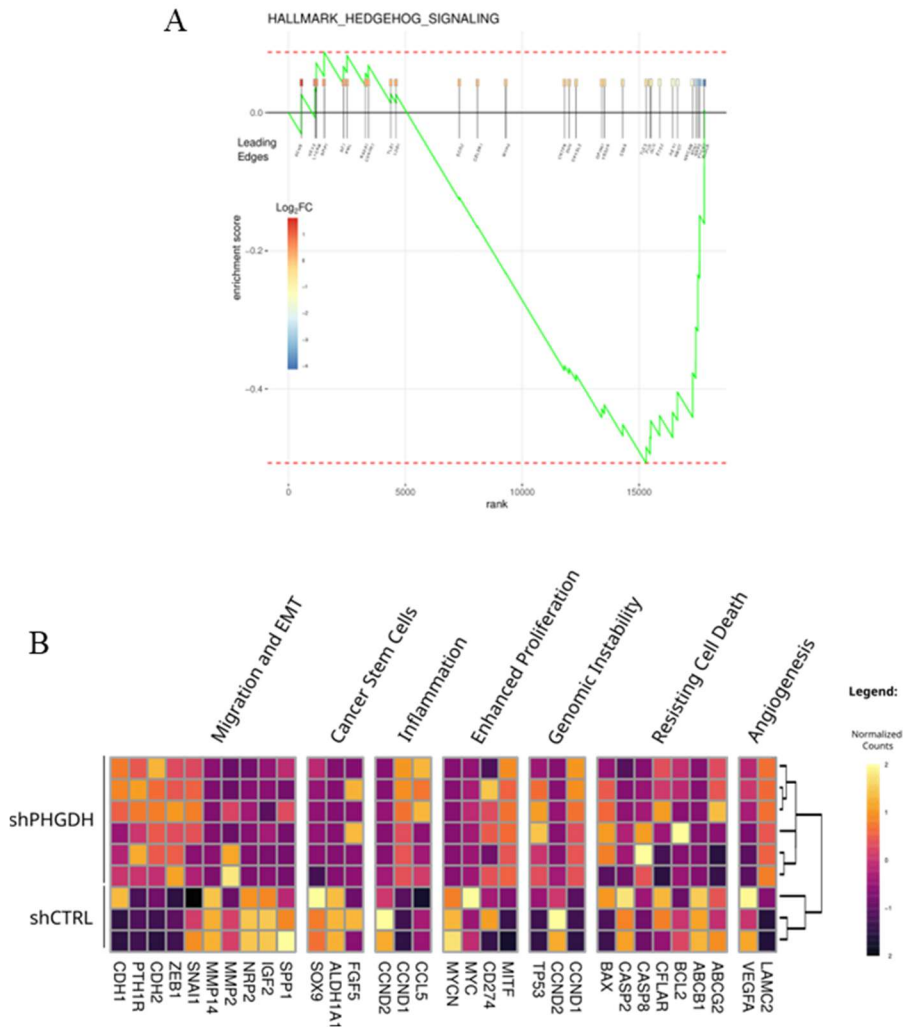

***Figure 25**: **A)** GSEA focused on the Hallmark HH Signaling pathway. The plot displays the resulting normalized enrichment score (NES, green line) of the ranked list of DEGs across the dataset. The leading edge, i.e. the genes contributing most significantly to the enrichment, are displayed below each bar which represents the position of the gene in the ranked list. Each gene is also annotated by the log2FC (boxes above the bars), providing an indication of its expression change in the comparison. The red dashed lines indicate the maximum and minimum NES achieved. **B)** Heatmap of HH Pathway Target Genes: displays the expression levels of HH pathway target genes across different samples. The genes are organized based on their involvement in specific cellular processes annotated on the top. Sample clustering is shown via a dendrogram at the top of the heatmap.*

To confirm these results, quantitative qPCR analysis was performed to validate expression of key HH target genes in HCT8 shPHGDH and RKO OE PHGDH cells. This analysis confirmed downregulation of HH target genes in HCT8 shPHGDH cells compared to wild-type controls and up-regulation in RKO OE PHGDH with respect to RKO cells (*Figure 26*), thereby establishing a positive correlation between PHGDH expression and HH pathway activity.

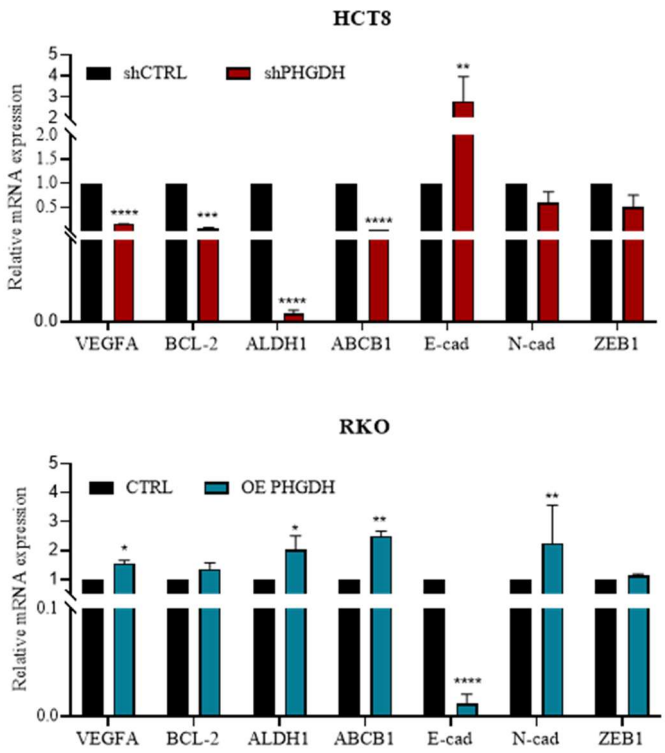

***Figure 26**: mRNA expression levels of genes involved in HH pathway analyzed by qPCR. Data are reported as mean ± SEM from three independent experiments; t-test; * $p < 0.05$, ** $p < 0.01$, *** $p < 0.001$, **** $p < 0.0001$.*

The link between PHGDH and HH signaling was additional validated by examining the expression of final effectors of the HH pathway, Glioma-associated oncogene 1 (GLI1), Glioma-associated oncogene 2 (GLI2), and the pathway-specific receptor Patched1 (PTCH1). Expression of GLI1, GLI2, and PTCH1 was reduced in HCT8 shPHGDH cells compared to controls, whereas RKO OE PHGDH cells exhibited elevated expression of these markers relative to parental ones (*Figure 27A*). To validate this association, qPCR analysis was performed comparing high-PHGDH-expressing LS174T cells with low-PHGDH-expressing RKO cells. Data confirmed the previous results (*Figure 27B*).

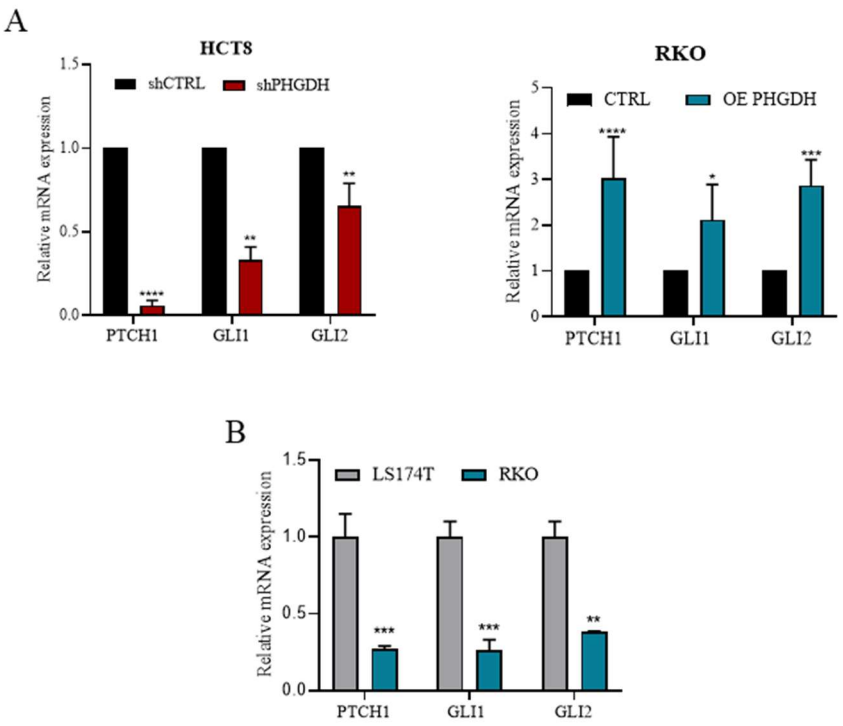

***Figure 27**: **A-B)** mRNA expression levels of PTCH1, GLI1 and GLI2 in PHGDH-silenced cells or PHGDH-overexpressing and in LS174T vs RKO analyzed by qPCR using parental cells as comparator. Data are reported as mean ± SEM from three independent experiments; t-test; * $p < 0.05$, ** $p < 0.01$, *** $p < 0.001$, **** $p < 0.0001$.*

Analysis of PDCOs revealed a strong positive correlation between PHGDH expression and HH pathway-related genes (*Figure 28*). Overall, these analyses suggest that PHGDH promotes activation of the HH pathway.

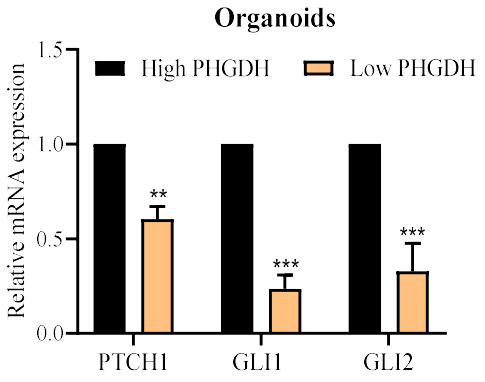

***Figure 28**: mRNA expression levels of PTCH1, GLI1 and GLI2 in PDCOs analyzed by qPCR using high PHGDH organoids as comparator. Data are reported as mean ± SEM from three independent experiments; t-test; ** $p < 0.01$, *** $p < 0.001$.*

4.5. PHGDH and GLI1: a Positive Feedback Loop that Mediates 5-FU Resistance

Previous studies have shown that the HH signaling pathway plays a role in maintaining stemness and promoting drug resistance across various tumor types. Specifically, HH pathway activation has been identified as a critical driver of 5-fluorouracil (5-FU) resistance in LoVo cells (142–145).

PHGDH silencing in HCT8 cells led to decreased GLI1 expression at both mRNA and protein levels (*Figure 27A* and *Figure 29*).

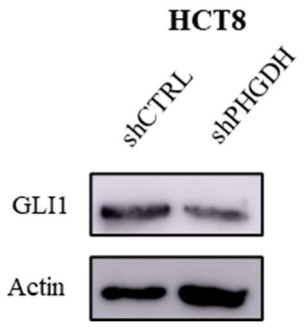

Figure 29: *GLI1 protein level in shCTRL and shPHGDH cells. β-Actin immunoblot was performed to ensure equal loading.*

To investigate whether GLI1 modulation could affect PHGDH expression, GLI1 silencing was performed (*Figure 30A*), which resulted in lowered PHGDH expression in HCT8 cells. Similarly, pharmacological inhibition of GLI1 with JC19, a 4-methoxy-8-hydroxyquinoline compound that blocks GLI1/2 transcriptional activity by interfering with DNA binding, decreased PHGDH expression levels (*Figure 30B*).

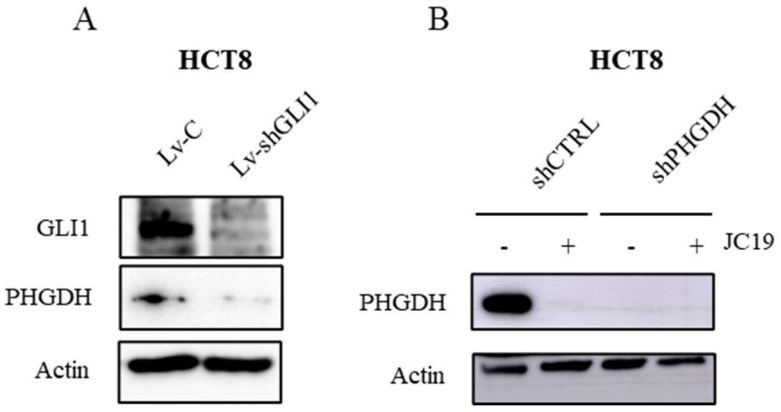

Figure 30*: **A)** Representative images of western blot for GLI1, PHGDH and β-Actin of HCT8 cells silenced with GLI1 shRNA. **B)** Immunoblot of PHGDH in HCT8 shCTRL or shPHGDH cells treated with 2 μM JC19 for 48 h. β-Actin immunoblot was performed to ensure equal loading.*

The reduction of PHGDH expression increased sensitivity to 5-FU treatment (*Figure 31*). These results showed a positive feedback loop between GLI1 and PHGDH.

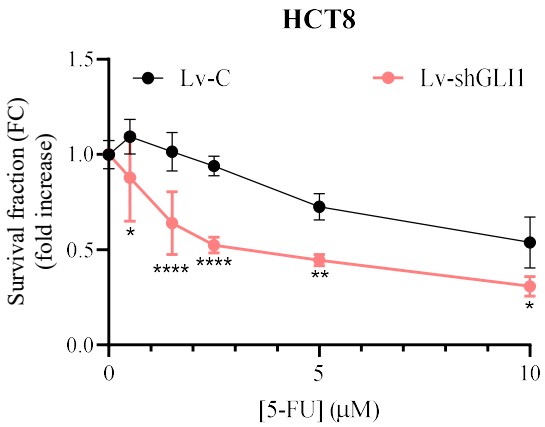

***Figure 31**: Effects of 5-FU on GLI1-silenced HCT8 cells. Cells were treated for 48 h with increasing concentration of 5-FU. Data are reported as mean ± SEM from three independent experiments; t-test; * $p < 0.05$, ** $p < 0.01$, **** $p < 0.0001$.*

This observation suggested that pharmacological inhibition of GLI transcription factors (using compounds such as JC19 or GANT61) could enhance CRC cell lines sensitivity to 5-FU treatment. The combination of 5-FU and JC19 (*Figure 32A*) or GANT61 (*Figure 32B)* increased chemosensitivity in both CRC cell lines and patient-derived 3D organoids (*Figure 32C*).

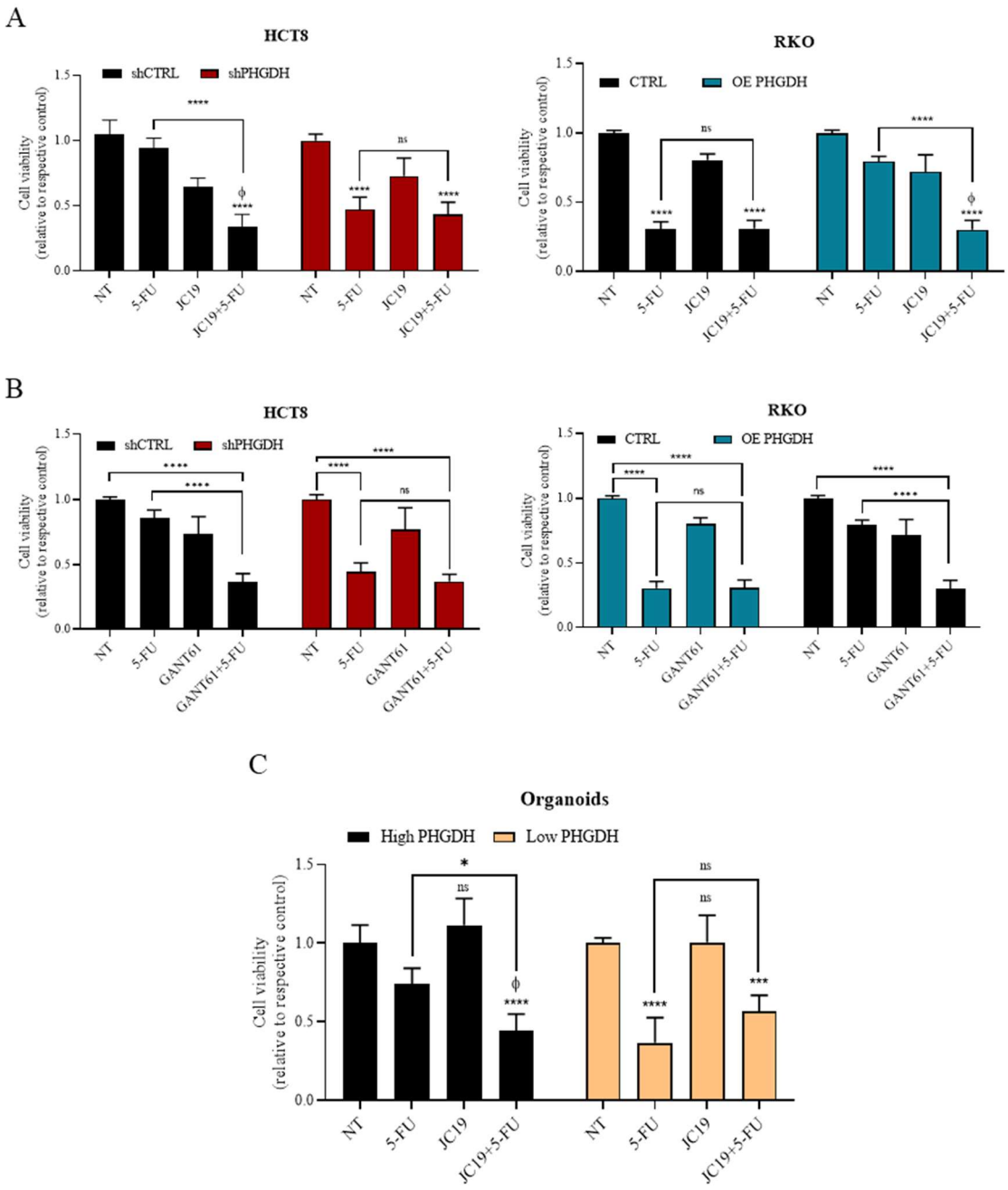

Figure 32: A) *Survival fraction of transfected cells treated or not with 5 µM 5-FU in combination with 2 µM JC19 for 48 h. Data are reported as mean ± SEM from three independent experiments; ANOVA; **** p < 0.0001. φ indicates synergistic effect (Bliss test > 0) with respect to single treatments.* ***B)*** *Survival fraction of HCT8, HCT8 shPHGDH, RKO and RKO OE PHGDH cells treated or not with 5 µM 5-FU in combination with 10 µM GANT61 for 48h. Data are reported as mean ± SEM from three independent experiments; ANOVA; **** p<0.0001.* ***C)*** *Survival fraction of PDCOs treated or not with 5 µM 5-FU in combination with 2 µM JC19 for or 7 days. Data are reported as mean ± SEM from three independent experiments; ANOVA; * p < 0.05, *** p < 0.001, **** p < 0.0001. φ indicates synergistic effect (Bliss test > 0) with respect to single treatments.*

Notably, the combination treatment showed synergistic effects (Bliss > 0) in cell lines and organoids with high PHGDH expression levels (HCT8 and RKO OE PHGDH). In

contrast, in cells and organoids with low PHGDH expression, JC19 did not enhance the effect of 5-FU (*Figure 32A* and *Figure 32C*). These results indicated that HH pathway inhibitors increased 5-FU chemosensitivity specifically in CRC cells and organoids expressing high levels of PHGDH.

To further examine the role of the PHGDH/HH axis in 5-FU resistance, the expression GLI1, GLI2 and PTCH1 was analyzed in 5-FU-resistant HCT116 cells (HCT116R), which had been previously established. Upregulation of GLI1, GLI2, and PTCH1 mRNA expression was observed in HCT116R cells compared to sensitive cells (*Figure 33A*). Additionally, downstream HH target genes showed increased expression in HCT116R cells (*Figure 33B*). These data confirmed the link between HH signaling activation and 5-FU resistance. Also, the combination treatment effectively enhanced 5-FU sensitivity in HCT116R cells (*Figure 33C*).

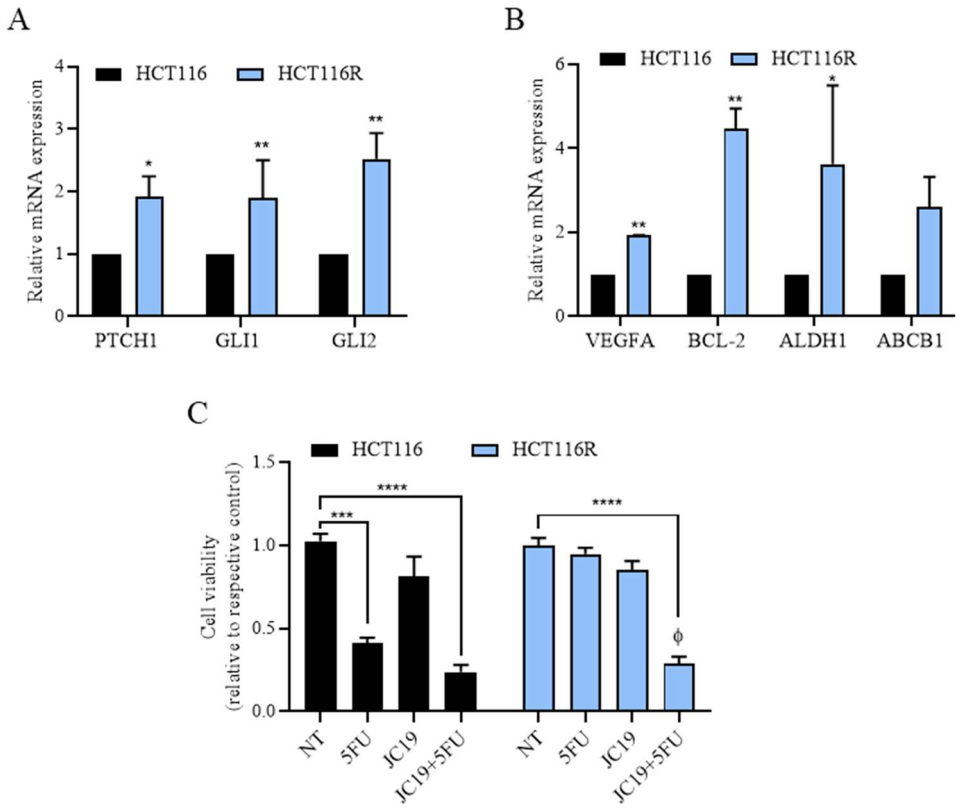

***Figure 33**: **A)** PTCH1, GLI1 and GLI2 mRNA expression level in HCT116 and HCT116R cells. HCT116 was used as comparator. Data are reported as mean ± SEM from three independent experiments; t-test; * $p < 0.05$, ** $p < 0.01$. **B)** mRNA expression levels of HH pathway target genes analyzed by qPCR. HCT116 was used as comparator. Data are reported as mean ± SEM from three independent experiments; t-test; * $p < 0.05$, ** $p < 0.01$. **C)** Survival fraction of HCT116 and HCT116R cells treated or not with 5 μM 5-FU in combination with 2,5 μM JC19 for 48 h. Data are reported as mean ± SEM from three independent experiments; ANOVA; *** $p < 0.001$, **** $p < 0.0001$. φ indicates synergistic effect (Bliss test > 0) with respect to single treatments.*

To validate the correlation between HH signaling and 5-FU resistance, RNA-sequencing data from The Cancer Genome Atlas (TCGA) were analyzed. The TCGA-COAD and TCGA-READ databases were examined, focusing on patients who had received 5-FU-based chemotherapy. Patients were classified as responders (R) or non-responders (NR) based on clinical outcomes following treatment (see Methods). Gene Set Enrichment Analysis (GSEA) revealed significant upregulation of the HH signaling pathway in the NR group (NES = 1.509, adjusted p-value = 0.0401) (*Figure 34*). This DATA confirmed the importance of this pathway in mediating resistance to 5-FU-based therapy.

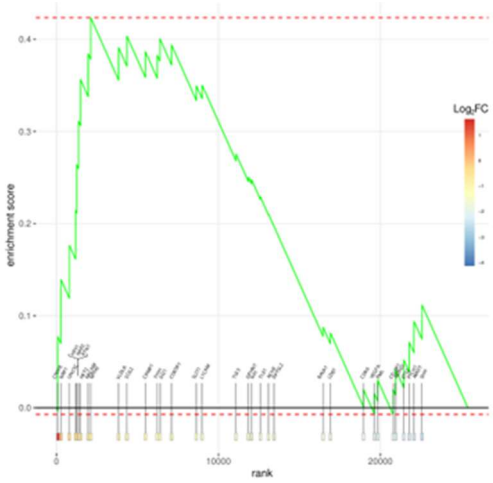

***Figure 34**: GSEA of HH in R vs NR colon cancer patients from publicly available TCGA datasets (TCGA-READ, TCGA-COAD).*

4.6. JC19 Enhances 5-FU Efficacy in CRC Xenograft mouse Models

These results were validated in an *in vivo* CRC xenograft model obtained by subcutaneously injecting HCT8 cells into the flanks of Fox1 nu/nu mice. Once tumors became palpable, mice were randomized and treated for two weeks with 5-FU or JC19 as monotherapy, or with a combination of the two treatments, as reported in the scheme in (*Figure 35*).

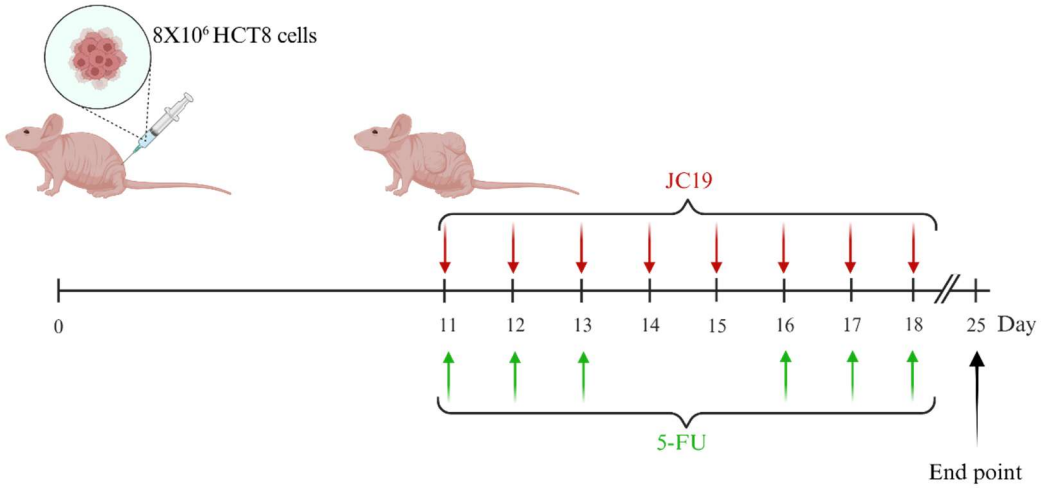

***Figure 35**: 8 × 106 HCT8 cells were injected into the flanks of nu/nu mice. When tumors became palpable (day 11) mice were randomly divided in 4 groups (n = 6) and treated for 2 weeks as reported: Vehicle, 5-FU (25 mg/kg), JC19 (15 mg/ kg) and a combination of both.*

As shown by tumor growth curves, ultrasound images, and tumor weight of excised tumors at the experiment endpoint, combining JC19 with 5-FU was more effective in impairing xenograft growth than 5-FU treatment alone (*Figure 36A-Figure 36C*).

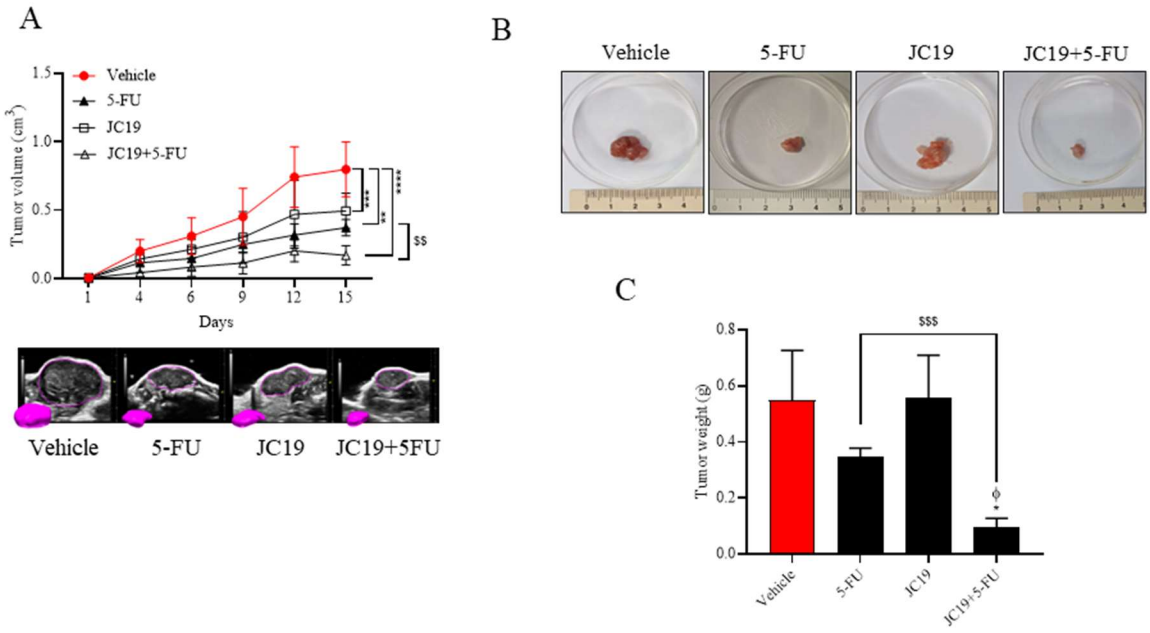

***Figure 36**: **A)** Tumor growth curve in mice treated as described in X figure. Day 1 represents treatment start; analysis of tumor volume by Vevo LAZR-X photoacoustic imaging (lower panel) at the end point of the in vivo experiment. Three-dimensional rendering of ultrasound images of representative subcutaneous tumor masses is shown in the insert. t-test; ** p < 0.01, *** p < 0.001, **** p < 0.0001; $$ p < 0.001. **B)** Representative images of dissected tumor samples. **C)** Tumor weight of explanted tumors. t-test; * p < 0.05; $$$ p < 0.001. φ indicates synergistic effect (Bliss test > 0) with respect to single treatments.*

In agreement with these results, immunohistochemical (IHC) staining revealed a significant reduction of Ki67-positive cells in tumor sections from combination-treated mice compared to those receiving single-drug treatments (*Figure 37*).

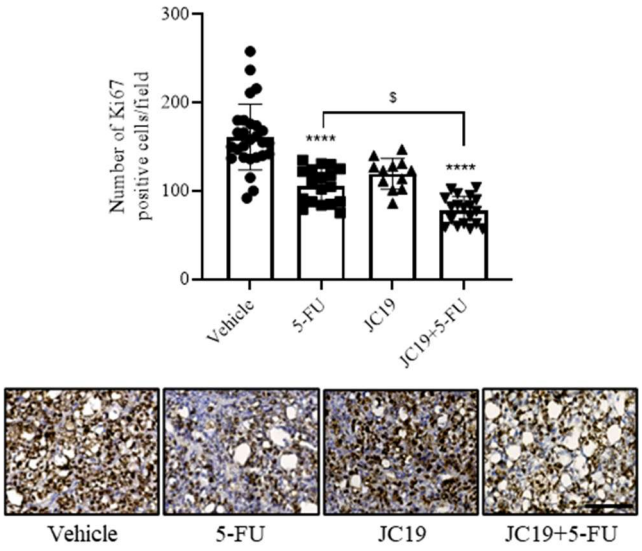

Figure 37*: Ki67 positive cells by immunostaining assay in tumor slices from mice treated. Representative staining of Ki67 and H&E is shown below the bargraph (magnification 40 ×, scale bar: 50 μm); t-test; **** $p < 0.0001$; $ $p < 0.05$*

The efficacy of the combination treatment was further confirmed by testing the activation/expression of proteins involved in proliferation and survival through western blotting analysis (*Figure 38A*). In particular, lower activation of key proteins such as phospho-ERK 1/2, phospho-P38, and c-Myc was observed combining 5-FU with JC19. Similarly, qPCR analysis conducted on tumor tissues highlighted strong downregulation of genes involved in invasion (SNAIL, VIM, ZEB1, ZEB2), cancer stem cells (CD133, EpCAM, NANOG, SOX2, KLF4, OCT4), and the HH pathway (ABCB1, GLI2, BCL2, VEGF-A) in the combination group compared to single drug treatments (*Figure 38B*).

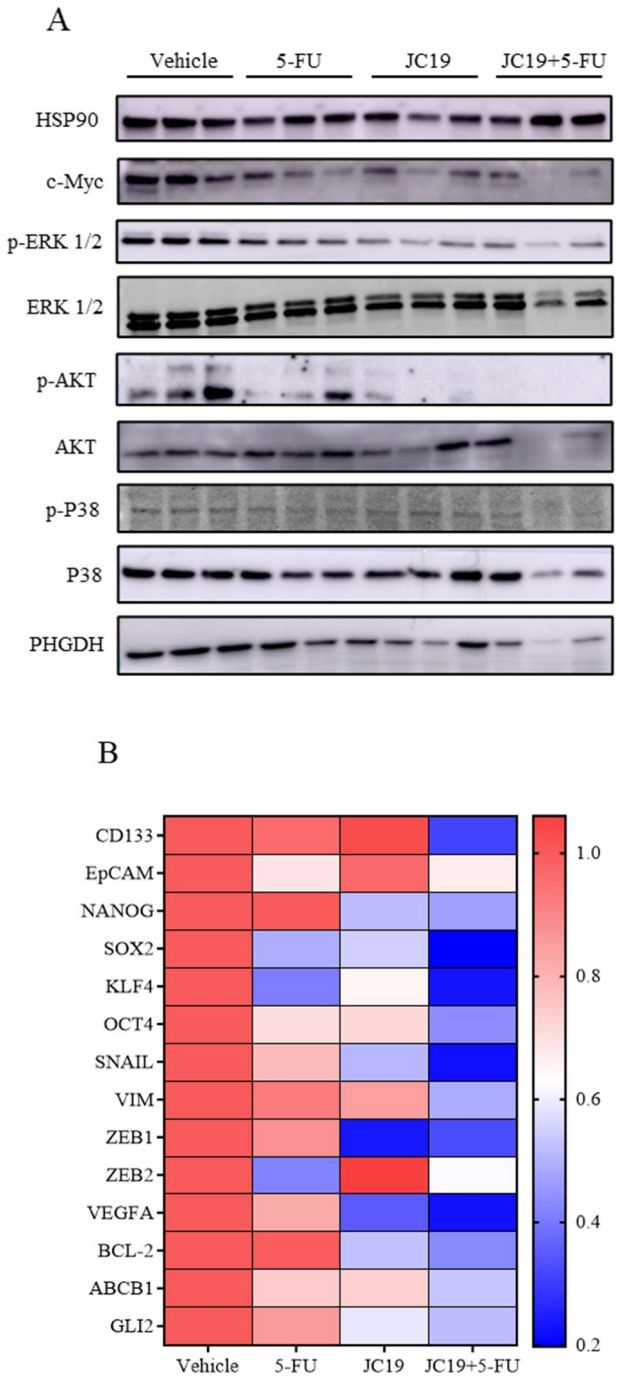

***Figure 38**: **A)** Immunoblot of proteins involved in proliferation and survival in explanted tumors. HSP90 immunoblot was performed to ensure equal loading. **B)** Heatmap plot of differentially expressed genes in tumor tissues from vehicle, 5-FU, JC19 and combo treated mice. Vehicle group was used as comparator. Gene expression levels are expressed in colour code from blue (low) to red (high) according to the colour key scale bar (n = 3 per group).*

Interestingly, a significant decrease in PHGDH expression was also confirmed in tumor tissues from mice treated with JC19 alone or with the combination (*Figure 38A*). Overall, these results demonstrated that combining 5-FU with inhibition of HH signaling synergistically decreased CRC xenograft growth in nude mice.

Chapter 5. DISCUSSION

In recent years, serine metabolism has emerged as a central player in tumor biology. PHGDH - the rate-limiting enzyme of the serine biosynthetic pathway - plays a fundamental role not only in supporting anabolic demands of neoplastic cells but also in activating adaptive mechanisms that enable tumor survival under metabolic and therapeutic stress (45). The data obtained in this thesis confirm and expand these observations, establishing PHGDH as a critical determinant of 5-FU resistance in CRC and identifying a previously uncharacterized PHGDH/HH axis. Through a series of experiments using CRC cell lines, patient-derived organoids, patient tissue samples, and xenograft mouse models, this study shows that PHGDH expression levels have a direct impact on the effectiveness of 5-FU-based chemotherapy. High PHGDH expression is linked to reduced treatment response, while lower levels improve sensitivity to the drug. These findings reveal a targetable weakness in chemoresistant tumors that could be exploited to enhance the success of current treatments.

The initial observation of heterogeneity in PHGDH expression in CRC tumor tissues and in PDCOs represents a fundamental discovery with significant translational implications. In contrast to the adjacent normal tissues, which showed relatively homogeneous PHGDH levels, tumor samples exhibited significant variability. This heterogeneity suggests that PHGDH expression is regulated by complex mechanisms during malignant transformation and tumor progression. Interesting, all four patients who developed disease recurrence showed elevated PHGDH levels, suggesting its potential as a prognostic biomarker. However, larger cohort studies with longer follow-up are needed to confirm this association. The retrospective analysis revealed that patients with higher PHGDH expression were significantly more prevalent in the non-responder group compared to responders. Kaplan-Meier survival analysis further corroborated these findings, demonstrating that elevated PHGDH expression was associated with reduced overall survival and reduced relapse-free survival. These data provided independent validation, showing that high PHGDH expression correlates with poorer clinical outcomes. Collectively, these clinical observations support the hypothesis that PHGDH expression levels may influence therapeutic response and disease outcomes in CRC patients. This establishes a strong rationale for studying how PHGDH mediates chemoresistance. These findings are also in line with reports from other cancers, where high PHGDH levels have been linked to more aggressive behavior, greater cellular

plasticity, and resistance to treatment (146) Based on these clinical observations, other studies confirmed that PHGDH plays a central role in promoting aggressive features and therapy resistance in CRC. Specifically, PHGDH expression was found to influence cellular sensitivity to 5-FU, modulate DNA damage responses and enhance hallmarks associated with tumor aggressiveness, including clonogenicity, invasion and stemness. These findings suggest that PHGDH plays a dual role in cancer biology, supporting not only metabolic adaptation but also contributing to the maintenance of cancer stem-like cells, critical for resistance to chemotherapy. Its association with increased expression of stemness and EMT markers further reinforces its role in driving tumor plasticity and therapeutic evasion, in line with observations in other tumors (147). Collectively, these data highlight PHGDH as a potential therapeutic target for overcoming chemoresistance and limiting tumor progression in CRC. To elucidate the molecular mechanisms underlying PHGDH-mediated aggressive phenotypes and chemoresistance, transcriptomic profiling was performed. Most notably, the HH signaling cascade emerged as one of the most significantly suppressed pathways following PHGDH silencing—a finding particularly intriguing given the well-established role of HH signaling in maintaining cancer stem cell properties and promoting chemoresistance across multiple malignancies. Targeted validation through qPCR and western blot analyses confirmed that PHGDH expression positively correlated with expression of key HH pathway, including GLI1, GLI2, and PTCH1, across multiple CRC cell lines and PDCOs. Downstream targets of HH signaling were consistently upregulated in high-PHGDH-expressing cells and downregulated following PHGDH silencing, consolidating the link between PHGDH and HH pathway activation. The mechanistic connection between PHGDH and HH signaling was further substantiated by immunoprecipitation experiments demonstrating physical interaction between PHGDH and c-Myc within the nuclear compartment. Given that c-Myc is both a target and a regulator of HH signaling, and that nuclear PHGDH has been reported to modulate transcriptional programs through interactions with transcription factors such as FOXM1 in glioma (75), these findings suggest that PHGDH may influence HH pathway activity through both metabolic and non-metabolic mechanisms. The nuclear localization of PHGDH and its interaction with transcription factors support a role in transcription regulation beyond its canonical metabolic function. This aligns with emerging evidence that metabolic enzymes can possess moonlighting functions, with PHGDH participating in transcriptional complexes that influence gene expression independently of its enzymatic activity (148).

Based on these observations, an integrated model can be proposed in which PHGDH, beyond its canonical role in serine biosynthesis, exerts a crucial non-metabolic function in transcriptional regulation and therapeutic response. Within the nucleus, PHGDH interacts with c-Myc to promote the transcriptional activation of genes involved in proliferation, stress response, and chemoresistance. Concurrently, activation of the HH pathway sustains a stem-like phenotype and promotes tumor survival under drug-induced stress, establishing a PHGDH–GLI1 axis that drives 5-FU resistance. These interactions position PHGDH at the intersection of metabolism, transcription, and nuclear signaling, suggesting that its inhibition could generate synergistic therapeutic effects through the repression of convergent oncogenic pathways. While PHGDH-mediated serine production supports one-carbon metabolism, nucleotide biosynthesis, and redox homeostasis—factors that could indirectly modulate signaling pathway activity—the physical interaction between PHGDH and c-Myc indicates a direct involvement in transcriptional complexes. The relative contributions of metabolic versus non-metabolic PHGDH functions to chemoresistance remain to be fully elucidated and require further studies employing catalytically inactive PHGDH mutants or metabolite supplementation experiments. The functional significance of HH pathway activation in PHGDH-mediated chemoresistance was confirmed through pharmacological intervention experiments. GLI1 silencing and pharmacological inhibition with JC19 and GANT61 resulted in decreased PHGDH expression and enhanced sensitivity to 5-FU. Treatment with these GLI inhibitors potentiated the cytotoxic effects of 5-FU in CRC cell lines and patient-derived organoids, with the strongest synergistic effects observed in models characterized by high PHGDH expression. In contrast, low-PHGDH-expressing cells and organoids derived minimal additional benefit from GLI inhibitor co-treatment, indicating that the therapeutic efficacy of targeting HH signaling to overcome 5-FU resistance is context-dependent. Consequently, PHGDH expression status could serve as a predictive biomarker for patient stratification in future clinical trials evaluating HH inhibitor combinations. Supporting the translational relevance of these findings, analysis of TCGA data focusing on CRC patients who received 5-FU-based chemotherapy revealed significant upregulation of HH signaling in non-responders compared with responders, underscoring the association between HH pathway activation and therapeutic failure in human patients. *In vivo* validation conducted on HCT8 murine xenograft models further corroborated these findings and established the preclinical efficacy of combining HH pathway inhibition with 5-FU chemotherapy. Combined treatment with 5-FU and JC19

was significantly more effective in suppressing tumor growth compared to either single treatment, as demonstrated by high-frequency ultrasound imaging, tumor volume measurements, growth curves, and excised tumor weight. Immunohistochemical analysis revealed reduced Ki67 proliferation index in combination-treated tumors, while western blot analysis demonstrated decreased activation of key proliferation and survival signaling pathways including ERK1/2, P38, and c-Myc. Molecular profiling through qPCR and western blot confirmed substantial downregulation of genes associated with invasion, EMT, stemness, and HH pathway activity in tumors receiving combination therapy. Notably, PHGDH expression itself was significantly reduced in tumors from mice treated with JC19 alone or in combination with 5-FU, providing *in vivo* confirmation of the reciprocal regulatory relationship between GLI1 and PHGDH and supporting the hypothesis of a reciprocal functional control between the enzyme and the HH pathway. The ability of GLI inhibition to suppress PHGDH expression in the tumor microenvironment suggests that this combination strategy may produce durable responses by disrupting the positive feedback loop that sustains chemoresistant phenotypes.

The findings from this study have several important clinical implications and open new therapeutic opportunities. First, PHGDH expression assessment in tumor biopsies could potentially serve as a predictive biomarker to identify CRC patients who are likely to respond poorly to 5-FU-based chemotherapy and who might benefit from alternative or intensified treatment strategies. Second, the demonstration that GLI inhibitors synergize with 5-FU specifically in high-PHGDH tumors provides a rational basis for biomarker-directed clinical trial design. The current landscape of HH pathway inhibitors includes FDA-approved Smoothened (SMO) inhibitors such as vismodegib and sonidegib for basal cell carcinoma (123). However, resistance to SMO inhibitors can develop through SMO mutations or activation of non-canonical HH signaling that bypasses SMO. GLI inhibitors offer the theoretical advantage of targeting downstream transcriptional effectors, potentially overcoming SMO inhibitor resistance, although clinical development has been hampered by chemical instability and pharmacological limitations (131). An alternative or complementary therapeutic strategy could involve direct targeting of PHGDH itself. Several PHGDH inhibitors have been developed and shown preclinical efficacy and given that high PHGDH expression appears to be a driver of chemoresistance rather than merely a marker, pharmacological PHGDH inhibition combined with 5-FU could potentially provide similar or superior benefit compared to GLI inhibitor

combinations. Furthermore, dietary interventions involving serine and glycine restriction have shown promise in preclinical models and could represent a low-toxicity adjunct to chemotherapy, particularly for tumors highly dependent on PHGDH-mediated serine biosynthesis. The identification of molecules capable of simultaneously interfering with PHGDH and Hedgehog pathway factors could represent the starting point for the development of personalized therapies and clinical trials aimed at improving prognosis and quality of life of oncology patients with tumors resistant to conventional treatments.

Several limitations of this study should be acknowledged to provide context for interpretation and future directions. While patient-derived organoid models offer substantial advantages over traditional cell lines by more accurately reproducing tumor heterogeneity and architecture, they still lack the complex tumor microenvironment, including immune cells, fibroblasts, and vascular components. Given that PHGDH has been reported to influence immune cell recruitment and that nuclear PHGDH can reshape the immune microenvironment in other cancer types (149), future studies employing syngeneic immunocompetent mouse models could reveal additional dimensions of PHGDH function in modulating anti-tumor immunity and chemotherapy response.

Another limitation concerns the incomplete understanding of the molecular mechanisms linking PHGDH to Hedgehog (HH) pathway activation. Although nuclear localization and c-Myc interaction provide initial evidence, further mechanistic studies—such as chromatin immunoprecipitation, metabolomic profiling to distinguish metabolic from non-metabolic contributions, and catalytic mutant rescue experiments—are required to clarify which functions predominate in mediating HH activation.

Moreover, although preliminary observations suggest that PHGDH expression correlates with disease recurrence, the patient cohort analyzed here was relatively small and the follow-up period limited. Larger retrospective and prospective studies will therefore be necessary to validate PHGDH as a reliable prognostic and predictive biomarker.

Finally, this work focused primarily on 5-FU resistance, whereas modern colorectal cancer treatment often involves combination regimens such as FOLFOX (oxaliplatin-based) or FOLFIRI (irinotecan-based). Determining whether PHGDH expression influences the response to these therapies, and whether GLI inhibitors might synergize with oxaliplatin or irinotecan, will be essential to establish broader clinical relevance. In addition, considering the increasing use of immune checkpoint inhibitors in microsatellite

instability–high CRC, exploring the potential interactions between PHGDH expression, HH signaling, and immunotherapy response represents an important avenue for future research with implications beyond chemotherapy-based combinations.

Looking ahead, further studies are needed to elucidate the molecular details of the PHGDH–HH axis and translate these findings into clinical applications. Future efforts should focus on identifying molecular partners and epigenetic regulators of nuclear PHGDH, and on clarifying whether GLI1 directly controls PHGDH transcription or acts through intermediate factors. Clinical validation in larger and more diverse patient cohorts will be essential, including the assessment of PHGDH expression in combination chemotherapy settings (FOLFOX, FOLFIRI) and its potential interaction with immunotherapy in selected subgroups. At the translational level, the development of more stable and pharmacologically optimized GLI inhibitors, along with the advancement of selective PHGDH inhibitors, will be crucial to fully exploit the therapeutic potential revealed by this study. Dietary interventions based on serine and glycine restriction could also represent a low-toxicity strategy to enhance chemotherapy efficacy, particularly in PHGDH-high tumors. Finally, mechanistic studies using catalytically inactive PHGDH mutants, metabolomic profiling, and proteomic characterization of the PHGDH–c-Myc–GLI1 complex will further clarify the relative contribution of metabolic and non-metabolic functions of PHGDH to chemoresistance. Overall, this study highlights PHGDH as a central mediator linking cancer metabolism to transcriptional control and chemoresistance, providing a foundation for future biomarker-driven and metabolism-oriented therapeutic strategies in colorectal cancer.

Chapter 6. CONCLUSIONS

This research has established PHGDH as a key element in the regulation of resistance to 5-fluorouracil in colorectal cancer, operating through both established metabolic mechanisms and non-canonical modalities involving activation of the Hedgehog signaling pathway. The comprehensive analysis performed on human samples, cellular models, patient-derived organoids, and animal models has demonstrated that high PHGDH expression levels are associated with more aggressive phenotypes, increased tumor survival, and augmented self-renewal capability, confirming the role of PHGDH as an independent predictor of poor prognosis and suboptimal therapeutic response.

The key findings can be summarized as follows: PHGDH expression exhibits marked heterogeneity in CRC patient samples and correlates with treatment response, with elevated expression associated with poor outcomes in patients receiving 5-FU-based chemotherapy and disease recurrence; PHGDH expression confers resistance to 5-FU through enhanced DNA damage repair capacity, evidenced by reduced γH2AX accumulation, alongside increased invasive potential and enrichment of cancer stem cell properties including enhanced colonosphere formation and elevated expression of stemness markers; comprehensive transcriptomic profiling identified Hedgehog signaling as a key pathway regulated by PHGDH, with expression positively correlating with GLI1, GLI2, and PTCH1 levels across multiple experimental models; a positive feedback loop exists between PHGDH and GLI1, whereby each factor promotes expression of the other, creating a self-reinforcing circuit that stabilizes chemoresistant phenotypes; pharmacological inhibition of GLI transcription factors with JC19 or GANT61 synergizes with 5-FU to overcome resistance in CRC cell lines, patient-derived organoids, and xenograft models, specifically in contexts of high PHGDH expression; *in vivo* validation demonstrated that combination treatment with 5-FU and GLI inhibitor JC19 significantly reduced tumor growth, proliferation markers, and expression of genes associated with stemness, invasion, EMT, and HH signaling, while also suppressing PHGDH expression itself.

These results suggest that combinatorial therapeutic targeting of PHGDH and the Hedgehog pathway represents an innovative and promising strategy for overcoming 5-FU chemoresistance in patients with colorectal cancer, especially in cases with high PHGDH expression. From a translational perspective, PHGDH expression assessment

could serve as a predictive biomarker to identify CRC patients unlikely to respond to standard 5-FU-based chemotherapy and who might benefit from alternative treatment strategies or combination approaches targeting HH signaling. The demonstration that GLI inhibitors restore 5-FU sensitivity specifically in high-PHGDH tumors provides a rational framework for biomarker-directed clinical trial design, potentially improving patient outcomes while avoiding unnecessary exposure to combination therapy toxicity in patients unlikely to benefit.

From a broader perspective, this work highlights the complex interplay between metabolic reprogramming and oncogenic signaling pathways in mediating therapeutic resistance. The discovery of the PHGDH-HH axis demonstrates that metabolic enzymes can influence treatment response through both catalytic functions affecting nucleotide availability and non-catalytic functions involving direct participation in transcriptional regulatory complexes. Recognition of these multifaceted roles opens new avenues for therapeutic intervention, as targeting either metabolic or signaling components of this axis can disrupt the resistance phenotype.

In light of these findings, future efforts should focus on validating PHGDH as a clinical biomarker in large patient cohorts, elucidating the detailed molecular mechanisms linking PHGDH to HH pathway regulation, and advancing clinical development of either PHGDH or GLI inhibitors suitable for combination with standard chemotherapy. Additionally, investigation of whether similar metabolic-signaling axes operate in other cancer types and therapeutic contexts could reveal generalizable principles for overcoming drug resistance through combination approaches targeting metabolism and signaling simultaneously. The identification of selective PHGDH and GLI inhibitors, alongside exploration of dietary interventions involving serine restriction, could represent the starting point for the development of personalized therapies and clinical trials aimed at improving the prognosis and quality of life of oncology patients with tumors resistant to conventional treatments. In conclusion, this study demonstrates that elevated PHGDH expression drives 5-FU resistance in colorectal cancer through activation of Hedgehog signaling and establishes proof-of-concept that pharmacological inhibition of this axis can restore chemosensitivity, providing a foundation for development of personalized treatment strategies in CRC and contributing to the growing understanding of how metabolic reprogramming influences therapeutic outcomes in cancer.

REFERENCES

1. Rawla P, Sunkara T, Barsouk A. Epidemiology of colorectal cancer: incidence, mortality, survival, and risk factors. Prz Gastroenterol [Internet]. 2019;14(2):89–103. Available from: https://pubmed.ncbi.nlm.nih.gov/31616522/

2. Xi Y, Xu P. Global colorectal cancer burden in 2020 and projections to 2040. Transl Oncol [Internet]. 2021 Oct 1; 14(10). Available from: https://pubmed.ncbi.nlm.nih.gov/34243011/

3. Toma M, Beluşică L, Stavarachi M, Apostol P, Spandole S, Radu I, et al. Rating the environmental and genetic risk factors for colorectal cancer. J Med Life [Internet]. 2012; 5(Spec Issue):152. Available from: https://pmc.ncbi.nlm.nih.gov/articles/PMC6880217/

4. Cherry LM. The genetic etiology of familial and nonfamilial colorectal cancer. Proc (Bayl Univ Med Cent) [Internet]. 2011 Apr; 24(2):139–41. Available from: https://pubmed.ncbi.nlm.nih.gov/21566761/

5. Sato Y, Tsujinaka S, Miura T, Kitamura Y, Suzuki H, Shibata C. Inflammatory Bowel Disease and Colorectal Cancer: Epidemiology, Etiology, Surveillance, and Management. Cancers (Basel) [Internet]. 2023 Aug 1; 15(16). Available from: https://pubmed.ncbi.nlm.nih.gov/37627182/

6. Song M, Garrett WS, Chan AT. Nutrients, foods, and colorectal cancer prevention. Gastroenterology [Internet]. 2015 May 1;148(6):1244-1260.e16. Available from: https://pubmed.ncbi.nlm.nih.gov/25575572/

7. B V, ER F, SR H, SE K, AC P, M L, et al. Genetic alterations during colorectal-tumor development. N Engl J Med [Internet]. 1988 Sep;319(9):525–32. Available from: https://pubmed.ncbi.nlm.nih.gov/2841597/

8. Sullivan BA, Noujaim M, Roper J. Cause, Epidemiology, and Histology of Polyps and Pathways to Colorectal Cancer. Gastrointest Endosc Clin N Am [Internet]. 2022 Apr 1;32(2):177–94. Available from: https://pubmed.ncbi.nlm.nih.gov/35361330/

9. Gore RM. Lower gastrointestinal tract tumours: diagnosis and staging strategies. Cancer Imaging [Internet]. 2005;5(1):99–102. Available from: https://pubmed.ncbi.nlm.nih.gov/16154828/

10. Gunderson LL, Jessup JM, Sargent DJ, Greene FL, Stewart AK. Revised TN categorization for colon cancer based on national survival outcomes data. J Clin Oncol [Internet]. 2010 Jan 10;28(2):264–71. Available from: https://pubmed.ncbi.nlm.nih.gov/19949014/

11. Salvatore L, Imperatori M, Arnoldi E, Carnaghi C, Cordio S, Cosimelli M, et al. Management of patients with early-stage colon cancer: Guidelines of the Italian Medical Oncology Association. ESMO Open [Internet]. 2020 Dec 1;5(6). Available from: https://pubmed.ncbi.nlm.nih.gov/33262200/

12. Baxter NN, Kennedy EB, Bergsland E, Berlin J, George TJ, Gill S, et al. Adjuvant Therapy for Stage II Colon Cancer: ASCO Guideline Update. J Clin Oncol [Internet]. 2022 Mar 10;40(8):892–910. Available from: https://pubmed.ncbi.nlm.nih.gov/34936379/

13. Chan GHJ, Chee CE. Making sense of adjuvant chemotherapy in colorectal cancer. J Gastrointest Oncol [Internet]. 2019 Dec 1;10(6):1183–92. Available from: https://pubmed.ncbi.nlm.nih.gov/31949938/

14. Neugut AI, Lin A, Raab GT, Hillyer GC, Keller D, O'Neil DS, et al. FOLFOX and FOLFIRI Use in Stage IV Colon Cancer: Analysis of SEER-Medicare Data. Clin Colorectal Cancer [Internet]. 2019 Jun 1;18(2):133–40. Available from: https://pubmed.ncbi.nlm.nih.gov/30878317/

15. Xie YH, Chen YX, Fang JY. Comprehensive review of targeted therapy for colorectal cancer. Signal Transduct Target Ther [Internet]. 2020 Dec 1 ;5(1). Available from: https://pubmed.ncbi.nlm.nih.gov/32296018/

16. Cotan HT, Emilescu RA, Iaciu CI, Orlov-Slavu CM, Olaru MC, Popa AM, et al. Prognostic and Predictive Determinants of Colorectal Cancer: A Comprehensive Review. Cancers (Basel) [Internet]. 2024 Dec 1 ;16(23). Available from: https://pubmed.ncbi.nlm.nih.gov/39682117/

17. Xu W, He Y, Wang Y, Li X, Young J, Ioannidis JPA, et al. Risk factors and risk prediction models for colorectal cancer metastasis and recurrence: an umbrella review of systematic reviews and meta-analyses of observational studies. BMC Med [Internet]. 2020 Jun 26 ;18(1):172. Available from: https://pubmed.ncbi.nlm.nih.gov/32586325/

18. Vodenkova S, Buchler T, Cervena K, Veskrnova V, Vodicka P, Vymetalkova V. 5-fluorouracil and other fluoropyrimidines in colorectal cancer: Past, present and future. Pharmacol Ther [Internet]. 2020 Feb 1 ;206. Available from: https://pubmed.ncbi.nlm.nih.gov/31756363/

19. Zhang N, Yin Y, Xu SJ, Chen WS. 5-Fluorouracil: mechanisms of resistance and reversal strategies. Molecules [Internet]. 2008 Aug ;13(8):1551–69. Available from: https://pubmed.ncbi.nlm.nih.gov/18794772/

20. Johnston PG, Kaye S. Capecitabine: a novel agent for the treatment of solid tumors. Anticancer Drugs [Internet]. 2001 ;12(8):639–46. Available from: https://pubmed.ncbi.nlm.nih.gov/11604550/

21. Biller LH, Schrag D. Diagnosis and Treatment of Metastatic Colorectal Cancer: A Review. JAMA [Internet]. 2021 Feb 16 ;325(7):669–85. Available from: https://pubmed.ncbi.nlm.nih.gov/33591350/

22. Hurwitz H, Fehrenbacher L, Novotny W, Cartwright T, Hainsworth J, Heim W, et al. Bevacizumab plus irinotecan, fluorouracil, and leucovorin for metastatic colorectal cancer. N Engl J Med [Internet]. 2004 Jun 3 ;350(23):2335–42. Available from: https://pubmed.ncbi.nlm.nih.gov/15175435/

23. Wohlhueter RM, McIvor RS, Plagemann PGW. Facilitated transport of uracil and 5-fluorouracil, and permeation of orotic acid into cultured mammalian cells. J Cell Physiol [Internet]. 1980 ;104(3):309–19. Available from: https://pubmed.ncbi.nlm.nih.gov/7419607/

24. Longley DB, Harkin DP, Johnston PG. 5-fluorouracil: mechanisms of action and clinical strategies. Nat Rev Cancer [Internet]. 2003 May ;3(5):330–8. Available from: https://pubmed.ncbi.nlm.nih.gov/12724731/

25. Mojardín L, Botet J, Quintales L, Moreno S, Salas M. New insights into the RNA-based mechanism of action of the anticancer drug 5'-fluorouracil in eukaryotic cells. PLoS One [Internet]. 2013 Nov ;8(11). Available from: https://pubmed.ncbi.nlm.nih.gov/24223771/

26. Santi D V., McHenry CS, Sommer H. Mechanism of interaction of thymidylate synthetase with 5-fluorodeoxyuridylate. Biochemistry [Internet]. 1974 Jan 1 ;13(3):471–81. Available from: https://pubmed.ncbi.nlm.nih.gov/4203910/

27. Maslarinou A, Manolopoulos VG, Ragia G. Pharmacogenomic-guided dosing of fluoropyrimidines beyond DPYD: time for a polygenic algorithm? Front Pharmacol. 2023 May 15;14:1184523.

28. Chang TH, Tsai MF, Su KY, Wu SG, Huang CP, Yu SL, et al. Slug confers resistance to the epidermal growth factor receptor tyrosine kinase inhibitor. Am J Respir Crit Care Med [Internet]. 2011 Apr 15 ;183(8):1071–9. Available from: https://www.atsjournals.org/doi/pdf/10.1164/rccm.201009-1440OC?download=true

29. Dagogo-Jack I, Shaw AT. Tumour heterogeneity and resistance to cancer therapies. Nat Rev Clin Oncol [Internet]. 2018 Feb 1 ;15(2):81–94. Available from: https://pubmed.ncbi.nlm.nih.gov/29115304/

30. Sun L, Ke J, He Z, Chen Z, Huang Q, Ai W, et al. HES1 Promotes Colorectal Cancer Cell Resistance To 5-Fu by Inducing Of EMT and ABC Transporter Proteins. J Cancer [Internet]. 2017 ;8(14):2802–8. Available from: https://pubmed.ncbi.nlm.nih.gov/28928869/

31. Kreso A, O'Brien CA, Van Galen P, Gan OI, Notta F, Brown AMK, et al. Variable clonal repopulation dynamics influence chemotherapy response in colorectal cancer. Science [Internet]. 2013 Feb 1 ;339(6119):543–8. Available from: https://pubmed.ncbi.nlm.nih.gov/23239622/

32. Gmeiner WH, Okechukwu CC. Review of 5-FU resistance mechanisms in colorectal cancer: clinical significance of attenuated on-target effects. Cancer Drug Resist [Internet]. 2023 ;6(2):257–72. Available from: https://pubmed.ncbi.nlm.nih.gov/37457133/

33. Chu E, Koeller DM, Casey JL, Drake JC, Chabner BA, Elwood PC, et al. Autoregulation of human thymidylate synthase messenger RNA translation by thymidylate synthase. Proc Natl Acad Sci U S A [Internet]. 1991 Oct 15 ;88(20):8977–81. Available from: https://pubmed.ncbi.nlm.nih.gov/1924359/

34. Varghese V, Magnani L, Harada-Shoji N, Mauri F, Szydlo RM, Yao S, et al. FOXM1 modulates 5-FU resistance in colorectal cancer through regulating TYMS expression. Sci Rep [Internet]. 2019 Dec 1 ;9(1). Available from: https://pubmed.ncbi.nlm.nih.gov/30728402/

35. Evrard A, Cuq P, Ciccolini J, Vian L, Cano JP. Increased cytotoxicity and bystander effect of 5-fluorouracil and 5-deoxy-5-fluorouridine in human colorectal cancer cells transfected with thymidine phosphorylase. Br J Cancer [Internet]. 1999 ;80(11):1726–33. Available from: https://pubmed.ncbi.nlm.nih.gov/10468288/

36. Leguisamo NM, Gloria HC, Kalil AN, Martins T V., Azambuja DB, Meira LB, et al. Base excision repair imbalance in colorectal cancer has prognostic value and modulates response to chemotherapy. Oncotarget [Internet]. 2017 ;8(33):54199–214. Available from: https://pubmed.ncbi.nlm.nih.gov/28903334/

37. Tajima A, Hess MT, Cabrera BL, Kolodner RD, Carethers JM. The mismatch repair complex hMutSα recognizes 5-fluorouracil-modified DNA: Implications for chemosensitivity and resistance. Gastroenterology [Internet]. 2004 ;127(6):1678–84. Available from: https://pubmed.ncbi.nlm.nih.gov/15578504/

38. Adamsen BL, Kravik KL, De Angelis PM. DNA damage signaling in response to 5-fluorouracil in three colorectal cancer cell lines with different mismatch repair and TP53 status. Int J Oncol [Internet]. 2011 Sep ;39(3):673–82. Available from: https://pubmed.ncbi.nlm.nih.gov/21674128/

39. Källberg J, Harrison A, March V, Bērziņa S, Nemazanyy I, Kepp O, et al. Intratumor heterogeneity and cell secretome promote chemotherapy resistance and progression of colorectal cancer. Cell Death Dis [Internet]. 2023 May 1 ;14(5). Available from: https://pubmed.ncbi.nlm.nih.gov/37142595/

40. Pavlides S, Whitaker-Menezes D, Castello-Cros R, Flomenberg N, Witkiewicz AK, Frank PG, et al. The reverse Warburg effect: aerobic glycolysis in cancer associated fibroblasts and the tumor stroma. Cell Cycle [Internet]. 2009 Dec 1 ;8(23):3984–4001. Available from: https://pubmed.ncbi.nlm.nih.gov/19923890/

41. Denise C, Paoli P, Calvani M, Taddei ML, Giannoni E, Kopetz S, et al. 5-fluorouracil resistant colon cancer cells are addicted to OXPHOS to survive and enhance stem-like traits. Oncotarget [Internet]. 2015 ;6(39):41706–21. Available from: https://pubmed.ncbi.nlm.nih.gov/26527315/

42. Vellinga TT, De Boer VCJ, Fatrai S, Van Schelven S, Trumpi K, Verheem A, et al. SIRT1/PGC1α-Dependent Increase in Oxidative Phosphorylation Supports Chemotherapy Resistance of Colon Cancer. Clin Cancer Res [Internet]. 2015 Jun 15 ;21(12):2870–9. Available from: https://pubmed.ncbi.nlm.nih.gov/25779952/

43. Pranzini E, Pardella E, Muccillo L, Leo A, Nesi I, Santi A, et al. SHMT2-mediated mitochondrial serine metabolism drives 5-FU resistance by fueling nucleotide biosynthesis. Cell Rep [Internet]. 2022 Aug 16 ;40(7). Available from: https://pubmed.ncbi.nlm.nih.gov/35977477/

44. Montrose DC, Saha S, Foronda M, McNally EM, Chen J, Zhou XK, et al. Exogenous and Endogenous Sources of Serine Contribute to Colon Cancer Metabolism, Growth, and Resistance to 5-Fluorouracil. Cancer Res [Internet]. 2021 May 1 ;81(9):2275–88. Available from: https://pubmed.ncbi.nlm.nih.gov/33526512/

45. Rathore R, Schutt CR, van Tine BA. PHGDH as a mechanism for resistance in metabolically-driven cancers. Cancer Drug Resist [Internet]. 2020 ;3(4):762–74. Available from: https://pubmed.ncbi.nlm.nih.gov/33511334/

46. Jia XQ, Zhang S, Zhu HJ, Wang W, Zhu JH, Wang XD, et al. Increased expression of PHGDH and prognostic significance in colorectal cancer. Transl Oncol [Internet]. 2016 Jun 1 ;9(3):191–6. Available from: https://pubmed.ncbi.nlm.nih.gov/27267836/

47. Locasale JW, Grassian AR, Melman T, Lyssiotis CA, Mattaini KR, Bass AJ, et al. Phosphoglycerate dehydrogenase diverts glycolytic flux and contributes to oncogenesis. Nat Genet [Internet]. 2011 Sep ;43(9):869–74. Available from: https://pubmed.ncbi.nlm.nih.gov/21804546/

48. Ravez S, Spillier Q, Marteau R, Feron O, Frédérick R. Challenges and Opportunities in the Development of Serine Synthetic Pathway Inhibitors for Cancer Therapy. J Med Chem [Internet]. 2017 Feb 23 ;60(4):1227–37. Available from: https://pubmed.ncbi.nlm.nih.gov/27959531/

49. Weinstabl H, Treu M, Rinnenthal J, Zahn SK, Ettmayer P, Bader G, et al. Intracellular Trapping of the Selective Phosphoglycerate Dehydrogenase (PHGDH) Inhibitor BI-4924 Disrupts Serine Biosynthesis. J Med Chem [Internet]. 2019 Sep 12 ;62(17):7976–97. Available from: https://pubmed.ncbi.nlm.nih.gov/31365252/

50. Zhao X, Fu J, Tang W, Yu L, Xu W. Inhibition of Serine Metabolism Promotes Resistance to Cisplatin in Gastric Cancer. Onco Targets Ther [Internet]. 2020 ;13:4833–42. Available from: https://pubmed.ncbi.nlm.nih.gov/32581546/

51. Pacold ME, Brimacombe KR, Chan SH, Rohde JM, Lewis CA, Swier LJYM, et al. A PHGDH inhibitor reveals coordination of serine synthesis and one-carbon unit fate. Nat Chem Biol [Internet]. 2016 Jun 1 ;12(6):452–8. Available from: https://pubmed.ncbi.nlm.nih.gov/27110680/

52. Furuya S. An essential role for de novo biosynthesis of L-serine in CNS development. Asia Pac J Clin Nutr. 2008;17(S1):312–5.

53. Yang M, Vousden KH. Serine and one-carbon metabolism in cancer. Nat Rev Cancer [Internet]. 2016 Sep 23 ;16(10):650–62. Available from: https://pubmed.ncbi.nlm.nih.gov/27634448/

54. De Koning TJ, Klomp LWJ. Serine-deficiency syndromes. Curr Opin Neurol [Internet]. 2004 Apr ;17(2):197–204. Available from: https://pubmed.ncbi.nlm.nih.gov/15021249/

55. Geeraerts SL, Heylen E, De Keersmaecker K, Kampen KR. The ins and outs of serine and glycine metabolism in cancer. Nat Metab [Internet]. 2021 Feb 1 ;3(2):131–41. Available from: https://pubmed.ncbi.nlm.nih.gov/33510397/

56. Hosios AM, Hecht VC, Danai L V., Johnson MO, Rathmell JC, Steinhauser ML, et al. Amino Acids Rather than Glucose Account for the Majority of Cell Mass in Proliferating Mammalian Cells. Dev Cell [Internet]. 2016 Mar 7 ;36(5):540–9. Available from: https://pubmed.ncbi.nlm.nih.gov/26954548/

57. Labuschagne CF, van den Broek NJF, Mackay GM, Vousden KH, Maddocks ODK. Serine, but not glycine, supports one-carbon metabolism and proliferation of cancer cells. Cell Rep [Internet]. 2014 May 22 ;7(4):1248–58. Available from: https://pubmed.ncbi.nlm.nih.gov/24813884/

58. Maddocks ODK, Berkers CR, Mason SM, Zheng L, Blyth K, Gottlieb E, et al. Serine starvation induces stress and p53-dependent metabolic remodelling in cancer cells. Nature [Internet]. 2013 Jan 24 ;493(7433):542–6. Available from: https://pubmed.ncbi.nlm.nih.gov/23242140/

59. Chaneton B, Hillmann P, Zheng L, Martin ACL, Maddocks ODK, Chokkathukalam A, et al. Serine is a natural ligand and allosteric activator of pyruvate kinase M2. Nature [Internet]. 2012 Nov 15 ;491(7424):458–62. Available from: https://pubmed.ncbi.nlm.nih.gov/23064226/

60. Ye J, Mancuso A, Tong X, Ward PS, Fan J, Rabinowitz JD, et al. Pyruvate kinase M2 promotes de novo serine synthesis to sustain mTORC1 activity and cell proliferation. Proc Natl Acad Sci U S A [Internet]. 2012 May 1 ;109(18):6904–9. Available from: https://pubmed.ncbi.nlm.nih.gov/22509023/

61. Hitosugi T, Zhou L, Elf S, Fan J, Kang HB, Seo JH, et al. Phosphoglycerate Mutase 1 Coordinates Glycolysis and Biosynthesis to Promote Tumor Growth. Cancer Cell [Internet]. 2012 Nov 13 ;22(5):585–600. Available from: https://pubmed.ncbi.nlm.nih.gov/23153533/

62. DeNicola GM, Chen PH, Mullarky E, Sudderth JA, Hu Z, Wu D, et al. NRF2 regulates serine biosynthesis in non-small cell lung cancer. Nat Genet [Internet]. 2015 Dec 1 ;47(12):1475–81. Available from: https://pubmed.ncbi.nlm.nih.gov/26482881/

63. Tedeschi PM, Markert EK, Gounder M, Lin H, Dvorzhinski D, Dolfi SC, et al. Contribution of serine, folate and glycine metabolism to the ATP, NADPH and purine requirements of cancer cells. Cell Death Dis [Internet]. 2013 Oct ;4(10). Available from: https://pubmed.ncbi.nlm.nih.gov/24157871/

64. Glasauer A, Chandel NS. Targeting antioxidants for cancer therapy. Biochem Pharmacol [Internet]. 2014 Nov 1 ;92(1):90–101. Available from: https://pubmed.ncbi.nlm.nih.gov/25078786/

65. Gorrini C, Harris IS, Mak TW. Modulation of oxidative stress as an anticancer strategy. Nat Rev Drug Discov [Internet]. 2013 Dec ;12(12):931–47. Available from: https://pubmed.ncbi.nlm.nih.gov/24287781/

66. Maddocks ODK, Labuschagne CF, Adams PD, Vousden KH. Serine Metabolism Supports the Methionine Cycle and DNA/RNA Methylation through De Novo ATP Synthesis in Cancer Cells. Mol Cell [Internet]. 2016 Jan 21 ;61(2):210–21. Available from: https://pubmed.ncbi.nlm.nih.gov/26774282/

67. Snell K. Enzymes of serine metabolism in normal, developing and neoplastic rat tissues. Adv Enzyme Regul [Internet]. 1984 ;22(C):325–400. Available from: https://pubmed.ncbi.nlm.nih.gov/6089514/

68. Newman AC, Maddocks ODK. Serine and Functional Metabolites in Cancer. Trends Cell Biol [Internet]. 2017 Sep 1 ;27(9):645–57. Available from: https://pubmed.ncbi.nlm.nih.gov/28601431/

69. Tajan M, Vousden KH. Dietary Approaches to Cancer Therapy. Cancer Cell [Internet]. 2020 Jun 8 ;37(6):767–85. Available from: https://pubmed.ncbi.nlm.nih.gov/32413275/

70. Tajan M, Hennequart M, Cheung EC, Zani F, Hock AK, Legrave N, et al. Serine synthesis pathway inhibition cooperates with dietary serine and glycine limitation for cancer therapy. Nat Commun [Internet]. 2021 Dec 1 ;12(1). Available from: https://pubmed.ncbi.nlm.nih.gov/33446657/

71. Dong JK, Lei HM, Liang Q, Tang Y Bin, Zhou Y, Wang Y, et al. Overcoming erlotinib resistance in EGFR mutation-positive lung adenocarcinomas through repression of phosphoglycerate dehydrogenase. Theranostics [Internet]. 2018 ;8(7):1808–23. Available from: https://pubmed.ncbi.nlm.nih.gov/29556358/

72. Wu X, Xia J, Zhang J, Zhu Y, Wu Y, Guo J, et al. Phosphoglycerate dehydrogenase promotes proliferation and bortezomib resistance through increasing reduced glutathione synthesis in multiple myeloma. Br J Haematol [Internet]. 2020 Jul 1 ;190(1):52–66. Available from: https://pubmed.ncbi.nlm.nih.gov/32037523/

73. Annibali D, Fendt SM. Nuclear PHGDH protects cancer cells from nutrient stress. Nat Metab [Internet]. 2021 Oct 1 ;3(10):1284–5. Available from: https://pubmed.ncbi.nlm.nih.gov/34663972/

74. Ma C, Zheng K, Jiang K, Zhao Q, Sha N, Wang W, et al. The alternative activity of nuclear PHGDH contributes to tumour growth under nutrient stress. Nat Metab [Internet]. 2021 Oct 1 ;3(10):1357–71. Available from: https://pubmed.ncbi.nlm.nih.gov/34663976/

75. Liu J, Guo S, Li Q, Yang L, Xia Z, Zhang L, et al. Phosphoglycerate dehydrogenase induces glioma cells proliferation and invasion by stabilizing forkhead box M1. J Neurooncol [Internet]. 2013 ;111(3):245–55. Available from: https://pubmed.ncbi.nlm.nih.gov/23229761/

76. Zhu H, Yu H, Zhou H, Zhu W, Wang X. Elevated Nuclear PHGDH Synergistically Functions with cMyc to Reshape the Immune Microenvironment of Liver Cancer. Adv Sci (Weinh) [Internet]. 2023 Jun 13 ;10(17). Available from: https://pubmed.ncbi.nlm.nih.gov/37078828/

77. Pacold ME, Brimacombe KR, Chan SH, Rohde JM, Lewis CA, Swier LJYM, et al. A PHGDH inhibitor reveals coordination of serine synthesis and one-carbon unit fate. Nat Chem Biol [Internet]. 2016 Jun 1 ;12(6):452–8. Available from: https://pubmed.ncbi.nlm.nih.gov/27110680/

78. Mullarky E, Mattaini KR, Vander Heiden MG, Cantley LC, Locasale JW. PHGDH amplification and altered glucose metabolism in human melanoma. Pigment Cell Melanoma Res [Internet]. 2011 Dec ;24(6):1112–5. Available from: https://pubmed.ncbi.nlm.nih.gov/21981974/

79. Osborn MJ, Freeman M, Huennekens FM. Inhibition of Dihydrofolic Reductase by Aminopterin and Amethopterin. Proceedings of the Society for Experimental Biology and Medicine [Internet]. 1958 ;97(2):429–31. Available from: https://pubmed.ncbi.nlm.nih.gov/13518295/

80. Gonen N, Assaraf YG. Antifolates in cancer therapy: structure, activity and mechanisms of drug resistance. Drug Resist Updat [Internet]. 2012 ;15(4):183–210. Available from: https://pubmed.ncbi.nlm.nih.gov/22921318/

81. Ducker GS, Chen L, Morscher RJ, Ghergurovich JM, Esposito M, Teng X, et al. Reversal of Cytosolic One-Carbon Flux Compensates for Loss of the Mitochondrial Folate Pathway. Cell Metab [Internet]. 2016 Jun 14 ;23(6):1140–53. Available from: https://pubmed.ncbi.nlm.nih.gov/27211901/

82. Ma X, Li B, Liu J, Fu Y, Luo Y. Phosphoglycerate dehydrogenase promotes pancreatic cancer development by interacting with eIF4A1 and eIF4E. J Exp Clin Cancer Res [Internet]. 2019 Feb 11 ;38(1). Available from: https://pubmed.ncbi.nlm.nih.gov/30744688/

83. Shu Y, Hao Y, Feng J, Liu H, Li S, Feng J, et al. Non-canonical phosphoglycerate dehydrogenase activity promotes liver cancer growth via mitochondrial translation and respiratory metabolism. EMBO J [Internet]. 2022 Dec ;41(23). Available from: https://pubmed.ncbi.nlm.nih.gov/36314841/

84. Chen J, Chung F, Yang GG, Pu M, Gao H, Jiang W, et al. Phosphoglycerate dehydrogenase is dispensable for breast tumor maintenance and growth. Oncotarget [Internet]. 2013 ;4(12):2502–11. Available from: https://pubmed.ncbi.nlm.nih.gov/24318446/

85. Cavodeassi F, Creuzet S, Etchevers HC. The hedgehog pathway and ocular developmental anomalies. Hum Genet [Internet]. 2019 Sep 11 ;138(8–9):917–36. Available from: https://pubmed.ncbi.nlm.nih.gov/30073412/

86. Dessaud E, McMahon AP, Briscoe J. Pattern formation in the vertebrate neural tube: a sonic hedgehog morphogen-regulated transcriptional network. Development [Internet]. 2008 Aug ;135(15):2489–503. Available from: https://pubmed.ncbi.nlm.nih.gov/18621990/

87. Le H, Kleinerman R, Lerman OZ, Brown D, Galiano R, Gurtner GC, et al. Hedgehog signaling is essential for normal wound healing. Wound Repair Regen [Internet]. 2008 Nov ;16(6):768–73. Available from: https://pubmed.ncbi.nlm.nih.gov/19128247/

88. Lowry WE, Richter L, Yachechko R, Pyle AD, Tchieu J, Sridharan R, et al. Generation of human induced pluripotent stem cells from dermal fibroblasts. Proc Natl Acad Sci U S A [Internet]. 2008 Feb 26 ;105(8):2883–8. Available from: https://pubmed.ncbi.nlm.nih.gov/18287077/

89. Huangfu D, Liu A, Rakeman AS, Murcia NS, Niswander L, Anderson K V. Hedgehog signalling in the mouse requires intraflagellar transport proteins. Nature [Internet]. 2003 Nov 6 ;426(6962):83–7. Available from: https://pubmed.ncbi.nlm.nih.gov/14603322/

90. Denef N, Neubüser D, Perez L, Cohen SM. Hedgehog induces opposite changes in turnover and subcellular localization of patched and smoothened. Cell [Internet]. 2000 Aug 18 ;102(4):521–31. Available from: https://pubmed.ncbi.nlm.nih.gov/10966113/

91. Yue S, Tang LY, Tang Y, Tang Y, Shen QH, Ding J, et al. Requirement of Smurf-mediated endocytosis of Patched1 in sonic hedgehog signal reception. Elife [Internet]. 2014 Jun 12 ;3(3). Available from: https://pubmed.ncbi.nlm.nih.gov/24925320/

92. Niewiadomski P, Kong JH, Ahrends R, Ma Y, Humke EW, Khan S, et al. Gli protein activity is controlled by multisite phosphorylation in vertebrate hedgehog signaling. Cell Rep [Internet]. 2014 ;6(1):168–81. Available from: https://pubmed.ncbi.nlm.nih.gov/24373970/

93. Stone DM, Murone M, Luoh SM, Ye W, Armanini MP, Gurney A, et al. Characterization of the human suppressor of fused, a negative regulator of the zinc-finger transcription factor Gli. J Cell Sci [Internet]. 1999 ;112 (Pt 23)(23):4437–48. Available from: https://pubmed.ncbi.nlm.nih.gov/10564661/

94. He M, Subramanian R, Bangs F, Omelchenko T, Liem KF, Kapoor TM, et al. The kinesin-4 protein Kif7 regulates mammalian Hedgehog signalling by organizing the cilium tip compartment. Nat Cell Biol [Internet]. 2014 ;16(7):663–72. Available from: https://pubmed.ncbi.nlm.nih.gov/24952464/

95. Ogden SK, Fei DL, Schilling NS, Ahmed YF, Hwa J, Robbins DJ. G protein Galphai functions immediately downstream of Smoothened in Hedgehog signalling. Nature [Internet]. 2008 Dec 18 ;456(7224):967–70. Available from: https://pubmed.ncbi.nlm.nih.gov/18987629/

96. Dorn K V., Hughes CE, Rohatgi R. A Smoothened-Evc2 Complex Transduces the Hedgehog Signal at Primary Cilia. Dev Cell [Internet]. 2012 Oct 16 ;23(4):823–35. Available from: https://pubmed.ncbi.nlm.nih.gov/22981989/

97. Bonifas JM, Pennypacker S, Chuang PT, McMahon AP, Williams M, Rosenthal A, et al. Activation of expression of hedgehog target genes in basal cell carcinomas. Journal of Investigative Dermatology [Internet]. 2001 ;116(5):739–42. Available from: https://pubmed.ncbi.nlm.nih.gov/11348463/

98. Duman-Scheel M, Weng L, Xin S, Du W. Hedgehog regulates cell growth and proliferation by inducing Cyclin D and Cyclin E. Nature [Internet]. 2002 May 16 ;417(6886):299–304. Available from: https://pubmed.ncbi.nlm.nih.gov/12015606/

99. Barnes EA, Kong M, Ollendorff V, Donoghue DJ. Patched1 interacts with cyclin B1 to regulate cell cycle progression. EMBO J [Internet]. 2001 May 1 ;20(9):2214–23. Available from: https://pubmed.ncbi.nlm.nih.gov/11331587/

100. Polizio AH, Chinchilla P, Chen X, Kim S, Manning DR, Riobo NA. Heterotrimeric Gi proteins link hedgehog signaling to activation of Rho small GTPases to promote fibroblast migration. Journal of Biological Chemistry [Internet]. 2011 Jun 3 ;286(22):19589–96. Available from: https://pubmed.ncbi.nlm.nih.gov/21474452/

101. Sasaki N, Kurisu J, Kengaku M. Sonic hedgehog signaling regulates actin cytoskeleton via Tiam1-Rac1 cascade during spine formation. Molecular and

Cellular Neuroscience [Internet]. 2010 Dec ;45(4):335–44. Available from: https://pubmed.ncbi.nlm.nih.gov/20654717/

102. Belgacem YH, Borodinsky LN. Sonic hedgehog signaling is decoded by calcium spike activity in the developing spinal cord. Proc Natl Acad Sci U S A [Internet]. 2011 Mar 15 ;108(11):4482–7. Available from: https://pubmed.ncbi.nlm.nih.gov/21368195/

103. Hahn H, Wicking C, Zaphiropoulos PG, Gailani MR, Shanley S, Chidambaram A, et al. Mutations of the human homolog of Drosophila patched in the nevoid basal cell carcinoma syndrome. Cell [Internet]. 1996 Jun 14 ;85(6):841–51. Available from: https://pubmed.ncbi.nlm.nih.gov/8681379/

104. Xie J, Murone M, Luoh SM, Ryan A, Gu Q, Zhang C, et al. Activating Smoothened mutations in sporadic basal-cell carcinoma. Nature [Internet]. 1998 Jan 1 ;391(6662):90–2. Available from: https://pubmed.ncbi.nlm.nih.gov/9422511/

105. Reifenberger J, Wolter M, Knobbe CB, Köhler B, Schönicke A, Scharwächter C, et al. Somatic mutations in the PTCH, SMOH, SUFUH and TP53 genes in sporadic basal cell carcinomas. Br J Dermatol [Internet]. 2005 Jan ;152(1):43–51. Available from: https://pubmed.ncbi.nlm.nih.gov/15656799/

106. Varnat F, Duquet A, Malerba M, Zbinden M, Mas C, Gervaz P, et al. Human colon cancer epithelial cells harbour active HEDGEHOG-GLI signalling that is essential for tumour growth, recurrence, metastasis and stem cell survival and expansion. EMBO Mol Med [Internet]. 2009 Sep ;1(6–7):338–51. Available from: https://pubmed.ncbi.nlm.nih.gov/20049737/

107. Kubo M, Nakamura M, Tasaki A, Yamanaka N, Nakashima H, Nomura M, et al. Hedgehog signaling pathway is a new therapeutic target for patients with breast cancer. Cancer Res [Internet]. 2004 Sep 1 ;64(17):6071–4. Available from: https://pubmed.ncbi.nlm.nih.gov/15342389/

108. Sheng T, Li C, Zhang X, Chi S, He N, Chen K, et al. Activation of the hedgehog pathway in advanced prostate cancer. Mol Cancer [Internet]. 2004 Oct 13 ;3. Available from: https://pubmed.ncbi.nlm.nih.gov/15482598/

109. Watkins DN, Berman DM, Burkholder SG, Wang B, Beachy PA, Baylin SB. Hedgehog signalling within airway epithelial progenitors and in small-cell lung cancer. Nature [Internet]. 2003 Mar 20 ;422(6929):313–7. Available from: https://pubmed.ncbi.nlm.nih.gov/12629553/

110. Szkandera J, Kiesslich T, Haybaeck J, Gerger A, Pichler M. Hedgehog signaling pathway in ovarian cancer. Int J Mol Sci [Internet]. 2013 Jan ;14(1):1179–96. Available from: https://pubmed.ncbi.nlm.nih.gov/23303278/

111. Yauch RL, Gould SE, Scales SJ, Tang T, Tian H, Ahn CP, et al. A paracrine requirement for hedgehog signalling in cancer. Nature [Internet]. 2008 Sep 18 ;455(7211):406–10. Available from: https://pubmed.ncbi.nlm.nih.gov/18754008/

112. Chen W, Tang T, Eastham-Anderson J, Dunlap D, Alicke B, Nannini M, et al. Canonical hedgehog signaling augments tumor angiogenesis by induction of VEGF-A in stromal perivascular cells. Proc Natl Acad Sci U S A [Internet]. 2011 Jun 7 ;108(23):9589–94. Available from: https://pubmed.ncbi.nlm.nih.gov/21597001/

113. Fan L, Pepicelli C V., Dibble CC, Catbagan W, Zarycki JL, Laciak R, et al. Hedgehog signaling promotes prostate xenograft tumor growth. Endocrinology [Internet]. 2004 Aug ;145(8):3961–70. Available from: https://pubmed.ncbi.nlm.nih.gov/15132968/

114. Tian H, Callahan CA, Dupree KJ, Darbonne WC, Ahn CP, Scales SJ, et al. Hedgehog signaling is restricted to the stromal compartment during pancreatic carcinogenesis. Proc Natl Acad Sci U S A [Internet]. 2009 Mar 17 ;106(11):4254–9. Available from: https://pubmed.ncbi.nlm.nih.gov/19246386/

115. Zhao C, Chen A, Jamieson CH, Fereshteh M, Abrahamsson A, Blum J, et al. Hedgehog signalling is essential for maintenance of cancer stem cells in myeloid leukaemia. Nature [Internet]. 2009 Apr 9 ;458(7239):776–9. Available from: https://pubmed.ncbi.nlm.nih.gov/19169242/

116. Cochrane CR, Szczepny A, Watkins DN, Cain JE. Hedgehog Signaling in the Maintenance of Cancer Stem Cells. Cancers (Basel) [Internet]. 2015 Aug 11 ;7(3):1554–85. Available from: https://pubmed.ncbi.nlm.nih.gov/26270676/

117. Clement V, Sanchez P, de Tribolet N, Radovanovic I, Ruiz i Altaba A. HEDGEHOG-GLI1 Signaling Regulates Human Glioma Growth, Cancer Stem Cell Self-Renewal, and Tumorigenicity. Current Biology [Internet]. 2007 Jan 23 ;17(2):165–72. Available from: https://pubmed.ncbi.nlm.nih.gov/17196391/

118. Sims-Mourtada J, Izzo JG, Ajani J, Chao KSC. Sonic Hedgehog promotes multiple drug resistance by regulation of drug transport. Oncogene [Internet]. 2007 Aug 16 ;26(38):5674–9. Available from: https://pubmed.ncbi.nlm.nih.gov/17353904/

119. Chen D, Kang X, Li Z, Chen L, Ma Q, Fan P. Hedgehog/GLI1 signaling pathway regulates the resistance to cisplatin in human osteosarcoma. J Cancer [Internet]. 2021 ;12(22):6676–84. Available from: https://pubmed.ncbi.nlm.nih.gov/34659557/

120. Das S, Samant RS, Shevde LA. Nonclassical activation of Hedgehog signaling enhances multidrug resistance and makes cancer cells refractory to smoothened-targeting Hedgehog inhibition. Journal of Biological Chemistry [Internet]. 2013 Apr 26 ;288(17):11824–33. Available from: https://pubmed.ncbi.nlm.nih.gov/23508962/

121. Wu X, Zhang LS, Toombs J, Kuo YC, Piazza JT, Tuladhar R, et al. Extra-mitochondrial prosurvival BCL-2 proteins regulate gene transcription by inhibiting the SUFU tumour suppressor. Nat Cell Biol [Internet]. 2017 Sep 29 ;19(10):1226–36. Available from: https://pubmed.ncbi.nlm.nih.gov/28945232/

122. Yauch RL, Dijkgraaf GJP, Alicke B, Januário T, Ahn CP, Holcomb T, et al. Smoothened mutation confers resistance to a Hedgehog pathway inhibitor in medulloblastoma. Science [Internet]. 2009 Oct 23 ;326(5952):572–4. Available from: https://pubmed.ncbi.nlm.nih.gov/19726788/

123. Axelson M, Liu K, Jiang X, He K, Wang J, Zhao H, et al. U.S. Food and Drug Administration approval: vismodegib for recurrent, locally advanced, or metastatic basal cell carcinoma. Clin Cancer Res [Internet]. 2013 May 1 ;19(9):2289–93. Available from: https://pubmed.ncbi.nlm.nih.gov/23515405/

124. D'Amato C, Rosa R, Marciano R, D'Amato V, Formisano L, Nappi L, et al. Inhibition of Hedgehog signalling by NVP-LDE225 (Erismodegib) interferes with growth and

invasion of human renal cell carcinoma cells. Br J Cancer [Internet]. 2014 Sep 9 ;111(6):1168–79. Available from: https://pubmed.ncbi.nlm.nih.gov/25093491/

125. Atwood SX, Sarin KY, Whitson RJ, Li JR, Kim G, Rezaee M, et al. Smoothened Variants Explain the Majority of Drug Resistance in Basal Cell Carcinoma. Cancer Cell [Internet]. 2015 Mar 9 ;27(3):342–53. Available from: https://pubmed.ncbi.nlm.nih.gov/25759020/

126. Zhao X, Pak E, Ornell KJ, Murphy MFP, Mackenzie EL, Chadwick EJ, et al. A Transposon Screen Identifies Loss of Primary Cilia as a Mechanism of Resistance to SMO Inhibitors. Cancer Discov [Internet]. 2017 Dec 1 ;7(12):1436–9. Available from: https://pubmed.ncbi.nlm.nih.gov/28923910/

127. Lauth M, Bergström Å, Shimokawa T, Toftgård R. Inhibition of GLI-mediated transcription and tumor cell growth by small-molecule antagonists. Proc Natl Acad Sci U S A [Internet]. 2007 May 15 ;104(20):8455–60. Available from: https://pubmed.ncbi.nlm.nih.gov/17494766/

128. Calcaterra A, Iovine V, Botta B, Quaglio D, D'Acquarica I, Ciogli A, et al. Chemical, computational and functional insights into the chemical stability of the Hedgehog pathway inhibitor GANT61. J Enzyme Inhib Med Chem [Internet]. 2018 Jan 1 ;33(1):349–58. Available from: https://pubmed.ncbi.nlm.nih.gov/29338454/

129. Pak E, Segal RA. Hedgehog Signal Transduction: Key Players, Oncogenic Drivers, and Cancer Therapy. Dev Cell [Internet]. 2016 Aug 22 ;38(4):333–44. Available from: https://pubmed.ncbi.nlm.nih.gov/27554855/

130. Kim J, Lee JJ, Kim J, Gardner D, Beachy PA. Arsenic antagonizes the Hedgehog pathway by preventing ciliary accumulation and reducing stability of the Gli2 transcriptional effector. Proc Natl Acad Sci U S A [Internet]. 2010 Jul 27 ;107(30):13432–7. Available from: https://pubmed.ncbi.nlm.nih.gov/20624968/

131. Maresca L, Crivaro E, Migliorini F, Anichini G, Giammona A, Pepe S, et al. Targeting GLI1 and GLI2 with small molecule inhibitors to suppress GLI-dependent transcription and tumor growth. Pharmacol Res [Internet]. 2023 Sep 1 ;195. Available from: https://pubmed.ncbi.nlm.nih.gov/37473878/

132. Lori G, Pastore M, Navari N, Piombanti B, Booijink R, Rovida E, et al. Altered fatty acid metabolism rewires cholangiocarcinoma stemness features. JHEP Reports [Internet]. 2024 Oct 1 ;6(10). Available from: https://pubmed.ncbi.nlm.nih.gov/39430578/

133. Sato T, Stange DE, Ferrante M, Vries RGJ, Van Es JH, Van Den Brink S, et al. Long-term expansion of epithelial organoids from human colon, adenoma, adenocarcinoma, and Barrett's epithelium. Gastroenterology [Internet]. 2011 ;141(5):1762–72. Available from: https://pubmed.ncbi.nlm.nih.gov/21889923/

134. Fujii M, Shimokawa M, Date S, Takano A, Matano M, Nanki K, et al. A Colorectal Tumor Organoid Library Demonstrates Progressive Loss of Niche Factor Requirements during Tumorigenesis. Cell Stem Cell [Internet]. 2016 Jun 2 ;18(6):827–38. Available from: https://pubmed.ncbi.nlm.nih.gov/27212702/

135. Marinucci M, Ercan C, Taha-Mehlitz S, Fourie L, Panebianco F, Bianco G, et al. Standardizing Patient-Derived Organoid Generation Workflow to Avoid Microbial Contamination From Colorectal Cancer Tissues. Front Oncol [Internet]. 2022 Jan 10 ;11. Available from: https://pubmed.ncbi.nlm.nih.gov/35083141/

136. Borrelli C, Roberts M, Eletto D, Hussherr MD, Fazilaty H, Valenta T, et al. In vivo interaction screening reveals liver-derived constraints to metastasis. Nature [Internet]. 2024 Aug 8 ;632(8024):411–8. Available from: https://pubmed.ncbi.nlm.nih.gov/39048831/

137. Taha-Mehlitz S, Bianco G, Coto-Llerena M, Kancherla V, Bantug GR, Gallon J, et al. Adenylosuccinate lyase is oncogenic in colorectal cancer by causing mitochondrial dysfunction and independent activation of NRF2 and mTOR-MYC-axis. Theranostics [Internet]. 2021 Feb 15 ;11(9):4011–29. Available from: https://pubmed.ncbi.nlm.nih.gov/33754045/

138. Patro R, Duggal G, Love MI, Irizarry RA, Kingsford C. Salmon provides fast and bias-aware quantification of transcript expression. Nat Methods [Internet]. 2017 ;14(4):417–9. Available from: https://pubmed.ncbi.nlm.nih.gov/28263959/

139. Soneson C, Love MI, Robinson MD. Differential analyses for RNA-seq: Transcript-level estimates improve gene-level inferences. F1000Res [Internet]. 2016 ;4. Available from: https://pubmed.ncbi.nlm.nih.gov/26925227/

140. Love MI, Huber W, Anders S. Moderated estimation of fold change and dispersion for RNA-seq data with DESeq2. Genome Biol [Internet]. 2014 Dec 5 ;15(12). Available from: https://pubmed.ncbi.nlm.nih.gov/25516281/

141. Hanover JA, Krause MW, Love DC. Bittersweet memories: linking metabolism to epigenetics through O-GlcNAcylation. Nat Rev Mol Cell Biol [Internet]. 2012 May ;13(5):312–21. Available from: https://pubmed.ncbi.nlm.nih.gov/22522719/

142. Liu Y, Du F, Zhao Q, Jin J, Ma X, Li H. Acquisition of 5-fluorouracil resistance induces epithelial-mesenchymal transitions through the Hedgehog signaling pathway in HCT-8 colon cancer cells. Oncol Lett [Internet]. 2015 ;9(6):2675–9. Available from: https://pubmed.ncbi.nlm.nih.gov/26137127/

143. Cong G, Zhu X, Chen XR, Chen H, Chong W. Mechanisms and therapeutic potential of the hedgehog signaling pathway in cancer. Cell Death Discov [Internet]. 2025 Dec 1 ;11(1). Available from: https://pubmed.ncbi.nlm.nih.gov/39900571/

144. Zhang L, Song R, Gu D, Zhang X, Yu B, Liu B, et al. The role of GLI1 for 5-Fu resistance in colorectal cancer. Cell Biosci [Internet]. 2017 Apr 13 ;7(1). Available from: https://pubmed.ncbi.nlm.nih.gov/28413604/

145. Yu B, Gu D, Zhang X, Liu B, Xie J. The role of GLI2-ABCG2 signaling axis for 5Fu resistance in gastric cancer. Journal of Genetics and Genomics [Internet]. 2017 Aug 20 ;44(8):375–83. Available from: https://pubmed.ncbi.nlm.nih.gov/28847472/

146. Zhang H, Kong W, Zhao X, Xie Y, Luo D, Chen S. Comprehensive analysis of PHGDH for predicting prognosis and immunotherapy response in patients with endometrial carcinoma. BMC Med Genomics [Internet]. 2023 Dec 1 ;16(1). Available from: https://pubmed.ncbi.nlm.nih.gov/36803157/

147. Ebrahimi N, Afshinpour M, Fakhr SS, Kalkhoran PG, Shadman-Manesh V, Adelian S, et al. Cancer stem cells in colorectal cancer: Signaling pathways involved in stemness and therapy resistance. Crit Rev Oncol Hematol [Internet]. 2023 Feb 1 ;182. Available from: https://pubmed.ncbi.nlm.nih.gov/36702423/

148. Boukouris AE, Zervopoulos SD, Michelakis ED. Metabolic Enzymes Moonlighting in the Nucleus: Metabolic Regulation of Gene Transcription. Trends Biochem Sci [Internet]. 2016 Aug 1 ;41(8):712–30. Available from: https://pubmed.ncbi.nlm.nih.gov/27345518/

149. Maddocks ODK, Athineos D, Cheung EC, Lee P, Zhang T, Van Den Broek NJF, et al. Modulating the therapeutic response of tumours to dietary serine and glycine starvation. Nature [Internet]. 2017 Apr 19 ;544(7650):372–6. Available from: https://pubmed.ncbi.nlm.nih.gov/28425994/